THE EFFECT OF SUSPENSION CASTING ON THE HOT WORKABILITY AND MECHANICAL PROPERTIES OF AISI TYPE 310 STAINLESS STEEL

ALISTAIR GEORGE SANGSTER FORBES

A Dissertation submitted to the Faculty of Engineering, University of the Witwatersrand, Johannesburg in fulfilment of the requirements for the Degree of Master of Science in Engineering.

Department of Metallurgy and Materials Engineering
University of the Witwatersrand
August 1987

DECLARATION

I declare that this dissertation is my own, unaided work. It is being submitted for the degree of Master of Science in Engineering at the University of the Witwatersrand, Johannesburg. It has not been submitted before for any degree or examination in any other university.

A G S Forbes

ALISTAIR GEORGE SANGSTER FORBES

25th day of August 1987

ABSTRACT

In processing austenitic stainless steels, certain grades stand out as being difficult to hot work, including AISI type 310. The poor hot workability is considered to be associated with the high resistance of the steel to plastic flow and the low ductile strength along the grain boundaries of the columnar crystals. The elimination of the columnar structure is expected to improve the hot workability and the internal quality of the steel as well as the mechanical properties.

This study was intended to investigate [illegible] solid structure by [illegible] and to find the effect of this structure on the as-cast properties and after hot deformation on the properties of the steel.

[illegible] using [illegible] of the decomposition of metallic powders [illegible] the melt [illegible] during casting. The metallic particles are considered as nucleating are evenly distributed in the form of a suspension in the melt. The purpose is to produce heat during solidification by [illegible] thermally heat zones which obtain heat from the metal in these zones are [illegible]. The metallic particles also act as nuclei for heat which [illegible] and which can [illegible].

The suspension casting process has been applied satisfactorily to sand castings and steel ingots in the Eastern Block countries. By using this process, the mechanical properties of steel castings were improved significantly, and better control of shrinkage porosity distribution and macro-segregation as well as macrostructure were obtained.

Ingots of AISI type 310 were produced by conventional and suspension casting methods. Microchilling was carried out by the addition of 2,1 mass percent of pure iron powder (53-105 μm in

size). Other casting conditions such as pouring time and temperature were similar for all castings. Ingots were then hot rolled by 20, 40, 60 and 80 percent reduction in area. Sectioning of the ingots was planned in such a way as to examine the properties of the microchilled castings and compare them with those of conventional castings in both the "longitudinal" and "transverse" directions. A "longitudinal" specimen is defined as one in which the dendrites are parallel to the specimen axis while in a "transverse" specimen the dendrites are perpendicular to the specimen axis.

It was found that the non-random dendritic structure common in conventional castings was altered by microchilling. The long dendrites with preferred orientations in conventional castings were replaced by fine randomly orientated dendrites. Chemical analyses showed that the composition of conventionally cast and microchilled material did not differ significantly.

The mechanical properties of the castings made by conventional methods and by microchilling were assessed by use of Charpy impact tests, tensile tests and Vickers hardness tests whereas the hot workability was assessed by use of hot compression test.

The hardness and therefore strength of the microchilled material was found to be higher than that of the conventionally cast material. The yield strength of the 80 percent hot rolled material increased from 400 MPa for conventionally cast material to 502 MPa for microchilled material.

The change in toughness of the material was however not conclusive. No decrease in impact energies was observed for microchilled material but an increase in the percentage reduction in area from 36 percent for conventionally cast longitudinally orientated specimens to 62 percent for microchilled longitudinally orientated specimens was obtained using tensile tests.

The suspension cast specimens had consistently better hot formability whereas the conventionally cast specimens showed greater frequency and severity of cracking.

ACKNOWLEDGEMENTS

The author is indebted to the following people and institutions for their invaluable advice, use of equipment and, particularly, their encouragement.

To Dr Andy Koursaris who persuaded me to embark on this project and for his interest and enthusiastic supervision during the course of this work.

To Professor Geoff Garrett for his recruitment and encouragement.

Middelburg Steel and Alloys for supplying the material and for their advice.

Members of Mintek for their advice and practical assistance.

Members of the Metallurgy Department at the University of the Witwatersrand, especially John Moore, Wayne Costopoulos, Johnson Ndengeza and Aubrey Xoseka for their advice and assistance.

My friends in the Metallurgy Department at the University of the Witwatersrand for their useful discussions, encouragement, time and help.

Yücel Sentarli of the CSIR for his time and help.

My family, particularly my wife Rosemarie for all their understanding, encouragement, time and help.

Finally, to Mintek, the CSIR and the University of the Witwatersrand for their financial support for the duration of this work.

CONTENTS

LIST OF FIGURES

LIST OF TABLES

1. INTRODUCTION

1.1 Background

In processing austenitic stainless steels, certain grades stand out as being difficult to hot work, including AISI type 310 (24-26 percent Cr, 19-22 percent Ni) and there appear to be two distinct workability problems.

First, ingot cracking may occur during the initial rolling operation which cannot be ascribed to hot shortness (defined as low ductility resulting from localised melting), and often slabs must be rolled to an intermediate size and conditioned to remove severe cracks prior to finishing. Secondly, hot band (~ 3-5 mm thick) may edge crack badly at normal finishing temperatures.

The two types of problem are illustrated in Figures 1 and 2 respectively.

These problems are erratic however and no widely applicable solution has been found through changes in melting, deoxidation, or casting practices. Each producer employs a particular furnace practise determined by trial and error to maximise yield on hot working.

Although it is recognised that many factors may affect the hot workability of steel, the poor hot workability of stainless steel AISI type 310 was considered to be primarily associated with two conditions namely the high resistance of the steel to plastic flow and the low cohesive strength along the periphery of the columnar crystals. Stainless steel AISI type 310 is a highly alloyed steel and the stress required to produce plastic flow during hot rolling is high. Furthermore, steels which are single phase with high alloy content also tend to develop long, columnar crystals showing pronounced preferred crystallographic orientation and AISI type 310 which is completely austenitic is no exception (Figure 3).

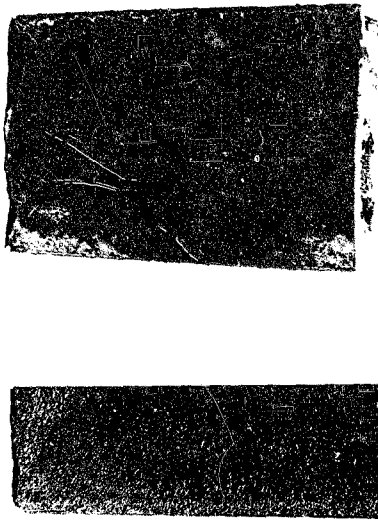

FIGURE 1 - Cracking of AISI Type 310 Stainless Steel Slab

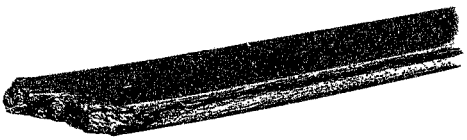

FIGURE 2 - Edge Cracking of AISI Type 310 Hot Band (~3-5mm Thick)

The combination of resistance to plastic flow and long, columnar crystals causes the steel to tear along the periphery of the columnar crystals (planes of weakness) and consequently decreases the hot workability.

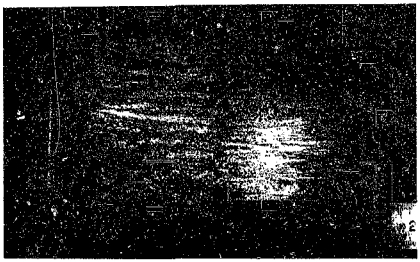

FIGURE 3 - Macrostructure of AISI Type 310 Stainless Steel

Since the elimination of the long columnar crystals is expected to improve the hot workability and the internal quality of the steel as well as the mechanical properties, this study was directed towards control of ingot structure and the effect of ingot structure on the properties of the steel.

The control of the ingot macrostructure was accomplished by the little known technique of suspension casting.

1.2 The Suspension Casting Process (Microchilling)

Several techniques have been used to obtain improved macrostructures in ingots. These include inoculation of the melt and dynamic grain refining techniques such as stirring of the melt or ultrasonic vibration. More recently microchilling of the melt has been investigated and appears to hold a lot of promise in this respect.

The suspension casting process consists of the introduction of metallic particles into the mould cavity during or prior to casting. The main object of this process is to obtain an even distribution of particles throughout the casting during solidification. The particles extract the superheat and a part of the latent heat of the alloy by acting as internal chills as well as forming effective nucleation sites. The amount of heat which is extracted by each metallic particle should be sufficient to melt down the particle and create a local thermal gradient. As a result of this faster cooling and formation of nucleation sites, the nucleation of equiaxed grains is promoted.

The suspension casting process has been applied satisfactorily to sand castings and steel ingots in the Eastern Block countries. By using this process, the mechanical properties of steel castings were improved significantly, and better control of shrinkage porosity distribution and macro-segregation as well as macrostructure were obtained.

The properties of steels made by conventional methods vary significantly in different orientations due to the coarse and non-random microstructures that form upon solidification. Microchilled steels may be expected to have isotropic properties due to the refining action of the microchills and the random distribution of microconstituents. This should prove beneficial to the hot workability of the steel.

1.3 Objectives of the Present Study

The purpose of this study was to investigate the control of ingot macrostructure by suspension casting and the influence of cast structure on the hot workability and the mechanical properties of AISI type 310 stainless steel.

The literature survey therefore concentrated on two major areas. Firstly, the cast structure of ingots was reviewed beginning with the fundamental aspects of solidification and progressing to a description of the ingot macrostructure. The theories on the formation of mixed structures in castings as well as the control and modification of the cast structure with particular reference to the suspension casting process were considered.

The second part of the literature survey is a discussion on the composition of some austenitic stainless steels and on the way in which AISI type 310 fits into this category. The hot workability of stainless steels is evaluated with reference to material type and process variables.

Experimental work included the establishment of a technique for microchilling, the production of conventional and microchilled ingots of AISI type 310 stainless steel and a study of ingot macrostructures and microstructures produced by the two routes. The mechanical properties and the hot workabilities of conventionally cast and microchilled material were determined in the as cast condition and after various amounts of deformation by hot rolling. Finally, the properties obtained in the two types of material were compared and the future of the suspension casting technique was assessed.

2. LITERATURE SURVEY

2.1 Review of Some Fundamental Aspects of Solidification

Before discussing the origin and control of the microstructure, it is necessary to review briefly some of the basic features of the process of solidification.

2.1.1 Nucleation and Latent Heat of Fusion

Crystalline solids, such as metals, have a definite melting point, Tm, above which they exist in the liquid state. However, it is possible to cool a liquid below the equilibrium melting point before solidification begins. A liquid metal below its melting point is described as "supercooled" or "undercooled".[1]

Supercooling a liquid is possible because the spontaneous aggregation of a few hundred atoms of the liquid in the geometrical pattern characteristic of the crystal involves the appearance of the solid/liquid interface which is associated with a positive energy change. The embryo must reach a certain size, r*, which depends on the temperature, in order to be sufficiently stable to have a reasonable chance of growing, when it is called a nucleus.

The critical nucleus size[2], r*, for homogeneous nucleation, as described above, is given by the equation :

$$r^* = \frac{2\,\gamma_{LC} \cdot T_m}{L_m \cdot \Delta T} \qquad \ldots\ (1)$$

where γ_{LC} is the specific surface energy of the liquid-crystal interface, T_m is the equilibrium melting point, L_m is the latent heat of fusion and ΔT is the amount of supercooling.

It can be shown[2] that the critical energy change, ΔG^*_{hom}, required for the formation of a nucleus of critical size, r*, is given by:

$$\Delta G^*_{hom} = \frac{16\pi \gamma_{LC}^3 \cdot T_m^2}{3 (L_m \cdot \Delta T)^2} \quad \ldots\ (2)$$

Metals nucleate homogeneously when the degree of undercooling is approximately 0,2 T_m. Iron, for example, whose equilibrium melting/solidification temperature is 1536 °C will nucleate homogeneously at a temperature of 1245 °C !

In practise it is almost always found that solidification starts at much lower degrees of supercooling because nucleation takes place heterogeneously due to the presence of solid particles in the melt and container walls. Solid particles and container walls, called "nucleation catalysts", make nucleation easier by acting as substrates on which an embryo can form and become a nucleus at much less supercooling than would otherwise be necessary.

It can be shown[2] that for heterogeneous nucleation, the critical nucleus size, r*, is the same as for homogeneous nucleation. However, the volume of the nucleus is reduced because the crystal adopts the "radius" of the substrate as its own (Figure 4). Thus, the work of nucleation, ΔG^*, decreases siginficantly and nucleation is facilitated. (It should be noted that in Figure 4 the formation of a spherical cap is assumed for simplicity although this may not be the case in actual systems).

For heterogeneous nucleation, ΔG^* is given as

$$\Delta G^*_{het} = \frac{4\pi \gamma_{LC}^3 T_m^2 (2-3\cos\theta + \cos^3\theta)}{3 (L_m \cdot \Delta T)^2} \quad \ldots\ (3)$$

Hence, the critical energy change differs from that for homogeneous nucleation by a factor of $1/4\ (2-3\cos\theta + \cos^3\theta)$.

The contact angle, θ, is defined by

$$\cos\theta = \frac{\gamma_{LS} - \gamma_{CS}}{\gamma_{LC}} \qquad \ldots\ (4)$$

where γ_{LC} is the liquid-crystal interface energy, γ_{CS} is the crystal-substrate interface energy and γ_{LS} is the liquid-substrate interface energy.

For $\theta = 180°$, $\cos\theta = 1$ and the expression $1/4\ (2-3\cos\theta+\cos^3\theta) = 0$. Thus, under these conditions $\Delta G^*_{het} = \Delta G^*_{hom}$.

For values of θ between $0°$ and $180°$, heterogeneous nucleation is more favourable thermodynamically.

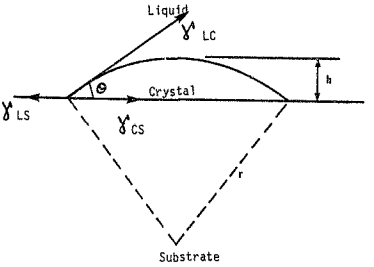

FIGURE 4 - Spherical Cap of Solid Formed on a Planar Substrate (Davies[2])

All metals processed under industrial conditions can be expected to contain potent nucleation sites such as oxide, carbide and carbonitride particles which promote nucleation at temperatures only a few degrees below T_m.[1]

When nucleation has occurred, subsequent growth of the crystal takes place by the addition of atoms from the liquid.[2] Each atom that attaches itself to the solid releases its latent heat of fusion and the rate of growth is determined by the rate at which this heat is removed.

If this heat is not removed, it very soon raises the temperature to the point at which no further solidification can occur.

It follows that the overall rate of the solidification process is controlled by the rate at which heat is extracted from the solidifying metal. The latent heat must be conducted outwards, into and through the mould in which the metal is solidifying[1]. Alternatively, as will be seen later, the addition of microchilling particles may provide local heat sinks for this heat.[3]

The quantity of heat that must be removed is considerable; iron for instance, has a latent heat of fusion of about 15,2 kJ mol^{-1} at 1536 °C and atmospheric pressure, while its specific heat is about 44,5 J mol^{-1} $°C^{-1}$ at 1536 °C.[4] The energy required to raise the temperature of the metal is given by $\int_{T_1}^{T_2} C_p \, dT$ where C_p is the specific heat capacity and T the absolute temperature. This expression reduces to $C_p \Delta T$ if C_p is assumed independent of temperature. The latent heat of fusion ΔH_f is the energy liberated when a metal solidifies and if this energy is equated to the term $C_p \Delta T$, the temperature rise corresponding to this energy can be obtained i.e. $\Delta T = \frac{\Delta H_f}{C_p}$. It

follows that the amount of heat that must be extracted to solidify a given quantity of iron would be sufficient to raise its temperature by 342 °C.

2.1.2 Rejection of Solute

One of the most important considerations in the solidification of an alloy is that the solid which forms almost always has a composition that differs from that of the liquid that is in contact with it.

The rejection of solute results in segregation and the enrichment in solute of the liquid at the solid-liquid interface, lowers the equilibrium liquidus temperature and gives rise to the phenomenon of constitutional supercooling.[1]

Originally, constitutional supercooling was analysed by Tiller et al[5] who demonstrated that the equilibrium liquidus temperature, T_L, for steady-state solidification of an alloy of initial composition C_o is given by :

$$T_L = T_i + \frac{m\, C_o\, (1-k_o)}{k_o} \left[1 - \exp\left(-\frac{Rx}{D}\right)\right] \qquad \ldots\ (5)$$

where T_i is the solid-liquid interface temperature, m is the slope of the liquidus line, R is the growth rate of the interface, D is the diffusivity, x is the distance ahead of the interface and k_o is the equilibrium distribution coefficient defined by the ratio :

$$k_o = \frac{\text{solute concentration in the solid at temperature T}}{\text{solute concentration in the liquid at the same temperature}}$$

The actual temperature T, in the liquid is given by :

$$T = T_i + G\, x \qquad \ldots\ (6)$$

where G is the temperature gradient in the liquid ahead of the interface and T_i and x are as in equation 5. As G varies, a situation can arise where the liquid ahead of the interface is at a temperature below its equilibrium liquidus temperature, in which case a region of constitutionally supercooled liquid exists ahead of the interface (Figure 5).

It has been shown[2] that for no constitutional supercooling,

$$\frac{G}{R} > \frac{m\,C_o}{D}\,\frac{(1 - k_o)}{k_o} \qquad \ldots\ (7)$$

This inequality allows those factors favouring constitutional supercooling to be identified as :

i) low temperature gradients in the liquid

ii) fast growth rates

iii) steep liquidus lines

iv) high alloy contents

v) low diffusivity in the liquid

vi) very low k_o for $k_o < 1$ or very high k_o for $k_o > 1$

The above treatment assumes that solute mixing in the liquid is the result of diffusion only. It can be modified[6] to allow for partial or complete mixing in the liquid.

2.1.3 Structural Effects Resulting from Solute Rejection

It has been found [1 7] that there are four recognisable morphologies that the solid-liquid interface can assume, depending on the composition of the alloy and on thermal conditions.

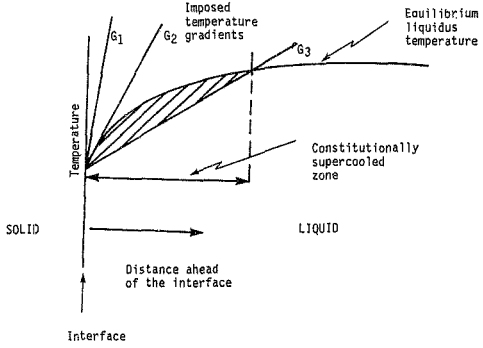

FIGURE 5 - Constitutional Supercooling ahead of an Interface (Davies[2])

These are : i) smooth interface

ii) cellular interface

iii) cellular-dendritic interface, and

iv) dendritic interface

These are shown diagrammatically in Figure 6 together with the conditions that give rise to each type.

In the absence of supercooling, pure metals as well as alloys will solidify with a planar solid-liquid interface. Thermal supercooling in pure metals and constitutional supercooling in alloys may be expected to result in a non-planar solid-liquid interface. Constitutionally supercooled liquid ahead of the interface stabilises interface perturbations and as the degree of supercooling increases, the planar interface goes through a number of distinct transitions becoming pock-marked at first followed by the formation of elongated cells and cellular dendrites. Under extreme conditions free dendritic growth takes place. There do not appear to be clear criteria for the transition from one type of interface to the next.[7]

The intercellular/interdendritic regions are enriched in solute for systems for which $k_o < 1$ and depleted in solute for systems for which $k_o > 1$. Long range segregation effects (macrosegregation) may also occur. A dendrite will show a variation in composition from its interior outwards, the phenomenon of coring.[6]

Dendrites grow preferentially along specific crystallographic directions (< 001 > in cubic metals) and dendritic structures may, therefore, be expected to exhibit strongly anisotropic properties.[7] Microsegregation may be eliminated with relative ease by a homogenisation anneal. Macrosegregation on the other hand is in most practical cases impossible to reduce significantly.

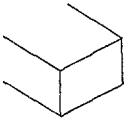

SMOOTH

Pure metal No supercooling

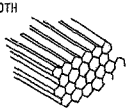

CELLULAR

Impure metal or dilute alloy Local supercooling

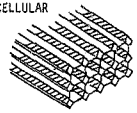

CELLULAR-DENDRITIC

Alloy Local supercooling

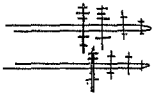

DENDRITIC

Alloy Extensive supercooling

FIGURE 6 - Types of Solid-Liquid Interfaces (Chalmers[1])

2.2 The Cast Structure

The macrostructure of ingots may contain the following three zones [2 6] : (Figure 7)

i) A peripheral zone of fine equiaxed grains, commonly called the chill zone;

ii) A zone of columnar grains extending inwards from the chill zone,

iii) A central zone of equiaxed grains; these are normally larger than the chill grains.

All the zones are not necessarily present in any particular ingot since their presence and extent depend upon the casting conditions and the composition of the cast material. Figure 8, for example, is the transverse section of a mild steel billet and, as can be seen, only the columnar zone is present.

Extensive research has been done in order to establish the origin and development of the three zones.

2.2.1 The Chill Zone

The chill crystals which are normally equiaxed and of random orientation nucleate on or near the mould wall as a result of heterogeneous nucleation.

An extensive chill zone is favoured by [6] :

i) nucleants which promote nucleation at very small supercooling,

ii) low pouring temperatures,

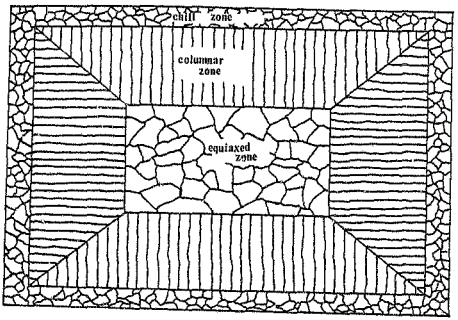

FIGURE 7 - Transverse Section of an as-cast Structure showing the Chill Zone, Columnar Zone and Equiaxed Zone (Walker[8])

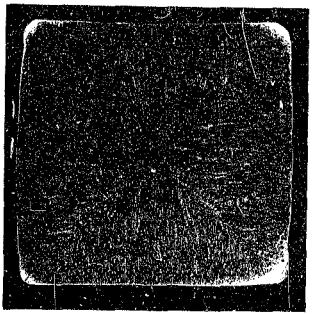

FIGURE 8 - Transverse Section of a Mild Steel Billet showing only a Columnar Zone

iii) low and high thermal diffusivities of the mould and the liquid metal respectively, and

iv) high alloy content

Crystal multiplication by the fragmentation of the initial dendrites was proposed by Bowers et al[9] and later verified by Jackson. [10]

The chill zone is only a few grain diameters thick and has little effect on ingot behaviour during deformation. The chill zone is, however, a desirable feature of ingots as it results in an improved surface finish after rolling.

2.2.2 The Columnar Zone

Columnar grains grow or nucleate on chill crystals and show a strong preferred crystallographic orientation, [11] [12] advancing inwards in a direction parallel to that of heat extraction. A few grains however do not originate in the chill zone.[13]

The columnar grains can grow with any one of the growth interfaces already discussed, e.g. planar, cellular, cellular dendritic or free dendritic growth.[13] During growth, the number of columnar crystals decreases, the cross-section of those remaining increases, and a preferred orientation is developed by the selection for survival of crystals having the steepest thermal gradient parallel to the preferred growth direction (the dendrite arm axis direction).

For a given alloy, the extent of the columnar region increases as the pouring temperature increases (Figure 9) whereas for given pouring conditions, the extent of the columnar region decreases as the alloy content increases[6] (Figure 10).

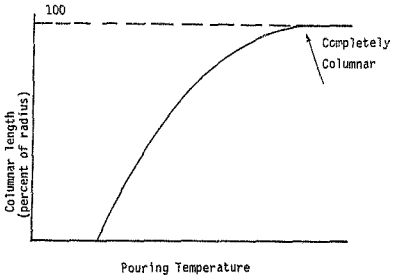

FIGURE 9 - Variation of the Length of the Columnar Zone with Pouring Temperature (Chalmers[6]).

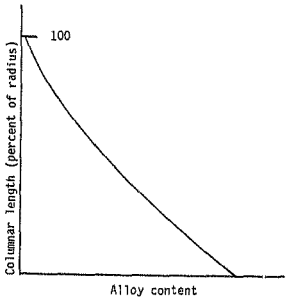

FIGURE 10 - Variation of the Length of the Columnar Zone with Alloy Content for Constant Pouring Temperature (Chalmers[6]).

Columnar grains may show segregation. Interdendritic segregation will lead to low-melting material or second phases between dendrite arms which can lead to hot shortness or poor ductility during rolling. Because the columnar crystals are extremely large, the overall grain boundary area is small and even small amounts of interdendritic segregation will have a significant influence on hot ductility.

During hot working cracks are likely to initiate in the columnar zone due to its inferior characteristics.

Since the columnar crystals will persist provided conditions are not favourable for the formation of equiaxed crystals, control over the columnar growth is normally exerted by inducing the formation of equiaxed crystals. It is this control which is foremost in the control of the overall cast structure. Suspension casting is one possible means of applying this control.

2.2.3 The Equiaxed Zone

The crystals in the equiaxed zone are usually larger than those in the chill zone and their orientation is effectively random.[2] As the pouring temperature increases, the tendency to form equiaxed grains decreases and those that do form are coarser.[6] It is however, important to recognise that there is a significant ingot size effect influencing the development of the equiaxed zone[14] and the above relationship may not hold for larger ingots where effects such as crystal settling influence the macrostructure.

Essentially six theories exist about the origin of the equiaxed zone :

i) Heterogeneous nucleation in constitutionally supercooled liquid ahead of the columnar grains. [15 16]

ii) Heterogeneous nucleations in a low density, solute enriched upper liquid layer[17]

iii) Nuclei formed in the chilled liquid adjacent to mould walls are carried to the centre of the ingot by convection (Big-bang theory)[1]

iv) Showering [18 19] of dendrites growing at the top surface

v) Crystal multiplication owing to melting of dendrite arms[10]

vi) Crystals nucleating on the mould wall grow with a necked shape and separate from the place of origin before the formation of a solid shell.[20 22]

Of these theories, the one postulating the detachment of dendrite arms owing to convective flow of the bulk liquid (postulate v above) is considered to be the most probable and has recently been demonstrated using a transparent succinonitrile-ethyl alcohol solution as a model material for steel.[22] It is however probable that two or more mechanisms may contribute to the formation of the equiaxed zone.

Interdendritic segregation is less in the equiaxed zone than the columnar zone as the grain size is smaller and hence the grain boundary area is larger which reduces the effect of segregation. Because of this and the random crystal orientation, the equiaxed zone is a desirable feature in ingots. The larger the equiaxed zone, the greater the ductility of the ingot.

2.2.4 Thermal Explanation of Mixed Structures in Castings

Because of the changing thermal conditions during freezing, the different structural zones encountered in castings may be explained solely on the basis of critical changes in the G/R ratio,[23] where G is the temperature gradient and R the rate of freezing.

Progressive change in this parameter from a high to a low value is accompanied by successive transitions in the mode of crystallisation as the effect of undercooling becomes more pronounced. With a very high ratio, columnar growth takes place with the advance of a planar interface (this corresponds to no constitutional supercooling). At very low values of G/R, heterogeneous nucleation in the constitutionally supercooled zone brings about the nucleation and growth of new grains in positions remote from the existing interface. These grains may themselves undergo dendritic growth, although there is some evidence that the radial growth of independent grains begins with a spherical morphology analogous to the plane interface condition in unidirectional freezing. The successive transitions from planar to cellular, to dendritic and thereafter to independently nucleated crystals, can be represented quantitatively as shown in Figure 11 which was derived from experimental observations under controlled thermal conditions.[23]

Because of the changing thermal conditions during freezing, therefore, the separate structural zones encountered in castings may be explained solely on the basis of critical changes in the ratio G/R. Figure 12(a) shows how initial solidification occurs under a marked temperature gradient (high G/R) which frequently suffices to bring about columnar dendritic growth in the outermost zone due to the lack of supercooling. In the central zone, and in some cases throughout the casting, the temperature gradient is shallow (low G/R) and lies below T_E the equilibrium liquidus temperature (Figure 12 (b)). Hence, the zone of constitutional supercooling is extensive so that solidification proceeds by the widespread nucleation and growth of equiaxed grains.

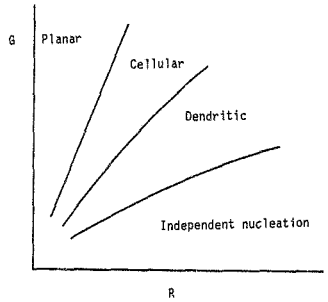

FIGURE 11 - Influence of Temperature Gradient G and Freezing Rate R on Solidification Morphology of a given Alloy (Beeley[23])

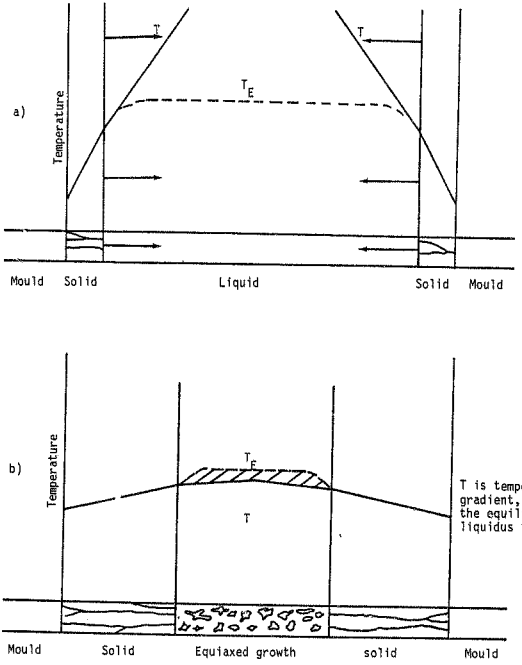

FIGURE 12 - Thermal Explanation of Mixed Structures in Castings. (a) Columnar Growth Stage, (b) Central Equiaxed Region (Beeley[23])

2.3 Control and Modification of the Cast Structure

The important characteristics of the cast structure include the type, the size, the uniformity and the orientation of grains in the different zones. These factors have a direct effect on the mechanical behaviour of castings as well as on their response to heat treatment and mechanical processing.[24]

For all but a few very specialised applications e.g. magnet alloys and single crystal turbine blades, fine-grained equiaxed structures are desirable in castings and ingots.[2] Equiaxed structures are isotropic and ensure reproducible behaviour during subsequent working. In particular they produce a uniform surface finish and reduce internal stresses in alloy castings which contain brittle constituents, by dispersing the latter. They also allow rapid solidification during continuous or semi-continuous casting and promote a uniform solidification pattern and sound product in small and intricate castings.[25]

To develop equiaxed structures requires the suppression of columnar growth and this can be achieved by promoting conditions favourable for the formation of equiaxed grains.[2] A necessary prerequisite is the establishment of a crystal network to act as an effective barrier to further columnar growth.

Davies[2] identifies two main approaches as having been adopted, namely the use of physical methods including dynamic refining techniques in which the alloy is s 'dified while applying mechanical action, and the control of nucleation by controlling the casting conditions and by the use of inoculants.

2.3.1 Dynamic Grain Refinement

Various methods have been used to produce dynamic fragmentation of the growing dendrites, and thus to promote equiaxed growth. All of these methods involve some degree of physical disturbance

and differ only in the way this disturbance is produced. Methods such as ultrasonic vibration, [26 27] mechanical vibration, [28 29] gas agitation, rotating magnetic fields, [28 30] magnetic-electric interaction[31-34] and mould oscillation[35] have been used by many investigators. Campbell[36] presents a comprehensive review on the subject.

In all cases, the principal mechanism for producing the nuclei for the equiaxed grains is dendrite fragmentation. The effect of the physical disturbance is to produce localised thermal fluctuations as the liquid metal flows backwards and forwards over the growing dendrites. It is these forced thermal fluctuations that produce the conditions conducive to dendrite arm remelting.

2.3.2 The Chill Effect

When molten metals contact the cold walls of the mould, or chills, the melt superheat is removed and the liquid becomes locally supercooled. The number of nucleation centres increases while the size of the centres decreases and nucleation occurs extensively in the liquid. Techniques such as splat-cooling, die casting and the application of chills utilise this approach in order to promote copious nucleation and a resulting fine grain size. [2 37]

In general, a rough mould surface, a very cold mould or a mould that can absorb large amounts of heat, a low pouring temperature and convection currents that stir the melt all favour a fine-grained structure. [2 6 37]

2.3.3 The Use of Inoculants

A simple and effective way for producing a fine grained structure in an alloy is to cast with a low degree of superheat so as to promote copious heterogeneous nucleation in the initially chilled

liquid.[2] This, however, is not always possible in practise especially in the case of castings of varying section thickness where the requirements for adequate fluidity may dictate the use of liquid with a high degree of superheat. It is also a rather haphazard process since without the deliberate introduction of nucleating agents, the nucleation process depends on the chance existance of suitable heterogeneous nucleants. For this reason it is usual to add inoculants.

Empirical methods are needed in determining the nucleating effectiveness of an inoculant. However, the general characteristics of a good refiner can be stated[37] : low surface energy between substrate and melt; low interfacial energy between solid and substrate and as a consequence low disregistry and high chemical affinity. In addition, settling of the inoculants must be prevented through a minimisation of density differences between inoculant and melt. The precipitation of a high-temperature compound which remains stable at the temperature of solidification assuring a clean and reactive surface is also desirable. Hence, on this simple basis, the principal problem is still to know, or to measure, the wetting angle θ, between the nucleated solid and the added catalytic substrate. Also, there remains the problem of evaluating factors such as surface area and surface character of the nucleant which present theory does not consider in detail.[37]

Furthermore, the growth of the nucleus requires that some supercooling exists in the liquid. This will usually be constitutional supercooling although at the beginning of the solidification process some thermal undercooling may occur.[2]

One approach to the introduction of heterogeneous nucleants is the use of mould coatings.[2] In this procedure, the mould walls are treated with a wash containing the nucleating agent; this ensures that all parts of the casting have access to the nucleant. Nucleant mould coatings are now well established for

the refining of superalloy investment castings[38] and of white iron castings intended for malleablizing.[39]

In the area of ladle inoculation, a typical example is the addition of Ti and B to aluminium. These elements quickly react with the aluminium and apparently suitable complexes are formed by a peritectic reaction. However, this mechanism is not the only one that has been postulated, and Glasson and Emley[40] discussed in detail the different possible mechanisms that are still under discussion.[41-44] Despite this uncertainty about details of the nucleation mechanisms, improvements have been made in the theory in order to predict the final grain size as a function of the dispersion and density of nucleant particles, at least in the case of grain refinement of aluminium alloys.[25 45]

In the model considered by Maxwell and Hellawell,[25 45] the ability of a substrate to act as a surface for heterogeneous nucleation was defined by the wetting angle, θ, and comparison was made between the final grain count per unit volume (N_V^G) and the initial substrate count per unit volume (N_V^P). The form of the cooling curves for a variety of freezing conditions was computed and it was found that for each set of freezing conditions a critical value of N_V^P exists, above which an increase in the initial substrate count per unit volume produces negligible further grain refinement. When the N_V^P is high, the as-cast grain size will be as fine as is possible for the particular casting conditions. They found that a high N_V^G i.e. a small grain size corresponded to a decrease in θ, an increase in the cooling rate and a decrease in the nucleant radii from 3,0 µm to 0,3 µm. Probably the most important information obtained was the influence of solute supercooling as it varies from system to system. In effect, the grain-refining activity of a good potential catalyst is precluded if the growth temperature is not significantly depressed below the freezing point of the alloy. This depression can be considered to be proportional to a parameter x_1 equal to $1/2\ C_o.m.(k - 1)$, a measure of

solute rejection in any system. In order to facilitate comparison, Figure 13 relates the contact angle $\theta = 4°$ and cooling rate $P = 0,5\ Ks^{-1}$ to N_V^G for the systems Al-Ti, Al-Zr and Al-Cr. The figure shows that the variation in the grain refining action is strongly dependent on the solute supercooling which varies inversely as x_1. The figure also confirms that the critical inoculant particle count per unit volume (critical N_V^P) beyond which further grain refinement is not achieved, increases as x_1 decreases.

An alternative method by which grain refinement and cast structure modification may be obtained is suspension casting (microchilling). Microchilling, or suspension casting as it is also known, also exerts its effects through the principle of nucleation behaviour control.

2.4 Microchilling (The Suspension Casting Process)

Sound castings possessing high strength and high ductility can be produced by taking precautions such as avoiding over-heating of the metal, controlling gas pick up during and after melting, controlling chemical composition, adopting the proper heat treatment cycle and so on. In spite of observing all these, microporosity occurs in castings which solidify in a "pasty" manner.[2] The dispersed microporosity caused by pasty solidification can be minimised by the use of chills. Chills extract heat from the casting at a faster rate than the mould, producing a steeper temperature gradient.[3]

External chills, however, have a limited effect in the case of thick castings. In such instances, the judicious location of chills inside the casting could be the only solution.[3]

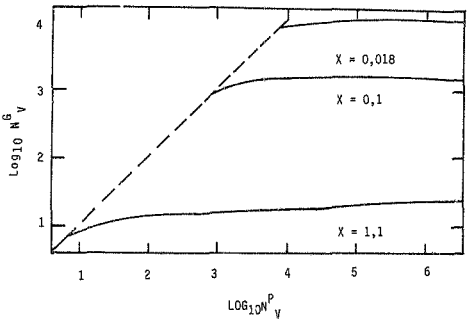

FIGURE 13 - A plot of the number of grains mm^{-3} (N_V^G) against number of particles mm^{-3} (N^P_V) for the systems Al-Ti (x = 0,018), Al-Zr (x = 0,1) and Al-Cr (x = 1,1), where x = 1/2 ($C_0 m$ (k-1)) • θ = 4° and P, the cooling rate is 0,5 $K.s^{-1}$ (Hellawell[23])

2.4.1 The Internal Chill

An internal chill differs from the conventional chill in that the internal chill is surrounded by the molten metal and becomes a part of the casting. Internal chills help in extracting the heat from the solidifying casting, prevent formation of shrinkage cavities, bring about reduction in porosity and grain size, and promote a more extensive equiaxed zone. This subsequently results in an increase in casting yield and density as well as improved mechanical and workability properties.[3]

Internal chills may be in the form of wires, rods, wire mesh and so on or, they may be in the form of powders (known as microchills).

For the internal microchilling process to be effective, the melting point of the microchills should be nearly equal to that of the parent metal and their composition should be compatible with that of the parent metal.[3]

When metal powders (microchills) are made use of, these are introduced along with the molten metal during pouring into the mould cavity. A uniform dispersion of the powder into the metal should be aimed at.[46] These metallic particles become numerous centres for the extraction of heat i.e. they serve as heat sinks and the action of the chills is thus accomplished.[3,47] Iron powder, molybdenum powder or ferromanganese powder can be used as microchills in carbon steels or alloy steels, and aluminium powder in aluminium-base alloys.

The mass of internal chills used must be 1 to 5 percent of the mass of the section to be cooled. The size of the metallic powder varies from a few microns to about 2mm[46] whereas in the case of rods or mesh, the mean diameter may vary depending on the section size of the casting.

The mass of the microchill can be established from the heat balance equation [3 48] :

$$M_c \{C_c(T_o-T_c)\} + L_c M_c = K (\frac{1}{m}) \{C_m (T_m-T_o)\} + L_m C_c\}$$

where the suffix 'c' refers to the chill side and 'm' to the metal side. M is the weight of metal/chill, C is the average specific heat, T_o is the temperature to which the metal must be cooled, T_c is the initial temperature of the chill, L is the latent heat, T_m is the superheat of the metal and K is the proportionality factor which depends on the metal, mould material and section being chilled. This equation assumes that the chills extract the superheat of the liquid metal rapidly prior to the commencement of metal solidification, and then extract part of the latent heat during solidification. It also assumes that heat is extracted simultaneously from all portions affected by the chill in the casting at a fairly uniform rate.

Finally, it should be noted that internal chills need more precautions compared to external chills in that chills should be free from gases, moisture, rust, oxide layers and so on.[3]

2.4.2 Methods of Microchilling

The two main approaches for the introduction of microchills are :

i) the entrainment of the microchill into the stream of molten metal during pouring and

ii) the introduction of the microchill to the mould prior to pouring.

Various techniques have been used by researchers to introduce microchills into a stream of molten metal during sand casting (Figure 14).

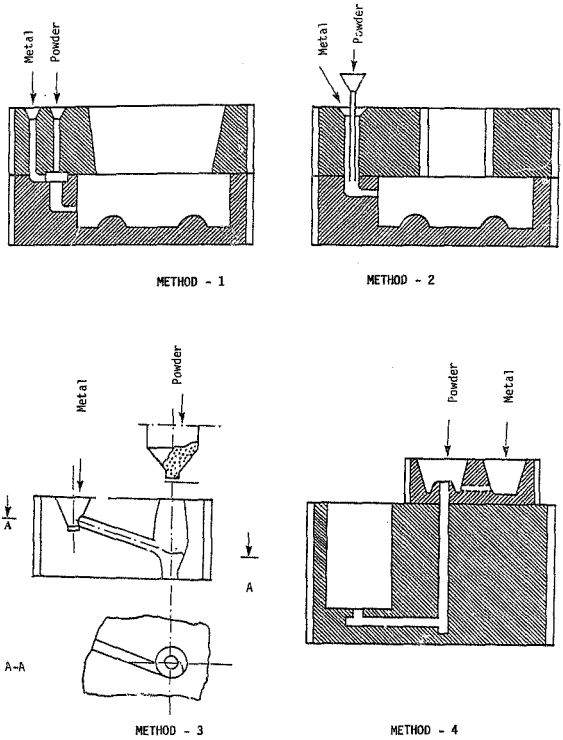

FIGURE 14 - Some Techniques for Microchilling (refs. 47,49,51)

In the first method [49] (Figure 14a), the metal passes down the sprue into a centrifugal metal receiver where it picks up the powder trickling down a separate channel; the suspension then flows to the ingate to fill the mould and the feeder.

In the second method[49] (Figure 14b), as the melt flows down the sprue to the ingate and the mould, it entrains the metal powder trickling down a graphite, chamotte or quartz tube placed within the sprue.

In both cases, up to 10 percent by mass of metal powder can be introduced into the molten metal.

Method 3 [49] [50] shows the most convenient of the known methods of introducing microchills during the production of castings. The most important feature of the gating system is that it imparts both forward and spinning motion to the stream of molten metal in the vortex cup and sprue. The spin throws the molten metal towards the walls of the cup and forms an axial cavity into which the metal powder is fed.

Method 4 [51] as shown in Figure 14d is a variant of Method 1.

An automatic device [52] for introducing the microchills into the metal stream (Figure 15) consists of a powder hopper mounted on a stoppered laddle and a dispensing slider which is connected to the stopper rod by an elastic link. When the stopper is raised for pouring, the slider opens and allows powder to enter the metal stream via a graphite sleeved powder guide. The elastic link compensates for any excess movement of the stopper rod. At the end of pouring, the stopper rod is lowered and a return spring pulls the slider back over the aperture in the hopper. It is possible with this device to introduce up to 6 or 7 percent by mass of micro-chills without extending the pouring time.

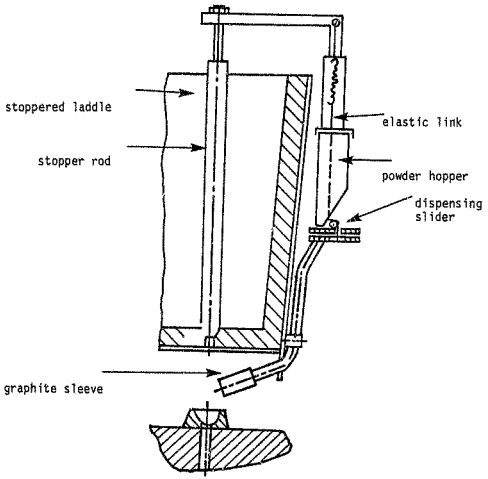

FIGURE 15 - Apparatus for Automatic Suspension Casting (Panferov[52])

Introduction of microchilling particles prior to pouring is accomplished by use of the 'full-mould' casting technique [48 53] viz. the powders are mixed with foamed polystyrene wetted with a binder and compacted in a die to form a pattern with powder particles distributed uniformly throughout its volume. When the molten metal contacts the pattern, the foamed polystyrene is gasified and the powder particles remain as solid nuclei scattered in large numbers throughout the casting.

2.4.3 Effect on Structure and Properties

Suspension casting has attracted much attention in the USSR especially in connection with sand castings and steel ingots. The microstructure of an ingot to which microchills have been added has been shown to exhibit a decrease in grain size of 1,5 times, a reduction in the zone of columnar grains by an average of 15-20 percent and a broadening of the zone of equiaxed grains in comparison to a standard ingot.[54]

Research already carried out shows that the microstructural improvements as a result of suspension casting resulted in improvements in tensile strength, transverse rupture strength and impact strength of certain cast steels.

Suspension pouring has been adopted in several USSR shipyards for the production of carbon and low-alloy steel castings with a mass of 100 - 10 000 kg.[47] Panferov et al [52] describe an automatic suspension pouring technique introduced at the "Petrov" Works in Volgograd (USSR).

Thinwalled and complex shaped castings can be made with much lower scrap rates (2 - 2,5 times less hot tearing and 3-5 times less chipping costs). Various massive castings with wall thicknesses exceeding 300mm have been made with reduced porosity under the feeders and greater homogeneity.[47] The mass of the feeder heads can also be reduced because the directionality of solidification is improved by the addition of metallic particles.[46]

Furthermore, suspension casting increases the rate of solidification [50 53 55 56] and hence decreases the time at high temperatures during which rapid diffusion occurs, thereby improving the distribution of impurities throughout the casting. Comparative investigations [55] into the solidification kinetics, structure and properties of carbon steel were made on 8

ton ingots produced by the conventional process and with the addition of 1 to 5 percent iron powder. Temperature measurements in forging ingots undergoing solidification showed that the iron particles substantially accelerate melt solidification, particularly in the vertical direction as can be seen in Figure 16.

The distribution of segregational heterogeneity in experimental and reference ingots studied with the aid of sulphur prints of longitudinal coupons obtained from the 8 ton ingots is shown in Figure 17.

The results of these [illegible]ns[55] show that the addition of iron powder during po[illegible] steel substantially reduces the size of the central and non central segregation zones, eliminates shrinkage porosity, slightly decreases the size of shrinkage pipe and promotes a more favourable distribution of segregating elements over the ingot cross-section.

Ryzhikov and Mikryukov[49] conducted experiments on steel 35L with additions of 0,1mm iron powder particles. They found that with 2 percent added powder, the density increased and the shrinkage defect volumes decreased when compared to steel cast without powder. They also found that the hot tearing tendency of steel 35L was reduced significantly by the addition of powder.

The effect of microchills on the structure and properties of G13L (GOST standard 2176-57 for austenitic steel castings) was investigated[49] by comparing an ingot cast without microchills and an ingot cast with a 2 percent addition of ferromanganese powder. The powder was introduced by method 1 (Figure 14a) at a pouring temperature of 1480 °C. The castings made with powder exhibited a transverse rupture strength of 10 kg. mm^{-2} with 4,5mm deflection compared to 4,6 kg. mm^{-2} and 1,5mm respectively in the absence of powder. The ferromanganese powder was found to produce a much finer grain structure and to suppress the extent of the columnar zone.

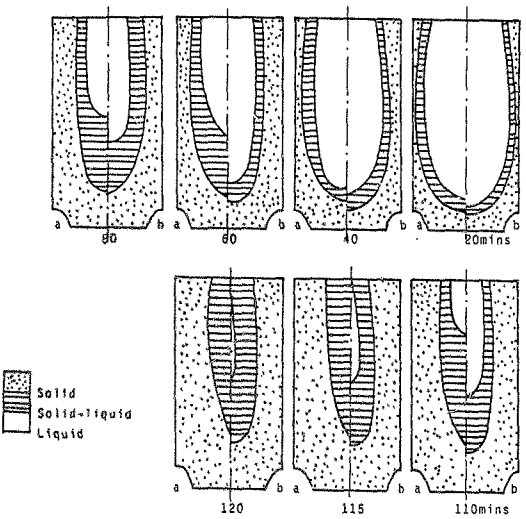

FIGURE 16 - Solidification Kinetics of Microchilled (a) and Conventionally Cast (b) Ingots (Zatulovskii[55])

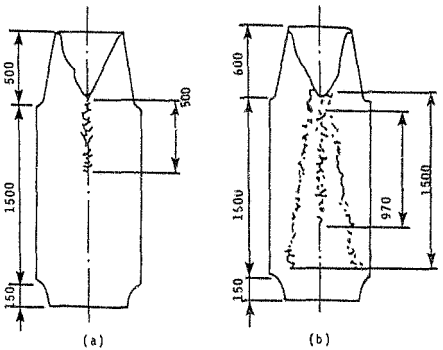

FIGURE 17 - Diagrammatic Representation of Macrostructural Heterogeneity of Microchilled (a) and Conventionally Cast (b) Ingots (Zatulovskii[38])

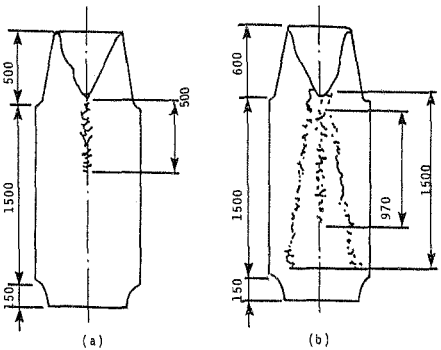

FIGURE 17 - Diagrammatic Representation of Macrostructural Heterogeneity of Microchilled (a) and Conventionally Cast (b) Ingots (Zatulovskii[55])

Chemical analyses on samples from different parts of the casting cross-section confirmed that the ferromanganese powder was uniformly distributed and the C and Mn contents remained within specification.

Using method 2 (Figure 14b), the internal microchill technique was developed further by Ryzhikov and Mikryukov[49] as a means of late alloying with powders introduced directly into the gating system as the mould was poured. A 0,4 percent C steel dieblock was cast in which 1 percent by mass of 0,1mm Mo powder was introduced as a powder in the metal stream, while another dieblock was cast with the Mo in the charge. The conventional casting was found to have a pronounced columnar dendritic structure, whereas late alloying with Mo powder produced a finer equiaxed dendritic structure. The Mo powder hence clearly influenced the crystallisation behaviour as well as the primary structure. The mean results of the mechanical tests are recorded in Table I.[49]

TABLE I - Results of Mechanical Tests on Conventional and Microchilled Steel Castings

Castings	Proof Stress (MPa)	Tensile Strength (MPa)	Elongation (Percent)	Impact Value (J)
Conventional	333	657	7	7,8
With Mo Powder added	588	785	21	23,5

Using the full-mould casting technique, Ivanov et al [53] investigated the influence of microchill additions on the mechanical properties, solidification time, macrostructure and density of steel 30L in the form of 210mm square slabs of thickness 40, 25, 15 and 8mm. Solidification time determinations

were made on slabs with 1-4 percent of iron powder in the pattern and compared with that for a conventional foamed polystyrene pattern. The relationships between the solidification time and microchill content were found to be nearly linear. The microchills were found to be more effective with the thicker castings - the solidification time being shortened by about 33 percent with 3 percent of iron powder, while at 4 percent iron powder solidification time was halved. Mechanical testing showed that impact values for slabs 25 and 40mm thick increased with microchill additions up to 2-2,5 percent followed by a decrease. The effects on tensile strength were the same for all thicknesses, with major improvements in material containing up to 2,5 percent of iron powder and little further response for material containing up to 5 percent; higher proof stress values were obtained with up to 3 percent microchill additions followed by a decrease in proof stress with further additions of powder. Thus the introduction of 2-3 percent of microchills gave the optimum combination of toughness, strength and ductility. The microstructure was effectively grain refined with the addition of 1 percent of iron powder and continued to improve up to 2-3 percent with no visible signs of porosity. The specimens containing 5 percent addition of iron powder had a fine but porous structure; the few specimens successfully made with 7 percent of iron powder by pouring at higher temperatures were affected by blowholes and skrinkage defects.

The extraction speed of continuous cast strands has been shown [55] to increase by 30 to 50 percent compared to conventional casting techniques.

The effect of microchill additions described above are purely thermophysical. Suspension treatments can be made still more effective by superimposing physico-chemical reactions between the microchill and the original melt. Ryzhikov et al [47] have shown that nucleating particles can be generated in the melt, in the form of stable complexes containing nitrides, carbides and refractory oxides.

Complex microchills may contain two or more components which can be classified as either active or stabilising. Active components may have a variety of functions, including notably the formation of stable nuclei, alloying the original metal (with V, Ti, Mo, Mn, Cr, Ni) and deoxidation in the mould (Mg, Al, Ti, V, Mn). Some components may have two or more functions. Stabilising components have a composition similar to that of the original melt and simply lower the overall surplus heat content of the metal, thereby refining the final structure and stabilising the effects produced by the active components.

Ryzhikov et al[42] were able to modify the microstructure of a 0,25 - 0,35 percent C steel with the addition of Fe powder as a stabilising agent and common ferro-alloys as active components. It was found that additions of less than 1,5 percent iron powder had no significant effect on the microstructure of the steel which consisted of pearlite and ferrite. Mixtures of iron powder and ferrochromium increased the ferrite content. Mixtures of iron powder and ferromolybdenum altered the pearlite content and distribution while mixtures of ferromanganese and ferromolybdenum localised the pearlite and ferrite distributions in the microstructure. The most pronounced structural effects were produced by mixtures of iron powder and ferrovanadium; the vanadium hardened the ferrite from HV 115 to 160 and also suppressed austenite grain growth, thereby producing a much finer ferrite-cementite eutectoid.

The above work has mainly been carried out in the USSR. Recently, Sentarli et al [46 47] have successfully used the suspension casting process to produce sand castings in high chromium white cast iron with a microstructure consisting of refined and equiaxed dendrites. They found the mechanical properties of the microchilled material, as determined by compression tests, to be isotropic in keeping with the random orientation of microconstituents in the material.

Hence, to summarise : The practical evidence on suspension pouring demonstrates that it has a wide scope and unique potential for effectively regulating the solidification behaviour of the steel directly inside the mould. It is particularly promising for the production of alloy steel castings in special purpose steels.

2.5 Composition of Some Austenitic Stainless Steels

As most stainless steels which give problems during hot working have austenite as their major phase, it is pertinent to review the austenitic stainless steels as a general class with respect to their development, composition and usage. A more complete discussion of different types of stainless steels has been given by Pickering[58] and Peckner and Bernstein.[59] The corrosion resistance of stainless steels in various environments is covered in reviews such as that by Sedriks.[60]

Typical analyses [61] of some austenitic stainless steels are given in Table II. The common AISI 304 steel is still the most used stainless steel but for applications in more aggressive environments a number of other steels have been developed. In AISI 316, an addition of 2 percent Mo is made to improve resistance to pitting and general corrosion (see Figure 18). Molybdenum is a strong ferrite stabiliser and hence, in order to keep the steel austenitic, the effect has to be compensated for by an increased Ni equivalent.[61]

In some even more aggressive environments, e.g. in the chemical industry, additions of 3 to 4 percent Mo might be necessary for good performance, and AISI 317 has been developed for such purposes following the same trend as AISI 316.[61]

In AISI 304, 316 and 317 steels subjected to welding, there is a risk of carbide precipitation along grain boundaries in the heat-affected zone (HAZ) causing intergranular corrosion in certain environments. Therefore the low-carbon variants 304L, 316L, and 317L are normally used in applications requiring welding. In steels AISI 321 and 347, the carbon is tied up by adding Ti and Nb-Ta, respectively, and these constitute alternative alloys especially suitable for service at elevated temperatures.[61]

2.5 Composition of Some Austenitic Stainless Steels

As most stainless steels which give problems during hot working have austenite as their major phase, it is pertinent to review the austenitic stainless steels as a general class with respect to their development, composition and usage. A more complete discussion of different types of stainless steels has been given by Pickering[58] and Peckner and Bernstein.[59] The corrosion resistance of stainless steels in various environments is covered in reviews such as that by Sedriks.[60]

Typical analyses [61] of some austenitic stainless steels are given in Table II. The common AISI 304 steel is still the most used stainless steel but for applications in more aggressive environments a number of other steels have been developed. In AISI 316, an addition of 2 percent Mo is made to improve resistance to pitting and general corrosion (see Figure 18). Molybdenum is a strong ferrite stabiliser and hence, in order to keep the steel austenitic, the effect has to be compensated for by an increased Ni equivalent.[61]

In some even more aggressive environments, e.g. in the chemical industry, additions of 3 to 4 percent Mo might be necessary for good performance, and AISI 317 has been developed for such purposes following the same trend as AISI 316.[61]

In AISI 304, 316 and 317 steels subjected to welding, there is a risk of carbide precipitation along grain boundaries in the heat-affected zone (HAZ) causing intergranular corrosion in certain environments. Therefore the low-carbon variants 304L, 316L, and 317L are normally used in applications requiring welding. In steels AISI 321 and 347, the carbon is tied up by adding Ti and Nb-Ta, respectively, and these constitute alternative alloys especially suitable for service at elevated temperatures.[61]

TABLE II - Typical Compositions of Some Austenitic Stainless Steels, Mass - %

AISI Steel	C max.	Si max.	Mn max.	Cr	Mo	Ni	Others
304	0,08	1	2	18-20	...	8-10,5	...
304L	0,03	1	2	18-20	...	8-12	...
304N	0,08	1	2	18-20	...	8-10,5	0,1-0,16%N
310	0,25	1,5	2	24-26	...	19-22	...
316	0,08	1	2	16-18	2-3	10-14	...
316L	0,03	1	2	16-18	2-3	10-14	...
316N	0,08	1	2	16-18	2-3	10-14	0,1-0,16%N
317	0,08	1	2	18-20	3-4	11-15	...
317L	0,03	1	2	18-20	3-4	11-15	...
321	0,08	1	2	17-19	...	9-12	(5x%C)%Ti
347	0,08	1	2	17-19	...	9-13	(10x%C)%(Nb+Ta)

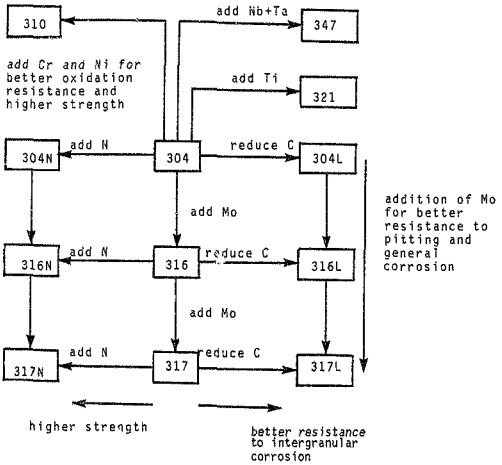

FIGURE 18 - Some compositional Modifications of 18Cr-8Ni austenitic stainless steels to improve certain properties, notations refer to AISI code system (Ahlblom[61])

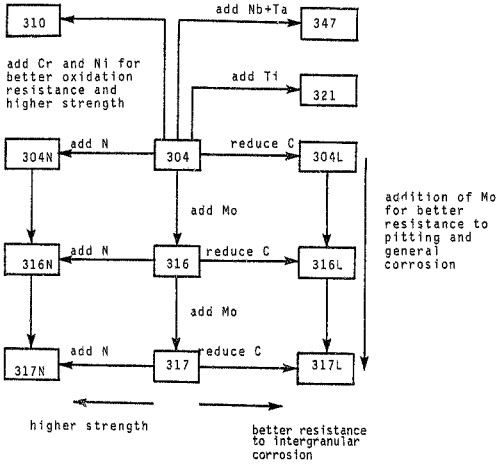

FIGURE 18 - Some compositional Modifications of 18Cr-8Ni austenitic stainless steels to improve certain properties, notations refer to AISI code system (Ahlblom[61])

Steels AISI 304N and 316N represent another category of austenitic stainless steels that meet the requirements for higher strength by means of alloying with N. The strong effect of N in stabilising the austenite is also used in some applications where the presence of very small amounts of δ-ferrite might be detrimental.[61]

Additions of Cr and Ni are also used to increase strength, especially at high temperatures as in AISI 310. This steel also shows better oxidation resistance than the steels mentioned so far. Steel AISI 310 as well as the N containing variants, all solidify more or less completely to austenite, which contributes to problems during hot working.[61]

2.6 Hot Workability

Hot workability refers to the ability of a material to deform at elevated temperatures and under specific conditions without cracking. It has been defined [61-63] by the relationship :

$$\text{Hot Workability} = f_1 \text{ (material)} \times f_2 \text{ (process)}$$

where f_1 is a function of the basic ductility of the material and f_2 is a function of the stress and strain systems imposed by the deformation process.

The predominant material parameters influencing hot workability are :

1. The composition and microstructure of the material
2. Recovery and recrystallisation characteristics
3. Second phase particles, and
4. Grain size

The factor f_2 is dependent on the following :

1. Test temperature

2. Strain rate

3. Environmental factors, and

4. Choice of hot working process, machine and design of work.

2.6.1 Material Variables Affecting Hot Workability (F1)

2.6.1.1 Composition and Structure

The effect of an element on the properties of an alloy depends on its concentration, its atomic radius, the other elements present in the alloy and generally its position in the periodic table of elements. In general, the hot ductility of an alloy will decrease as the extent of alloying is increased.[64]

The influence of composition on the micro-structure of stainless steel[65] may be determined from the Schaeffler diagram modified by Schneider (Figure 19). This figure shows the structures that form upon rapid cooling from 1050 °C to room temperature. The nickel and chromium equivalent values are given by the equations:

$$\%\ Ni\ equivalent = \%Ni + \%\ Co + 30\ (\%C) + 25\ (\%N) + 0{,}5\ (\%Mn) + 0{,}3\ (\%Cu)$$

$$\%\ Cr\ equivalent = \%\ Cr + 2\ (\%Si) + 1{,}5\ (\%Mo) + 5\ (\%V) + 5{,}5\ (\%Al) + 1{,}75\ (\%Cb) + 1{,}5\ (\%Ti) + 0{,}75\ (\%W)$$

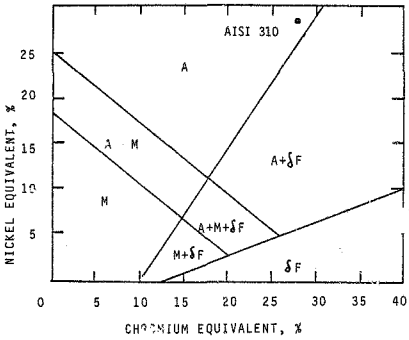

FIGURE 19 - Schaeffler Diagram with Modifications by Schneider (Pickering[58])

The ASTM 167-75 specification for stainless steel type AISI 310 is as follows :

C max.	Mn max.	P max.	S max.	Si max.	Cr	Ni
0,25	2,00	0,045	0,030	1,5	24,00-26,00	19,00-22,00

Hence, the % Ni equivalent and % Cr equivalent are 28,5 and 28,0 respectively. Using the Schaeffler diagram a fully austenitic structure is predicted for type 310 at room temperature.

Furthermore, from solidus and liquidus data[66] (Figure 20a and 20b), isothermal sections of the Fe-Ni-Cr diagram can be readily constructed[66] (Figure 21 a-d) showing that while steel type 310 solidifies as austenite, the other 300 series stainless steels such as type 304 can be fully feritic below the solidus. On the basis of this, it has been stated[67] that the hot workability of type 310 should resemble that of the higher nickel alloys rather than that of the steels in the 300 series.

The isothermal sections also show that microsegregation of chromium in type 310 can lead to interdendritic δ-ferrite.[67]

Compositional control to ensure the presence of some δ-ferrite is thought to improve ingot workability by increasing the recrystallisation rate of the ingot.[67] This rate is increased with the presence of δ-ferrite because the δ-γ interface acts as a recrystallisation site. Ferrite also retards grain boundary migration following solidification leading to a corrugated γ-γ grain boundary structure which is resistant to crack propagation.[67]

Aluminium and titanium may be added to steel type 310. Aluminium reduces the oxygen level and promotes formation of ferrite.[67] It also protects titanium from oxidation. Amounts of aluminium in excess of normal deoxidising additions do not cause hot shortness due to the high solid solubility of this element in austenite. The effect of aluminium on ductility is strongly influenced by the amount of nitrogen.[65] In maraging steels, for example, if the nitrogen content is 0,012 percent to 0,018 percent the ductility increases with the addition of aluminium. If the nitrogen content is between 0,008 percent and 0,010 percent addition of aluminium causes a mild decrease in ductility.[65]

Titanium stabilises ferrite, forms a large number of finely dispersed titanium nitride particles which can act as recrystallisation sites, and removes nitrogen from solid

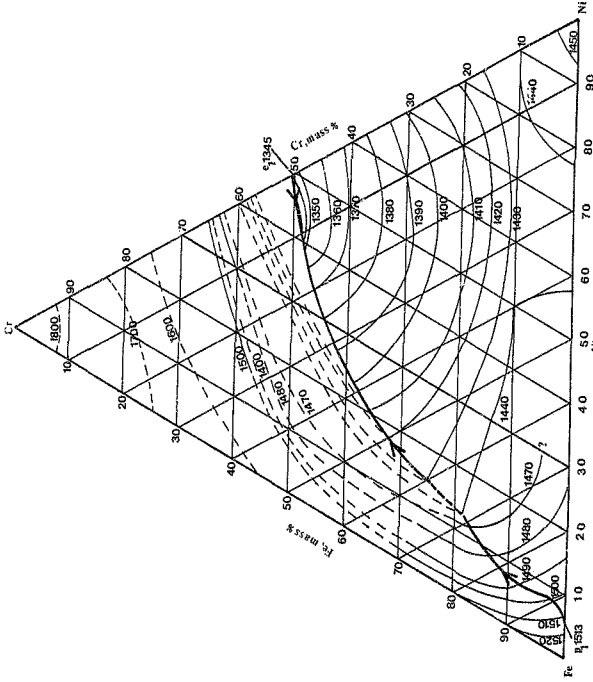

FIGURE 20(a) - Liquidus Projection of Cr-Fe-Ni System (Rivlin[66])

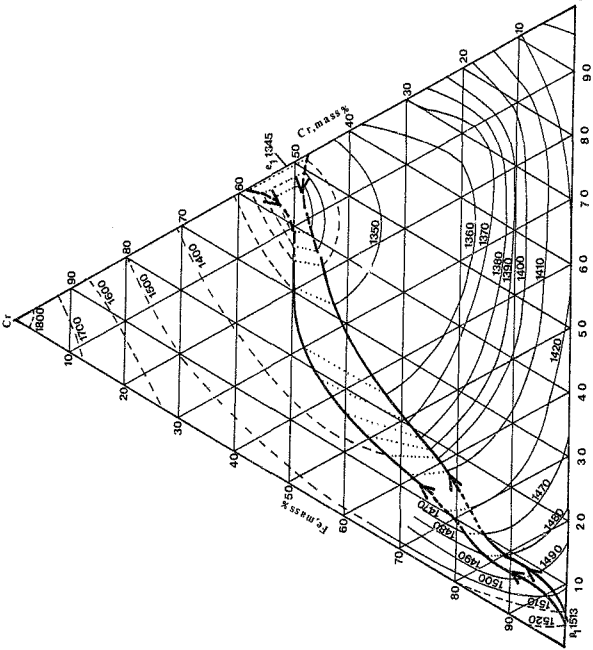

FIGURE 20(b) - Solidus Projection of Cr-Fe-Ni System (Rivlin[66])

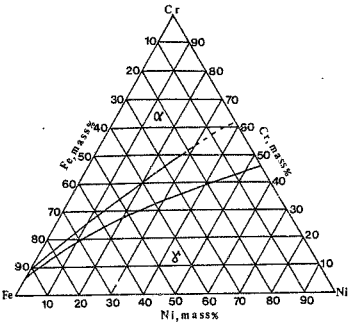

FIGURE 21(a) - 1300 °C Isotherm of Cr-Fe-Ni System (Rivlin[66])

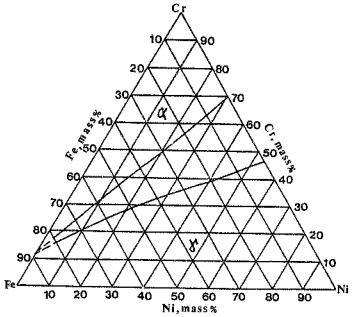

FIGURE 21(b) - 1200 °C Isotherm of Cr-Fe-Ni System (Rivlin[66])

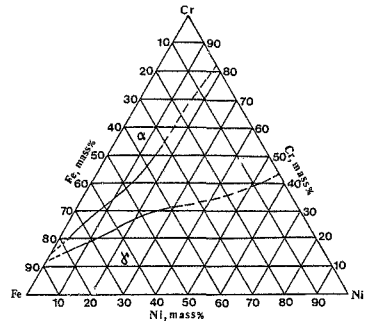

FIGURE 21(c) - 1100 °C Isotherm of Cr-Fe-Ni System (Rivlin[66])

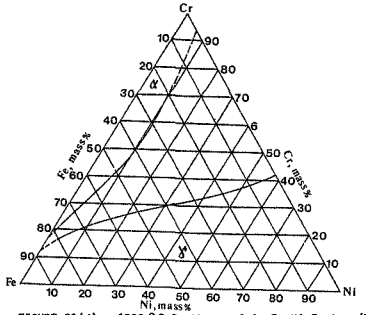

FIGURE 21(d) - 1000 °C Isotherm of Cr-Fe-Ni System (Rivlin[66])

solution.[67 69] In other steels of the 300 series titanium additions lower hot ductility since the presence of δ-ferrite is detrimental.[68 70]

Regarding the effect of nitrogen in steel type 310, it has been established that increasing nitrogen content increases the frequency of intergranular cracks. Manganese additions can improve hot ductility.[67] The amount of manganese required to ensure good workability at any nitrogen level is depicted in Figure 22. This also shows that the size of ingot influences the manganese requirement - probably as a result of chromium segregation.

The amounts of manganese required however, at nitrogen contents above about 0,08% are large - above the 2% specification limit. The control of N content by raw material selection [illegible] as the use of low nitrogen ferrochromium and highest man[illegible]ganese levels permissible by specification should yield practic[illegible] in workability. Nitrogen is, however, a strong austenite stabiliser and hence is used where the presence of even small amounts of δ-ferrite are detrimental.[61 69 71]

While rare earths have been reported[72] to improve the workability of type 310, Kane[67] found that these had no effect on the hot workability or the structure.

Finally, chromium and nickel increase strength at high temperatures and give very good oxidation resistance to steel. No clear effect of the Cr/Ni ratio on the hot workability of type 310 stainless steel could be found in the literature.

2.6.1.2 Restoration Characteristics

The restoration phenomena of recovery and recrystallisation take place in worked materials at suitable temperatures. During the recovery stage, the physical and mechanical properties that

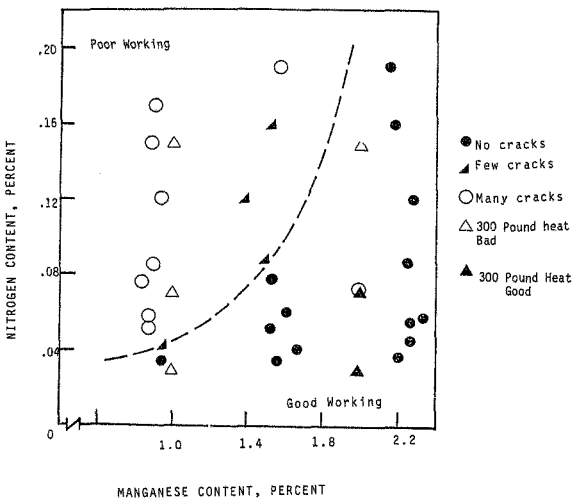

FIGURE 22 - Relationship of Mn and N for Good Hot Workability of AISI type 310 Stainless Steel (Kane[67])

underwent changes as a result of deformation tend to recover their original values.[73] In austenitic steels after high amounts of deformation, recrystallisation results in the formation of smaller, strain-free, equiaxed crystals which are independent of the old shattered grains.[74] Lower amounts of deformation result in a substructure within the distorted original grains.[74] Ferritic steels, however, are known to develop subgrains when the materials are cooled rapidly after either small or large amounts of deformation.[74]

Recrystallisation can be determined microscopically and during deformation it is evidenced by a decrease in the yield stress and an increase in ductility.[65] Other effects of recrystallisation are the decrease in hardness and dislocation density. Recrystallisation is strongly influenced by temperature, the time at temperature, the amount of deformation, the initial grain size, the composition and the strain rate.[65]

It has been suggested[75] that the onset of recrystallisation may be related to a critical structure, S_c, which in turn is uniquely related to stress, strain rate and temperature. The critical structure is defined by the relationship :

$$S_c = \frac{\dot{\varepsilon} \exp (Q/RT_D)}{T_D \sinh (\alpha \sigma_R)} \qquad \ldots . (8)$$

where σ_R is the stress at onset of recrystallisation,
$\dot{\varepsilon}$ is the strain rate,
T_D is the deformation temperature,
Q is the activation energy for recrystallisation,
R is the gas constant and
α is a constant

If $Z = S_c \sinh (\alpha\sigma_R)$, a plot of log Z vs. $\log\{\sinh(\alpha\sigma_R)\}$ should have a slope of unity.

underwent changes as a result of deformation tend to recover their original values.[73] In austenitic steels after high amounts of deformation, recrystallisation results in the formation of smaller, strain-free, equiaxed crystals which are independent of the old shattered grains.[74] Lower amounts of deformation result in a substructure within the distorted original grains.[74] Ferritic steels, however, are known to develop subgrains when the materials are cooled rapidly after either small or large amounts of deformation.[74]

Recrystallisation can be determined microscopically and during deformation it is evidenced by a decrease in the yield stress and an increase in ductility.[65] Other effects of recrystallisation are the decrease in hardness and dislocation density. Recrystallisation is strongly influenced by temperature, the time at temperature, the amount of deformation, the initial grain size, the composition and the strain rate.[65]

It has been suggested[75] that the onset of recrystallisation may be related to a critical structure, S_c, which in turn is uniquely related to stress, strain rate and temperature. The critical structure is defined by the relationship :

$$S_c = \frac{\dot{\varepsilon} \exp (Q/RT_D)}{T_D \sinh (\alpha \sigma_R)} \qquad \ldots\ (8)$$

where σ_R is the stress at onset of recrystallisation,
$\dot{\varepsilon}$ is the strain rate,
T_D is the deformation temperature,
Q is the activation energy for recrystallisation,
R is the gas constant and
α is a constant

If $Z = S_c \sinh (\alpha\sigma_R)$, a plot of log Z vs. $\log\{\sinh(\alpha\sigma_R)\}$ should have a slope of unity.

At very high strain rates, [75] [76] there is insufficient time for recrystallisation whereas at low strain rates, sufficient driving force is needed to start recrystallisation. The greater the degree of working, the lower the recrystallisation temperature, and the smaller the resultant grain size. A minimum amount of deformation is necessary to cause recrystallisation.[77] [78] As the temperature of annealing is lowered, the time necessary to produce a given amount of recrystallisation increases and near the minimum recrystallisation temperature time increases greatly.[77] [78] Soluble impurities raise the recrystallisation temperature.[64] [77] [78]

Since hot working is generally performed in several steps, the restoration processes can be divided into two main groups[61] [74] : those that occur during deformation and those that take place during pause times at the working temperature. These are referred to as dynamic and static processes respectively. In both cases, both recovery and recrystallisation can be operating. Recovery occurs rapidly during deformation but, when straining is interrupted, the rate of recovery decreases rapidly to a negligible value. The two types are usually called dynamic and static recovery respectively.

If the material has been deformed to a critical strain[61], $\varepsilon >$ 0,05-0,1, and is kept at the working temperature, the material starts to recrystallise statically. In some materials, the dynamic recovery is not fast enough and, after straining to a critical value, the material can start to recrystallise dynamically.

Since recrystallisation comprises a nucleation phase and a growth phase, dynamic recrystallisation can proceed after the deformation by a static growth process. This phenomenon is usually called metadynamic recrystallisation.[61] The critical strain for dynamic recrystallisation is, however, so large that it is only of interest in a few forming processes such as extrusion and piercing.

Recrystallisation, or partially recrystallised structures in cast slabs of AISI 3[illegible] stainless steel have been found to exhibit the following characteristics[67] :

1. The fraction recrystallised increased with depth in the sample after rolling. This can be expected from the variable temperature profile which arises during rolling.

2. Recrystallisation was always associated with an interface. In order of decreasing frequency, these were γ-γ grain boundaries, γ-δ interfaces in steels containing ferrite, γ-carbide boundaries for high carbon steels or γ-TiN interfaces where titanium had been added, γ-γ twin boundaries and lastly, at silicate - chromite inclusions.

3. Recrystallisation began by the formation of a continuous necklace of new grains[67 79 80] at the prior ingot grain boundaries (or at δ-ferrite or TiN inclusions).

4. Recrystallisation occurred to a greater extent in the equiaxed zones of all the samples examined, rather than in the columnar zones, and this appeared to be due to the greater grain boundary area per unit volume in the former locations. It would appear therefore that a greater proportion of equiaxed material in ingots or continuous cast slabs may be expected to enhance hot workability.

5. Steels containing δ-ferrite recrystallised to a larger degree in all cases. The alloys containing ferrite along with aluminium and titanium showed the highest recrystallisation due to TiN and ferrite acting as sites for new grain nucleation.

6. Recrystallisation inhibited crack propagation. No cracking was observed in recrystallised zones except those which had formed on the as-cast boundaries or at δ-γ interfaces. In partially recrystallised areas cracks were stopped by new grains.

7. Grain sizes in recrystallised regions were much smaller in the alloys containing titanium (due to the effect of TiN on boundary migration) or carbon (due to the high carbide density).

8. New grain formation apparently occurred by a bulge "nucleation" mechanism at γ-γ boundaries. This process could only be observed in alloys where boundary migration rates were retarded by second phases. Details of recrystallisation processes at γ-δ or γ-TiN interfaces, however, could not be determined.

These results bear out, at least partially, the premise that the greater the degree of recrystallisation, the better the workability of the ingot is likely to be.

2.6.1.3 **Influence of Second Phase Particles**

The effects of oxygen and sulphur on the properties of steel are normally counteracted by the additions of Al and Mn respectively to form oxide and sulphide inclusions. The effect of the inclusions on hot workability depends on their nature, distribution and size.[61 71 81-83]

Inclusions found in steels may be divided into five categories based on their deformation behaviour.[84]

1. Al_2O_3 and calcium aluminates - these are brittle solids, which are undeformable at all temperatures.

2. Spinel type oxides $AO-B_2O_3$ which are undeformable in the range room temperature to 1200 °C, but may be deformed above this tempe· ·re.

3. Silicates of calcium, manganese, iron and aluminium which are brittle at room temperature, but increasingly deformable at higher temperatures. The formability increases with decreasing melting point of the silicate, e.g. from aluminium silicate to iron and manganese silicates.

4. FeO, MnO and (FeMn)O - these are plastic at room temperature, but appear gradually to become less plastic above 400 °C.

5. Manganese sulphide MnS - this common inclusion type is deformable, becoming increasingly so as the temperature falls.

Although sulphides do not lead to problems in hot working, the same cannot be said of oxide and silicate type inclusions.[85] In an alloy of Fe-25Ni, the occurrence of hard undeformable oxides was found to reduce the hot ductility significantly.[86]

The distribution and shape of second phases and compounds have a strong influence on workability. Components existing at grain boundaries as distinct globules or isolated inclusions are less harmful than they are when they form continuous grain boundary films.[71 81 87] Sulphides exemplify this point. The most favourable location for second phases is within the grains as this is where they lower workability to the least extent.[87]

Kane,[67] investigating the workability of ingots of AISI 310 found that alloys containing carbides (which may also be considered as second phase particles) were suprisingly resistant to cracking. Carbides were of two types - eutectic carbides observed at grain boundaries and in intradendritic spaces due to C and Cr segregation to these regions during solidification, and secondary carbides found on annealing as a result of C diffusion out of prior ferrite regions. Where cracks did occur they were found to be usually short and of two types; cracks occurred at interfaces between carbide and γ, or through carbide particles leading to 'wedge cracking' on the adjacent boundary in the austenite. Cracks of the latter type were rare and were stopped by neighbouring particles on the boundary, usually only a few microns away.

Furthermore, it was found that recrystallisation in AISI 310 was always associated with interfaces such as those between austenite and carbide in the higher C version of the steel, γ and TiN in Ti-containing alloys and occasionally between silicate and chromite inclusions.

In general, good hot working properties were associated with alloys of high homogeneity containing a few fine, evenly distributed non-metallic inclusions.[88]

2.6.1.4 Grain Size

The grain size influences the workability of metals and alloys and its influence may differ from one material to another.[89]

Generally, a decrease in grain size and a decrease in the prior austenite grain size is believed to increase ductility.[61 89] The increase in ductility is due to the fact that fine grains promote rapid recrystallisation and reduce intercrystalline cracking.[61] Furthermore, a small grain size implies that the relative velocity of two adjacent grains will be low so they can slide more easily hence increasing ductility.[90] The orientation of the grains also has a strong effect on ductility.[90-92]

Bywater and Gladman[93] studied the influence of the grain size obtained after different soaking procedures in 25 Cr - 20 Ni steels and found that a decrease in grain size increased the ductility (Figure 23). Grünbaum[94] is reported by Ahlblom et al[61] as showing that for steel AISI 316, the reduction in area was reduced by 20 percent as the grain size was increased from 50 to 200 μm.

Gittins et al[85] working on 18 Cr - 8 Ni steel (Figure 24) showed that when the grain size is increased (broken curve), the ductility maximum at 1100 °C caused by dynamic recrystalisation is decreased. Also, at lower strain rates and a lower temperature (800 °C), when grain-boundary sliding governs the ductility, a large grain size (broken curve) gives a lower ductility. At very low strain rates and high temperatures, the effect seems to be reversed.

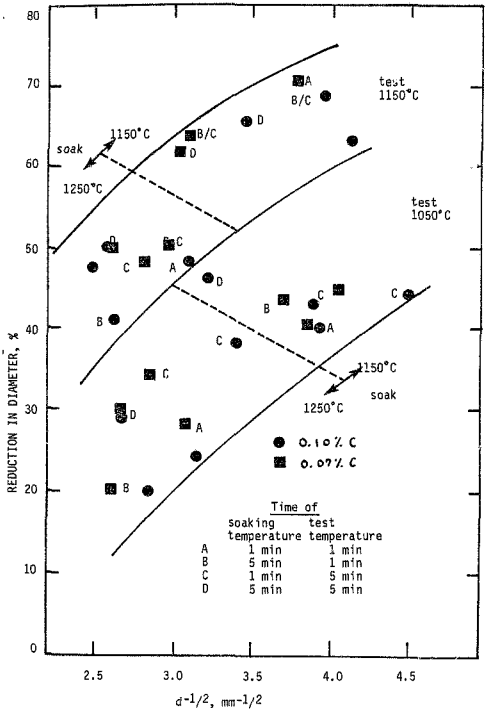

FIGURE 23 - Variation of Ductility of 25 Cr-20 Ni Steels with As-Soaked Grain Size, d (Bywater[93])

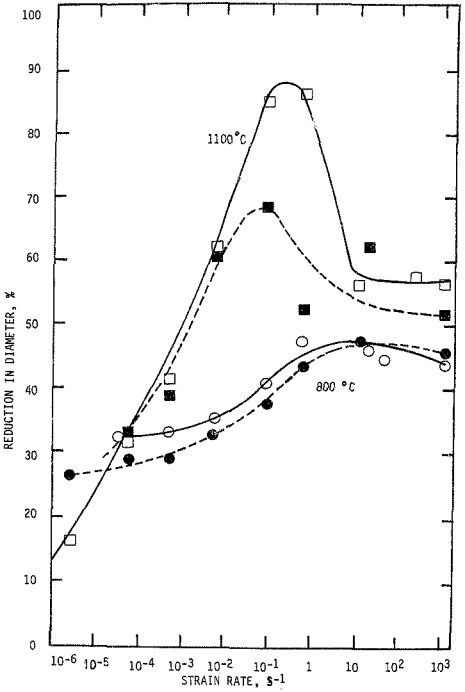

FIGURE 24 - Effect of strain rate on ductility of 18Cr-8Ni steel; full lines mean specimen heated directly to test temperature; dashed lines mean specimens annealed for 1h at 1150 °C before testing (i.e. larger grain size) (Gittins[85])

Surprisingly little has been published on the effect of grain size on the hot ductility of stainless steels. A possible reason for this might be that grain growth occurs at hot working temperatures. It is also difficult to distinguish between grain size effects and other phenomena. For example, Ahlblom et al[61] report Mase[96] as finding that although a high nickel content in 304 steel can improve the ductility owing to a reduction in the δ-ferrite content, at high temperatures (1250 °C - 1300 °C) the effect of Ni was reversed owing to grain growth.

There are also some investigations of materials worked to different reductions in area after casting and probably having different grain sizes.[96-98] These results are affected, however, by a decreasing amount of δ-ferrite which has a stronger effect than that of the changing grain size (Figure 25).

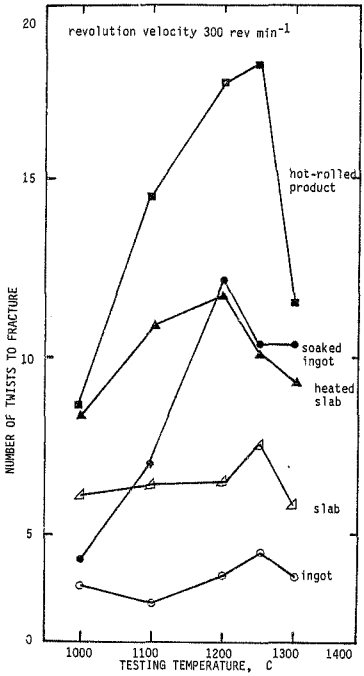

FIGURE 25 - Variation of the hot ductility of type 304 steel measured as number of twists to fracture in hot torsion (Mase[96])

2.6.2 Process Variables Affecting Hot Workability (F2)

The behaviour of a metallic material during deformation is influenced by the inherent ductility of the material and the process variables. Important process variables include temperature, stress system, strain rate and environmental conditions.

2.6.2.1 The Effect of Temperature in Metalworking

The forming properties of a material are determined by its strength and ductility, both of which are dependent on temperature.[65]

In general, strength decreases and ductility increases with increasing temperature. The effect of temperature and strain rate on the flow stress of various austenitic stainless steels is shown in Figure 26.[61]

The effect of temperature on ductility was investigated by Keown[69] using the hot tensile test and a constant strain rate of 6 s^{-1}. The hot ductility was measured as a percentage reduction of diameter (R of D). The results for stainless steel types 430, 304 and 316 are shown in Figure 27. It can be seen that ductility increases with increasing temperature until burning occurs.

Tegart[99] reports that the behaviour of strength and ductility with temperature can vary, depending on crystal structure and on structural changes produced by temperature e.g. precipitation effects or order-disorder transformations. For pure metals, the ductility is usually high over a wide range of temperatures but for impure metals and alloys, the temperature ranges for hot working can be restricted and knowledge of the variation of both strength and ductility with temperature is necessary in order to establish hot working conditions. Temperature limits[61] in hot

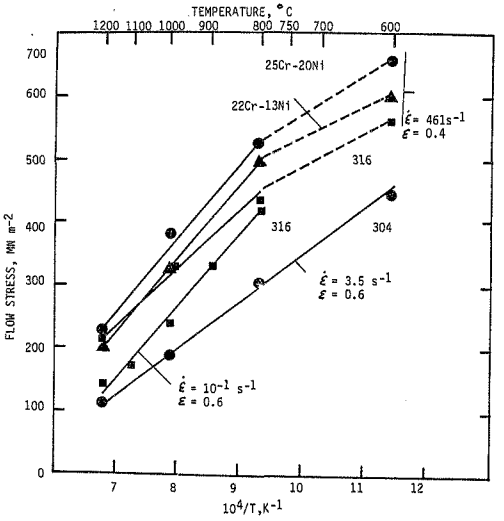

FIGURE 26 - Flow Stress v. Inverse Absolute Temperature for Various Austenitic Stainless Steels (Ahlblom[61])

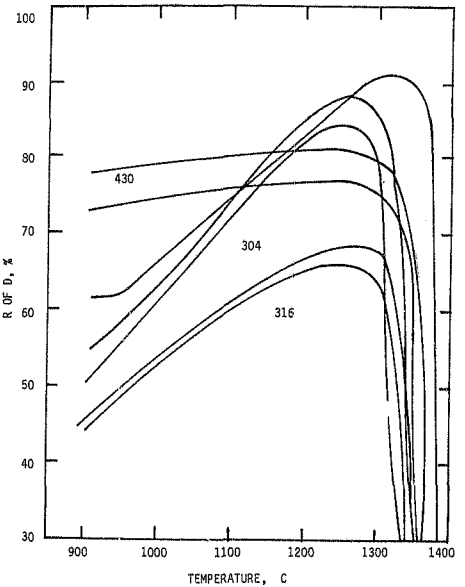

FIGURE 27 - The Hot Ductility of Types 430, 304 and 316 Stainless Steels (The Different Curves Correspond to Different Cast Numbers) (Keown[69]).

working are set by the lowest temperature at which recovery processes can take place for a given hot working process. The maximum temperature of working is set by the temperature at which burning occurs (see Figure 27) or at which oxidation is excessive.

In metal working processes, much of the mechanical work of deformation is converted into heat. Some of this heat is conducted away by the tools or lost to the atmosphere, but a portion remains to increase the temperature of the workpiece.[62] If the speed of processing is high, heat losses will be low and the temperature of the workpiece will increase accordingly. If the rate of processing is low, heat will be lost rapidly and the workpiece will cool. Cooling of the workpiece will increase the flow stress of the material making hot working more difficult.

2.6.2.2 Strain Rate

True strain rate $\dot{\varepsilon}$ is given by the relationship[65]

$$\dot{\varepsilon} = \frac{d\varepsilon}{dt} \qquad \ldots\ (9)$$

where ε is the strain and t is the time.

For the tensile test,[100]

$$\dot{\varepsilon} = \frac{d\ (\ln\ (\ell/\ell_0))}{dt} = \frac{v}{\ell} \qquad \ldots\ (10)$$

where ℓ is the instantaneous length
ℓ_0 is the initial length and
v is the instantaneous velocity

In the case of uniaxial compressive tests,[101] the strain rate may be expressed as :

$$\dot{\varepsilon} = \frac{d\ (\ln\ (H_o/H))}{dt} \qquad \ldots\ (11)$$

where H_o and H are the initial and the instantaneous heights of the specimen during the test.

Samanta,[101] working on tool steels, found that the above relationship (equation 11) gives reasonable results for compression tests at strain rates from 290 s^{-1} to 906 s^{-1} and at a temperature of 1000 °C.

In rolling,[102] the strain rate may be calculated for either slipping or sticking friction conditions by use of the relationships :

$$\dot{\varepsilon} = \frac{v}{H_o}\left(\frac{2\ (H_o - H_f)}{D}\right)^{1/2} \qquad \ldots\ (12)$$

- for slipping friction conditions

and

$$\dot{\varepsilon} = v\left(\frac{2}{D\ (H_o - H_f)}\right)^{1/2} \times \ln\ \frac{H_o}{H_f} \qquad \ldots\ (13)$$

- for sticking friction conditions

where v is the peripheral speed of the rolls
D is the roll diameter and
H_o and H_f are the initial and final thicknesses respectively

Ludwig[103] was the first to find that the flow stress σ of a material is related to the true strain rate by the formula

$$\sigma = \sigma_0 + \sigma_1 \ln \frac{\dot{\varepsilon}}{K} \qquad \ldots\ (14)$$

where σ_0, σ_1 and K are constants.

Later, the same relationship was used by many other investigators.[62 74 82 102 104]

The influence of strain rate[74] on the stress vs strain curves for an Fe-25% Cr alloy at 1100 °C as derived from torsion data is shown in Figure 28. As can be seen, increasing rates of strain for a fixed temperature result in an increase in strength.

Little work has been carried out on the influence of strain rate on the hot ductility of stainless steels. Hot torsion tests on an Fe-36 Ni alloy by White and Rossard[80] showed a straight line on a log-log plot of revolutions to rupture against rev. min^{-1}. For a 316 and a 25Cr-5Ni-1Mo steel Nikkilä,[105] using hot torsion, found that the hot ductility increased with increasing strain rate. Observations on type 316N[106] steels also show that a high strain rate improves the workability, in spite of the high loads applied.

An investigation by Gittins et al[85] of a 302 steel at 1100 °C by means of hot tensile tests shows a maximum reduction in area around a $\dot{\varepsilon} = 1\ s^{-1}$ (Figure 24). A decreasing strain rate implies an increasing amount of grain boundary sliding and more grain-boundary cracking. Around $\dot{\varepsilon} = 1\ s^{-1}$ the material undergoes dynamic recrystallisation before rupture, hence increasing the ductility. At higher strain rates dynamic recrystallisation is probably too slow to be of importance and hence, since the influence of grain boundary sliding is negligible, the reduction

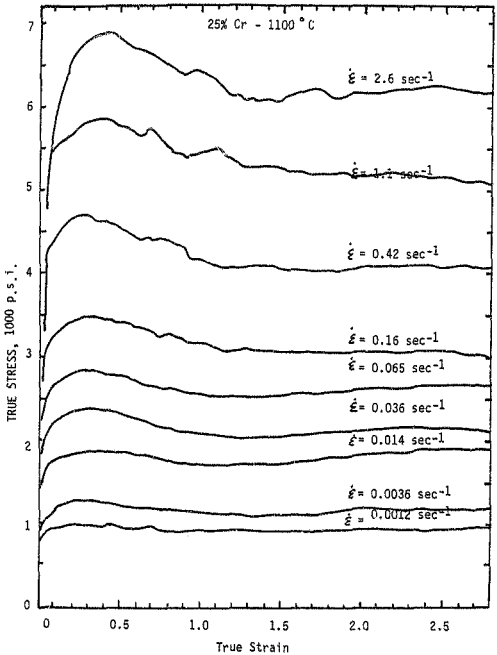

FIGURE 28 - Influence of Strain Rate on Stress v. Strain Curves Derived from Hot-Torsion Data at 1100 °C for an Fe-25% Cr Alloy (Jonas[74])

in area will be determined by cavitation at inclusions. It should also be noted in Figure 24 that at 800 °C no dynamic recrystallisation occurs and therefore the ductility peak is absent.

2.6.2.3 Environmental Conditions

Environment has a strong effect on ductility. Oxidation predominantly takes place on the surface of the specimen. Oxidation inside the specimen is strongly dependent on the porosity of the material. To protect the specimens from oxidation some researchers [107] [108] used vacuum and some others an argon[109] or a nitrogen atmosphere.

It has been shown that ductility is higher in vacuum compared with the ductility in air. Fontana and Green[110] showed that selective oxidation of chromium occurred in stainless steels at 982 °C when the alloys were exposed to low oxygen atmospheres. During oxidation, the elements with higher free energy are oxidised to a greater extent than the other elements.

2.7 Hot Workability Tests

Workability tests are usually aimed at the determination of deformation stresses and maximum amount of deformation possible. The major requirements of tests designed to simulate hot working operations may be summarised as follows :

1. The test method should allow the determination of the stress required for the deformation.

2. The temperature at which testing is undertaken should be known.

3. The strain rate should be determinable.

4. The amount of deformation that the material has withstood before fracture should be determinable.

5. The test method should allow rapid cooling of specimens so that high temperature structures can be examined at room temperature.

Simulative tests in the laboratory can give a very useful guide to correct metallurgical practise, in reheating, rolling, extrusion and other processes. Some of the tests are :

Scaled-Down Working Operations

Tensile Tests

Torsion Tests

Bend Tests and

Compression Tests

2.7.1 Scaled-Down Working Operations

Moore[111] has pointed out that the advantage of methods of this nature is that the mode of deformation in the test method and the practical working operation for which the data is required are the same.

For extrusions, scaled down extrusion experiments are the best method of determining extrusion pressures and optimum extrusion speeds, reductions and temperatures. In addition, variables such as die face angle and lubrication conditions can be studied with the same equipment.

However, in the case of rolling, a high speed multistand mill would be required to reproduce the high deformation rates and intermittent deformation cycles associated with modern

continuous hot rolling. This would be extremely expensive and therefore impractical. Lower rolling speeds and relatively longer intervals between successive deformations pertaining to the early stages of hot rolling (cogging and slabbing) can be simulated on laboratory scale single stand mills. Laboratory mills suffer from the limitation that large reductions cannot be imposed. It is therefore difficult to assess the sensitivity of a material to rolling conditions.[111]

Thus, scaled down practical working operations can give some useful data, such as recrystallisation characteristics for a given amount of deformation under given conditions of temperature and strain rate, but in general scaled-down working tests are not versatile for comprehensive studies of hot workability and therefore, the techniques of tensile, torsion, bending and compression testing, are utilised.

2.7.2 Tensile Tests

The ductility of a material may be evaluated from the uniform elongation, total elongation and reduction in area obtained in a tensile test. Reduction in area is the most structure sensitive ductility parameter.[112]

Although the simplicity of the tension test makes it useful as a means of evaluating workability, it is limited by necking, since the strain up to necking is less than that achieved in most deformation processes.[63]

The tension test is mainly used to determine the ductility of a material as a function of temperature.[81 100 101 113-115] With increasing temperature, the ductility (as measured by the reduction in area) increases to attain a maximum value at a specific temperature[100] (Figure 29). Beyond the characteristic temperature, ductility drops suddenly due to incipient

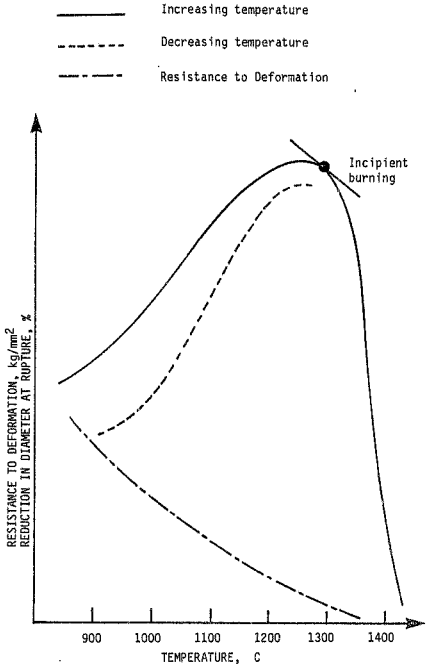

FIGURE 29 - Typical Hot Ductility Diagram from the Hot Tensile Test (Decroix[100])

fusion.[116 117] The strength decreases to zero at temperatures which cause the formation of enough liquid to wet the grain boundaries extensively. These temperatures are strongly influenced by the amount and distribution of second phases.

2.7.3 Torsion Tests

Torsion tests are normally carried out on cylindrical specimens either at room temperature or elevated temperature. The formability of the specimen which may be solid or tubular, is assessed from the number of revolutions sustained at failure. Tests can be carried out on modified lathe type machines in which the specimen is held fast at one end and twisted at the other.[79]

Deformation is by pure shear and larger strains are achieved without the limitations of plastic instability.[63] Large values of strain rate are also readily obtained since the strain rate is proportional to the rotational speed.[118]

The technique is limited by the fact that the strain rate in solid specimens varies linearly along the radius being maximum at the surface and zero at the axis.[65] This difficulty can be reduced by making use of tubular test pieces.[119] A second limitation of the torsion test is that the deformation is not an accurate simulation of actual processes.[119] Furthermore, difficulties may arise at high strain rates due to heat generation.[65] This problem, however, is not so pronounced with tubular specimens.

2.7.4 Bend Tests

These tests involve the three-point bending of rectangular specimens. The stress and strain states on the outer surface of the bend test specimen may be altered by adjusting the width-to-thickness ratio.[120] The strain rate in bend tests is difficult to assess as it varies significantly through the thickness of the specimen and is therefore influenced by specimen design.[65]

The bend test, in which necking problems do not arise, can be used as a method to assess formability. The determination of limiting tensile and compressive strains for the bend test is identical to that used for the compression test. The bend test can be used when the geometry of the material available is not convenient for the preparation of compression test specimens in the desired orientation, as shown in Figure 30.[115]

Bend tests have been used[121] to study the effect of anisotropy and the surface condition on forming limits in cold and hot forming, the orientation in specimens, the effect of atmosphere on surface cracking in steels and the degree of hot shortness[113] of carbon steels.

2.7.5 Compression Tests

The most basic hot ductility test consists of compressing a series of cylindrical (or square) specimens to various thicknesses, or to the same thickness with varying specimen length : diameter ratios.[122] The limit for compression without failure by radial or peripheral cracking is considered to be a measure of workability.

Historically this has been one of the tests most widely used by the forging industry. Longitudinal notches are sometimes machined into the specimens prior to compression because it is believed that the notches cause more severe stress concentrations, providing a more reliable index of the workability to be expected.[122] Because of the stress-concentration effect, fracture in the form of ruptures is most likely to occur in the notched areas and may be assumed to have been initiated by hot shortness, triple-point cracking and grain boundary cavitation.[123]

These ruptures may be classified[124 125] according to the rating system shown in Figure 31. A rating of 0 is applied if no

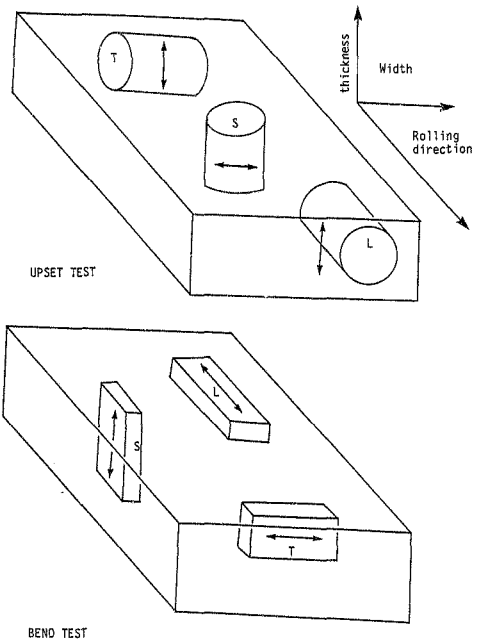

FIGURE 30 - Illustration of possible test specimen orientation and critical tensile stress direction of upset tests and bend tests for fracture surface anisotropy determination (Ertürk[115])

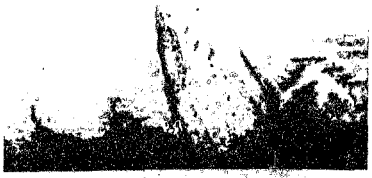

R=1

R=2

R=3

R=4

FIGURE 31 - Suggested rating system for notch-bar upset test specimens that exhibit progressively poorer forgeability. A rating of 0 would indicate freedom from ruptures in the notched area.[149]

ruptures are observed. If they are small, discontinuous and scattered, the rating is 1. Higher rating numbers indicate increasing incidence and depth of rupture.

During compressive deformation, the cross-sectional area of the specimen increases and the load requirements for further deformation also increase. This may present problems due to limitations in press capacity.

Another important factor in relation to compression tests, is the fact that for a constant cross-head speed the strain rate increases, as the height of the specimen decreases during deformation. This difficulty may be overcome by using machines of special design such as the cam plastometer.[111] [122] In a cam plastometer, the bottom platen compresses the specimen through cam action at a constant true strain rate to a strain limit of $\varepsilon = 0,7$. A cam plastometer is a rather rare device : there are probably no more than ten in the world.[122] It should be recognised, however, that although a constant strain rate is important in rigorous research studies, much useful workability data can be obtained by hot compression testing under conditions where the strain rate varies throughout deformation. The above holds as long as both the specimen height and the type of press are the same in order to obtain reproducible and comparable results.

Examples of the application of the notched-bar test are those reported by Sabroff et al[124] and by De Ridder and Koch.[126] Haberling et al [127] applied the rating system to unnotched cylindrical compression specimens to determine the effect of increased sulphur content on the hot workability of high speed steels. Sabroff et al [124] found that rolled rings of type 403 stainless steel with a notched-bar rating of 0 were sound whereas those with a rating of 4 ruptured extensively. In a similar vein, De Ridder and Koch[126] demonstrated the rupture sensitivity of Inconel 718 with the notched-bar upset test. The alloy was

shown to be much more notch-sensitive as the test temperature was increased.

It has been reported[123] that the notched-bar upset test is more sensitive than the simple upset test. In fact, a notched-bar rating of 3 has been shown to be perfectly sound after similar reductions in simple upsetting. Thus, the simple upset test may indicate a deceptively higher degree of workability than can be realised in an actual processing operation, and the notched-bar upset test may be particularly useful for identifying materials having marginal workability.

Compression tests may also be used to evaluate the limiting strains at fracture for bulk forming processes.[118] When, for the points of failure, tensile strain is plotted against compressive strain for varying height to diameter ratios and frictional conditions, a so-called "forming limit line" (FLL) with a positive intercept on the tensile axis and a slope of 0,5 is formed (Figure 32).[118] The intercept is known as the workability index and is a measure of the influence of the material variables on workability.[63] For further details on the utilisation of the forming limit line, the reader is referred to reference 63.

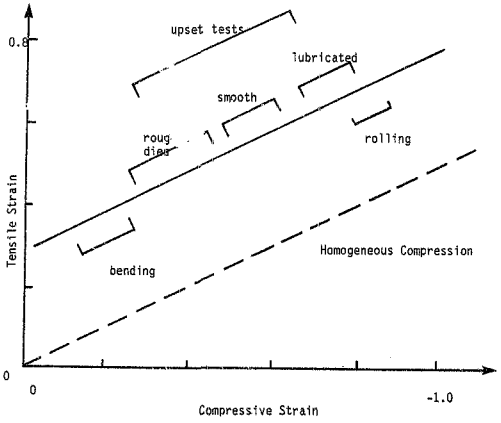

FIGURE 32 - Forming Limit Line Diagram (Kuhn[118])

3. EXPERIMENTAL PROCEDURES

3.1 Introduction

The experimental work refers to conventional and microchilled (suspension) ingot castings with similar chemical compositions. It covers the optimisation of a laboratory suspension casting procedure and the comparative examinations of microchilled and conventional ingots in the as cast condition and after mechanical deformation.

3.2 Alloy Preparation and Pouring

The following equipment was used : an air melting induction furnace fitted with a generator capable of delivering 50 kW at 3000 Hz, flake graphite cast iron moulds (with 8 kg capacity), a chrome oxide crucible with magnesite pouring spouts and a digital infrared pyrometer.

The crucible was charged with commercially supplied plate of AISI 310 stainless steel and preheated for 30 minutes. Melting was carried out without the use of a protective atmosphere hood at 30 kW for 30 minutes. The power was then boosted to 40 kW until the casting temperature was reached. The metal was held at temperature for about 6 minutes. After skimming the surface, the molten metal was poured within 21s into ingots (64mm square and 250mm long) and allowed to air cool.

The first ingot was cast from a temperature of 1600 °C in order to confirm that no significant change in chemical composition occurred during air melting. As can be seen from Table III, none did :

TABLE III - Chemical Analyses of the AISI 310 Stainless Steel in the As-Received and Remelted Conditions

Element	Mass Percent in the As-Received Condition	Mass Percent in the Remelted Condition
C	0,058	0,079
S	0,012	0,011
P	0,026	0,031
Mn	1,83	1,53
Si	0,65	0,53
Cr	24,44	24,04
Ni	19,40	19,29
N	0,037	0,050

The melting range of the metal was given as 1400 to 1455 °C[128] but in order to increase the extent of the columnar zone, a high degree of superheat was imparted to the melt. Hence, subsequent ingots were cast from 1750 °C. Problems were encountered with burn in of the mould (Figures 33 and 34) and dispersed porosity (Figure 35). Attempts to decrease the superheat and to preheat the mould by 200 °C aggravated the burn-in problem.

These problems were eventually eliminated, while maintaining a fully columnar structure, by the use of a zircon and silica flour alcohol based mould coat, more rapid melting and casting (20 minutes at 30 kW and immediate rapid pouring for 10 ± 5 s once the casting temperature of 1750 °C was reached), the use of an aluminium and iron oxide based exothermic powder poured on top of the ingot immediately after casting and a mould preheat of 60 to 80 °C.

FIGURE 33 - Burn in of the Ingot Mould Surface

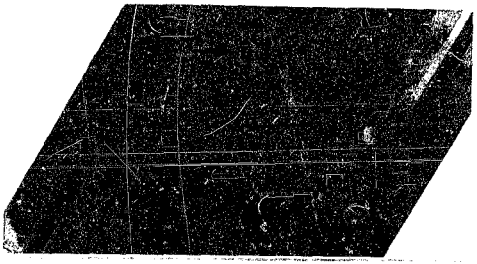

FIGURE 34 - Enlarged View of the Ingot Mould Burn-in

FIGURE 35 - Dispersed Ingot Porosity Obtained During Initial Ingot Casting Attempts

3.3 Powder Preparation and Characterisation

The iron powder used for the experiments was characterised with reference to its chemical composition, its particle size distribution, its microstructure, morphology and flow properties.

The carbon and oxygen contents of the powder were determined by infrared absorption of CO_2, nitrogen by thermal conductivity and the remaining elements by X-ray fluorescence. The results of the chemical analysis are shown in Table IV.

TABLE IV - Chemical Composition of the Iron Powder

Element	Percent
C	0,022
O	0,44
N	0,005
Mn	0,03
S	0,005
P	< 0,005
Si	< 0,0[illegible]
Cr	0,02
Mo	< 0,01
Ni	0,03
Cu	0,02
V	0,04
Fe	98,4

A sample splitter was used to obtain a representative sample of the powder for dry screen analysis. A sample of powder weighing 270g was vibrated for 15 minutes on a sieving machine utilising the following mesh sizes : 48 (297 µm), 70 (210 µm), 100 (149 µm), 140 (105 µm), 200 (74 µm), 300 (53 µm), 350 (45 µm) and 400 (38 µm). The mass retained on each sieve was measured and proportioned to the total mass as a percentage (Table V). The mass percent-size frequency distribution and the cumulative

mass-size curve are shown in Figure 36 and Figure 37 respectively. From the cumulative mass-size curve it was decided to utilise the 53 µm to 105 µm particle size range as this very narrow range represented 47,6 percent of the total powder by mass.

After sieving, the powder was dried at 200 °C for 2 hours and then stored in a dessicator for further use.

TABLE V - Percentage Iron Powder Retained on each Mesh Size

Mesh Number	Size (µm)	Percentage Powder Retained
48	297	-
70	210	-
100	149	8,77
140	105	22,40
200	74	25,16
300	53	18,78
350	45	7,09
400	38	4,18
Pan	<38	13,62

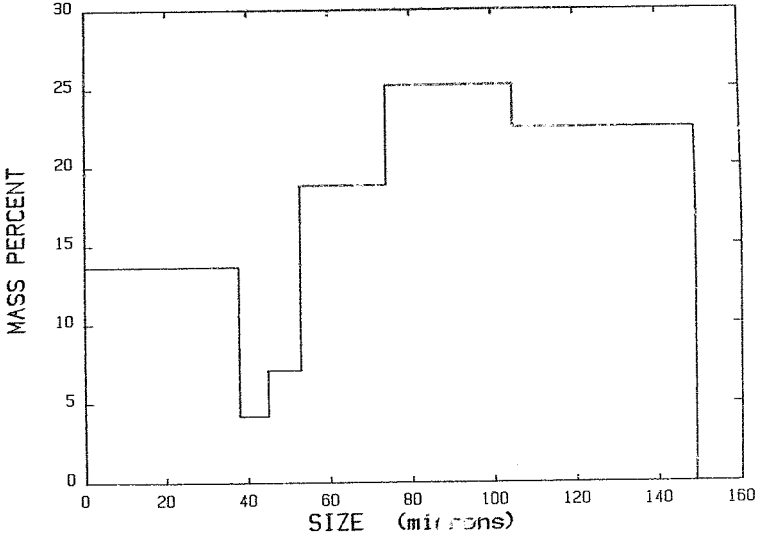

FIGURE 36 - The Mass Percent-Size Frequency Distribution of the Iron Powder

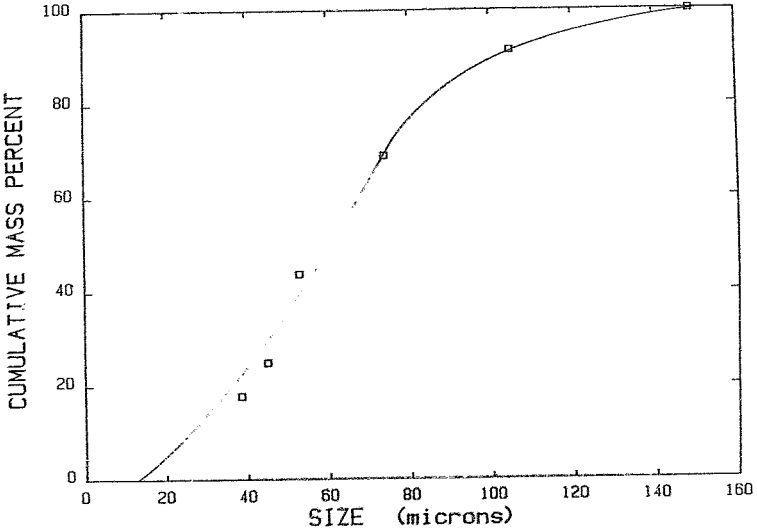

FIGURE 37 - Plot of the Cumulative Mass Percent Retained against Size for the Iron Powder

The powder was prepared for optical microscopy by mounting in lucite powder and grinding on successive grades of carbide paper up to 1000 grit. Final polishing was achieved by the use of a 2 μm alumina paste and the specimen was etched for 10 seconds in a 3 percent solution of HNO_3 in ethanol.

Metallographic examination showed the powder to be polycrystalline (Figure 38). Oxide inclusions were present in the grains. The presence of sponge microporosity was difficult to assess due to the irregular particle shape viz. any micropores observed may have been due to the orientation of the section through the particle. Hence, it was decided to determine the presence of open microporosity by scanning electron microscopy which would also allow investigation of the powder particle morphology.

The particles showed a low angularity and a topography typical of powders produced by the oxide reduction process (Figure 39). Furthermore, the particles showed some, but not extensive, open porosity as can be seen from Figure 40.

FIGURE 38 - Polycrystalline Nature of the Iron Powder

Note also the presence of oxide inclusions (A). Etched, 3% Nital, 500x.

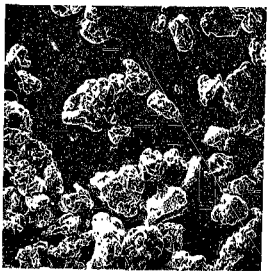

FIGURE 39 - The Morphology of the Iron Powder. SEM, 20x

FIGURE 40 - Detailed View of Iron Powder Particle Surface

SEM, 1000x

3.4 Technique of Microchilling

3.4.1 Preliminary Timing Studies for the Introduction of Powder

The technique of microchilling was mainly based on trial runs to obtain an even rate of powder addition. This was achieved by adjusting the powder flow rate to the pouring time of the ingot. The experimental timing studies were done in "mock" trials initially.

A refractory fused silica tube of length 500mm and 17mm in inner diameter was held in a stand. The iron powder was introduced into a funnel located at the top of the tube. Various angles of the tube with respect to the vertical axis and various funnel sizes were tested in order to obtain the desired flow rate.

The ideal positioning angle between the tube axis and the vertical axis was found to be 5 degrees.

This was determined by :

i) the limited space in the layout of the apparatus and,

ii) the need to maintain a gentle collusion of the powder particles with the stream of the molten metal to obtain rapid wetting of the particles by the molten metal.

Using 200g alliquots of iron powder, the following average flow rates of powder based on 30 trial runs each, were determined for various aperture diameters of funnels.

Aperture Diameter of Funnel (mm)	2,50	4,15	5,30	6,35	9,5
Average Flow rate of Powder (g s^{-1})	8,91	13,09	21,06	31,90	79,37

Once the metal flow rate and the time for pouring had been stabilised at 6 s by the introduction of a pouring basin (see next section on 'The Experimental Castings'), it was possible to determine what mass percentage of powder would be delivered to the 6kg ingots by the various aperture diameters.

Aperture Diameter of Funnel (mm)	2,50	4,15	5,30	6,35	9,5
Mass Percentage Addition of Powder (Percent)	0,89	1,31	2,10	3,19	7,94

Attempts to determine the variation in powder flow rate as the powder head in the funnel decreased were unsuccessful.

3.4.2 The Experimental Castings

Initially, it was conjectured that the microchilling would be accomplished by simultaneous pouring of the iron powder and the molten metal directly into the ingot mould. However, problems were experienced in obtaining sufficient mixing of the powder and the melt. This was thought to be due to the lack of change in flow direction and the absence of any change in cross-sectional area of the flow path after the initial impingement of the powder and the melt. It was also found that this method did not give a highly reproducible metal pouring rate resulting in uneven powder distribution in the ingot. Use of this simultaneous direct pouring technique resulted in pouring times of between 5 and 15s. In order to limit these variations to a minimum a pouring basin was used resulting in pouring times with acceptable reproducibility.

Using a mild steel template, the pouring basin (Figure 41) was moulded with a magnesite based refractory and coated with air setting magnesium-based mortar. The pouring basin was filled to a constant height, and the angle of the runner varied until a satisfactory reproducible pouring time of 6 ± 1s was obtained. (The experimental assembly for suspension casting can be seen in Figure 42).

In order to avoid chilling of the metal by the pouring basin, the latter was preheated to 1100 °C.

The refractory tube used to deliver the powder from the funnel into the ingot mould was positioned so that collusion of powder particles with the metal stream occurred immediately below the rim of the ingot mould surface. Positioning of the tube above the rim resulted in the deflection and scattering of iron particles outside the mould. Attempts to improve the mixing of the powder in the molten metal by positioning the tube in the pouring basin resulted in excessive chilling and solidification of the alloy in the launder.

The pouring procedure for suspension casting was the same as for conventional casting except for the addition of the iron powder. It was found that problems occurred obtaining satisfactory mixing of the powder and the melt when additions of 3,19 percent powder were used. The addition of 2,1 percent powder resulted in ingots with the largest equiaxed zone. All microchilled ingots used for subsequent experiments were therefore made with this percentage addition of iron powder.

3.4.3 Microchilled and Conventionally Cast Ingots

Following the establishment of the casting procedure, five conventionally cast and five suspension cast ingots of steel AISI 310 were produced. These were coded as CC and SC respectively

a) Side View

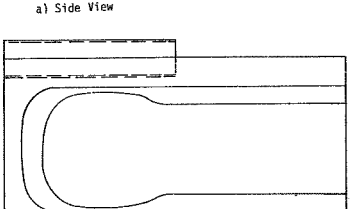

b) Top View

c) Front View

FIGURE 41 - A Schematic Diagram of the Pouring Basin

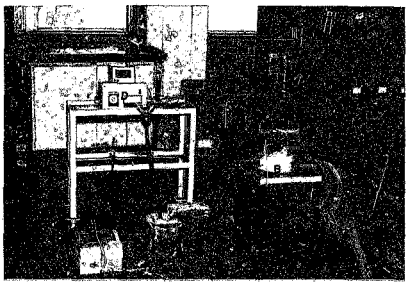

FIGURE 42 - The Experimental Set up for Suspension Casting

A is the induction unit
B is the melting pot containing the chrome oxide crucible
C is the infrared pyrometer sensory head
D is the infrared pyrometer control unit
E is the pouring basin
F is the flake graphite ingot mould
G is the silica tube
H is the funnel

Each series was coded further as 0, 20, 40, 60 and 80 referring respectively to the as cast material and to material reduced in hot rolling by 20, 40, 60 and 80 percent.

All the ingots were checked for unsoundness by X-ray radiography. The method also enabled the length of the primary pipe in each of the ingots to be measured.

3.5 Macrostructural Examination

All conventional and microchilled ingots cast during the establishment of the casting procedure were sectioned longitudinally while the hot-rolled ingots were sectioned transversely.

The surfaces were then surface ground and macroetched in boiling mixed acids (38 ml HCl, 12 ml H_2SO_4 and 50 ml H_2O) for two hours. After etching, the surfaces were examined visually to determine the effect of suspension casting and hot working on the ingot macro-structure.

3.6 Rolling

The ingots were rolled in a two-high reversing mill with a capacity of 50 tonnes. During rolling, the temperature was constantly monitored using a digital infrared pyrometer. All rolling was done using flat rolls of 200mm diameter and a roll speed of 25 rpm (equivalent to a linear speed of 0,26 ms^{-1}).

To maintain a square section, the ingots were rotated through 90° between passes and straightened in a press as necessary before being returned to the furnace.

Details of the rolling procedure are given in Table VI below :

TABLE VI - Rolling Procedure for the Suspension and Conventionally Cast Ingots

Rolling temperature	1100 °C
Soaking time	1,5 hours
Rolling temperature range	1100 °C - 800 °C
Number of intermediate reheats	0 for 20% reduction 1 for 40% reduction 2 for 60% reduction 3 for 80% reduction
Reheating times between reductions	30 minutes between roll periods 1 and 2 and 15 minutes between roll periods 2 and 3, and 3 and 4

A schematic representation of the rolling procedure followed is given in Figure 43.

After rolling, the ingots were water quenched and their surfaces examined visually for cracks and other defects. A transverse section was taken from each ingot and examined to establish the extent of recrystallisation.

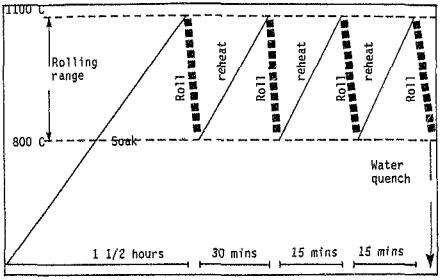

FIGURE 43 - Schematic Diagram for Rolling Procedure

3.7 Specimen Preparation and Testing

Charpy, tensile and compression specimens were prepared from the conventional and suspension cast ingots in the as-cast and as-rolled conditions. The specimens were cut in the longitudinal direction for all ingots and where ingot cross section size allowed, in the transverse direction as well (Figure 44).

3.7.1 Charpy Impact Tests

Standard Charpy V-notch impact specimens were cut and machined in the longitudinal direction for both suspension and conventionally cast ingots in the as cast and hot rolled conditions. Transverse specimens, however, could only be obtained in the as cast ingots and those reduced by 20 percent.

The specimens were machined and tested in accordance with the requirements of BS Specification 131 part 2, 1972.

The tests were performed at ambient temperature on a Tinius Olsen machine capable of registering absorbed impact energies of up to 358J. The energies are indicated to within 0,5 Joules and each value quoted is the average of four tests.

3.7.2 Tensile Tests

Hounsfield tensile specimens (Figure 45) were machined in the longitudinal and transverse directions for all ingots. Transverse specimens, however, could not be obtained for the ingots reduced by 80 percent. The tests were carried out according to BS 18 : Part 2 : 1971. All tests were carried out at ambient temperature.

The tensile tests were performed on an Instron servo-hydraulic testing machine of a 50 kN capacity at a constant displacement of 0,1mm s^{-1}. Engineering stress versus displacement data were stored with a Commodore microcomputer and converted to engineering stress-strain curves.

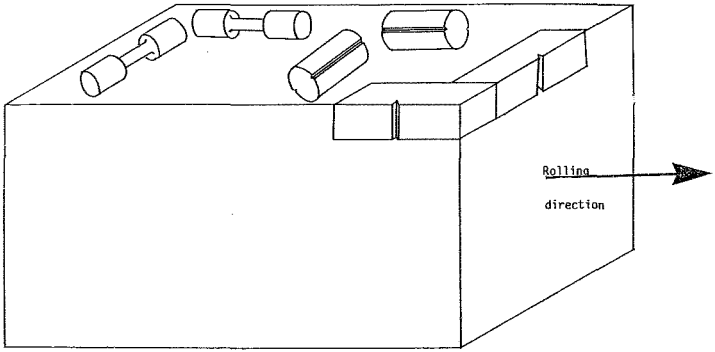

FIGURE 44 - Specimen Orientation

The yield strength, ultimate tensile strength, percentage reduction in area and percentage elongation of all the specimens were measured and the results quoted are the means of at least 3 tests.

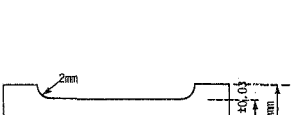

FIGURE 45 - Dimensions of the Hounsfield Tensile Specimens

3.7.3. Hardness Tests

The variation of hardness with increasing amount of deformation for the conventional and suspension cast ingots was measured using a Vickers hardness testing machine with a load of 30kg. The specimen surfaces were prepared by grinding and polishing to a finish of one micron. The hardness values given are the means of at least five tests.

3.7.4 Compression Tests

3.7.4.1 Compression Specimens

Cylindrical compression specimens (Figure 46) of 30mm height and 20mm diameter were machined from the as cast ingots and from material rolled by between 20 and 80 percent. Longitudinal and transverse specimens were obtained from both types of ingots in all conditions except in the case of material rolled by 80 percent from which transverse specimens could not be obtained.

The flat specimen surfaces were parallel to within ± 0,01mm, flat to within 0,005mm and had a surface finish of 0,4 µm arithmetic average measured in accordance with ASTM specification E9-77-81.

Two notches with a radius of 0,25mm and 0,5mm deep were cut from end to end on the lateral surface of the cylindrical specimens and at opposite ends of a diametral plane. The purpose of these notches was to magnify the effects of circumferential secondary tensile stresses caused by barrelling of the specimens.

3.7.4.2 Compression Test Dies

Cylindrical dies, 90mm in diameter were machined from AISI D2 tool steel and hardened and tempered to a hardness of 30 RC. The dies were knurled (Figure 47) in order to increase the friction between the dies and the specimen thereby promoting barrelling of specimens and increasing the likelihood for crack formation.

After machining and heat treatment, the dies were shrink fitted into mild steel blocks in order to prolong die life by decreasing the tensile forces acting in the surface layers of the dies during testing.

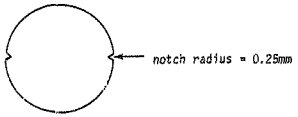

a) Top View

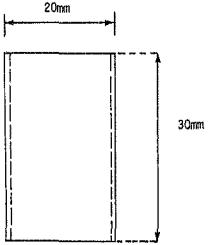

b) Side View

FIGURE 46 - Compression Specimen Dimensions

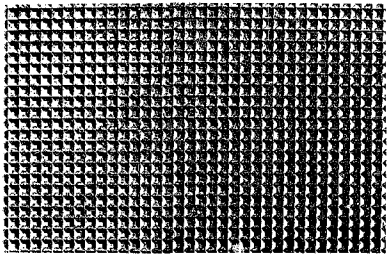

FIGURE 47 - Knurled Surface of the Compression Dies 1,5x

3.7.4.3 The Test Procedure

A load cell was built and through its use attempts were made to obtain curves of load against time. The circuit diagram for the load cell is shown in Figure 48. The wheatstone bridge shown in the circuit comprised four strain gauges mounted on the load cell such that two were parallel and two were vertical to the applied load vector. During compression, these would be in compression and in tension respectively.

It was hoped, that the load-time curve would show a deflection in the force at the time of crack initation thus allowing accurate determination of the amount of deformation at fracture. However, while a deflection was obtained on specimens of height 12,25mm and diameter 10,00mm at ambient temperature, a deflection in the

load-time curve could not be detected for the full size compression specimens tested at 1100 °C. It was therefore decided to perform upset tests on notched specimens as described below.

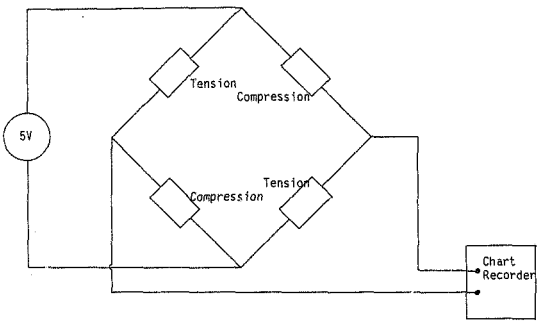

FIGURE 48 - Circuit Diagram for the Proposed Load Cell

The notched compression specimens were heated for 15 minutes at 1100 °C and compressed to various heights by use of a 150 ton hydraulic press. A constant displacement rate of 20mm min^{-1} was used for all tests. Each ingot series e.g. CC0 longitudinal, CC20 longitudinal, SC0 transverse etc was given a 50, 60, 70 and 80 percent reduction in height. Immediately after compression, the specimens were water quenched. (The experimental rig is shown in Figure 49).

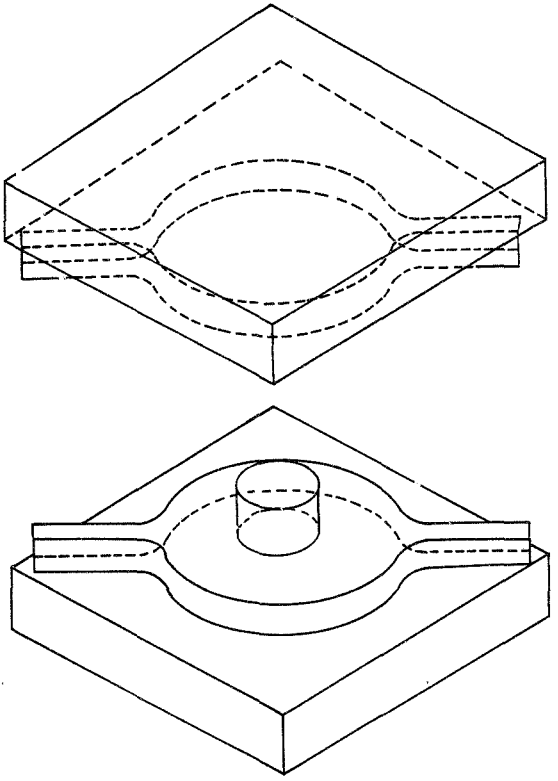

FIGURE 49 - Drawing of the Test Rig for the Compression Tests

The cracks occurring in the notches were then classified according to the rating system shown in Figure 31. A rating of 0 is applied if no cracks are observed. If they are small, discontinuous and scattered, the rating is 1. Higher rating numbers indicate increasing incidence and depth of rupture.

3.8 Microscopy

3.8.1 Optical Microscopy

Metallographic specimens were prepared and examined with a Nikon Optiphot microscope at magnifications of up to 1000x.

The specimens were prepared by grinding on successive grades of carbide paper up to 1200 grit. Final polishing was achieved by the use of 3 μm and 1 μm diamond lapping compounds. An electrolytic etch was used to reveal the grain structure. The samples were etched in a saturated solution of oxalic acid for about 15 seconds. A voltage of 8V was applied.

The grain size was measured by the linear intercept method.

3.8.2 Scanning Electron Microscopy (SEM)

Transverse sections of the Charpy specimens were polished and etched as before for examination in a Cambridge Stereoscan S4 scanning electron microscope. The matrix and inclusions were analysed by use of an energy dispersive X-ray spectrometer (EDS) which allowed detection of elements having an atomic mass number (Z) of greater than 11.

The SEM was also used to study the fracture surfaces of the tensile specimens.

4. RESULTS

4.1 The Chemical Composition of the Castings

The C and O_2 contents of the castings were determined by combustion and infrared absorption of CO_2. Cr, Ni, Mo, Ti, Co, Cu, Si, Mn, P and S were determined by XRF analysis and N_2 by the thermal conductivity method. The analyses of all the castings used in this study are shown in Table VII. The nominal composition of AISI 310 is also shown in Table VII for comparison.

From Table VII it can be seen that the C, Mn, P, S and Si contents were all maintained within the required composition maxima. The Ni content for SC20 and SC40 and the Cr content for a number of the castings were below the desired minimum. However, the deviations were small and are not considered to be significant. Except for the casting SC80, the deviations of the N_2 and O_2 levels were negligible. The casting SC80 had a high N_2 level and this could be expected to result in higher strength and lower ductility values.

TABLE VII - Chemical Compositions of the Castings

Casting Code	% C	% S	% P	% Mn	% Si	% Cu	% Co	% Ti	% Mo	% Cr	% Ni	% O_2	% N_2
CC0	0,054	0,010	0,026	1,41	0,46	0,11	0,08	0,005	0,19	24,02	19,52	0,0336	0,0488
CC20	0,057	0,010	0,017	1,38	0,38	0,08	0,02	0,003	0,11	23,95	19,20	0,0354	0,0500
CC40	0,058	0,008	0,020	1,46	0,36	0,08	0,02	0,003	0,10	23,96	19,19	0,0353	0,0389
CC60	0,060	0,009	0,017	1,40	0,38	0,08	0,02	0,003	0,10	23,84	19,23	0,0430	0,0406
CC80	0,058	0,009	0,020	1,52	0,36	0,08	0,02	0,003	0,10	23,99	19,18	0,0406	0,0492
Mean	0,057	0,009	0,020	1,43	0,38	0,08	0,03	0,003	0,12	23,95	19,26	0,0376	0,0455
S.D.	±0,002	±0,001	±0,003	±0,05	±0,04	±0,01	±0,02	±0,001	±0,03	± 0,06	±0,14	±0,0040	±0,0053
SC0	0,049	0,005	0,023	0,80	0,60	0,11	0,08	0,008	0,14	24,76	19,21	0,0348	0,0461
SC20	0,059	0,011	0,017	1,37	0,35	0,08	0,03	0,003	0,11	23,80	18,99	0,0348	0,0506
SC40	0,056	0,010	0,017	1,36	0,38	0,08	0,02	0,003	0,11	23,63	18,94	0,0362	0,0562
SC60	0,062	0,012	0,016	1,27	0,42	0,08	0,03	0,004	0,11	23,73	19,06	0,0316	0,0500
SC80	0,060	0,009	0,017	1,13	0,34	0,08	0,03	0,003	0,10	24,04	19,05	0,0374	0,1090
Mean	0,057	0,009	0,018	1,18	0,41	0,08	0,03	0,004	0,11	23,99	19,05	0,0350	0,0624
S.D.	±0,005	±0,002	±0,002	±0,23	±0,10	±0,01	±0,02	±0,002	±0,01	± 0,45	±0,10	±0,0022	±0,0263
AISI 310	0,08 max.	0,03 max.	0,045 max.	2,0 max.	1,5 max.	-	-	-	-	24,0-26,0	19,0-22,0	-	-

TABLE VII - Chemical Compositions of the Castings

Casting Code	% C	% S	% P	% Mn	% Si	% Cu	% Co	% Ti	% Mo	% Cr	% Ni	% O_2	% N_2
CC0	0,054	0,010	0,026	1,41	0,46	0,11	0,08	0,005	0,19	24,02	19,52	0,0336	0,0488
CC20	0,057	0,010	0,017	1,38	0,38	0,08	0,02	0,003	0,11	23,96	19,20	0,0364	0,0500
CC40	0,058	0,008	0,020	1,46	0,36	0,08	0,02	0,003	0,10	23,96	19,19	0,0353	0,0389
CC60	0,060	0,009	0,017	1,40	0,38	0,08	0,02	0,003	0,10	23,84	19,23	0,0430	0,0406
CC80	0,058	0,009	0,020	1,52	0,36	0,08	0,02	0,003	0,10	23,99	19,18	0,0406	0,0492
Mean	0,057	0,009	0,020	1,43	0,38	0,08	0,03	0,003	0,12	23,95	19,26	0,0376	0,0455
S.D.	±0,002	±0,001	±0,003	±0,05	±0,04	±0,01	±0,02	±0,001	±0,03	± 0,06	±0,14	±0,0040	±0,0053
SC0	0,049	0,005	0,023	0,80	0,60	0,11	0,08	0,008	0,14	24,76	19,21	0,0348	0,0461
SC20	0,059	0,011	0,017	1,37	0,35	0,08	0,03	0,003	0,11	23,80	18,99	0,0348	0,0506
SC40	0,056	0,010	0,017	1,36	0,38	0,08	0,02	0,003	0,11	23,63	18,94	0,0362	0,0562
SC60	0,062	0,012	0,016	1,27	0,42	0,08	0,03	0,004	0,11	23,73	19,06	0,0316	0,0500
SC80	0,060	0,009	0,017	1,13	0,34	0,08	0,03	0,003	0,10	24,04	19,05	0,0374	0,1090
Mean	0,057	0,009	0,018	1,18	0,41	0,08	0,03	0,004	0,11	23,99	19,05	0,0350	0,0624
S.D.	±0,005	±0,002	±0,002	±0,23	±0,10	±0,01	±0,02	±0,002	±0,01	± 0,45	±0,10	±0,0022	±0,0263
AISI 310	0,08 max.	0,03 max.	0,045 max.	2,0 max.	1,5 max.	-	-	-	-	24,0-26,0	19,0-22,0	-	-

4.2 Ingot Macrostructure

4.2.1 The As Cast Macrostructure

The longitudinal sections of conventional ingots cast from 1650°C and 1750 °C are shown in Figures 50 and 51 respectively. A longitudinal section of an ingot microchilled with 2,1 percent by mass of iron powder is shown in Figure 52.

As can be seen, problems with porosity and insufficient mixing were eliminated. The conventionally cast ingot poured from a temperature of 1750 °C is totally columnar and only a few equiaxed crystals are discernible in the centre of the ingot poured from 1650 °C. The suspension cast ingot which was poured from a temperature of 1750 °C and therefore had 100 °C more superheat than the 1650 °C conventionally cast ingot would ordinarily be expected to show a more extensive columnar zone. This however was not the case. Suspension casting resulted in a significantly greater equiaxed zone than that of the conventional ingots cast from the same temperature and the conventional ingots cast with 100 °C less superheat. Furthermore, the grain size in the equiaxed zone of the suspension cast ingot is smaller than that of the conventionally cast ingot.

The length of the primary pipe was measured from X-ray radiographs and the results are listed in Table VIII. It would appear that suspension casting decreases the length of the primary pipe, expressed as a percentage of the ingot length, from an average of 43,34 percent for conventional castings to an average of 36,40 percent.

The improved grain structure should enhance mechanical and hot workability properties while the reduction in the length of the central pipe should improve material utilisation and therefore economic viability.

FIGURE 50 - Longitudinal Section of Conventionally Cast Ingot Poured from a Temperature of 1650 °C. Etched with Boiling Mixed Acids

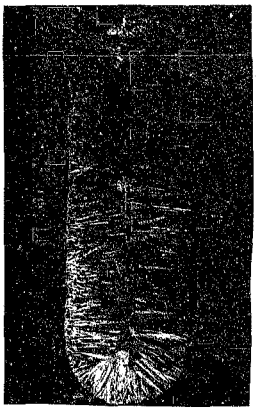

FIGURE 51 - Longitudinal Section of Conventionally Cast Ingot Poured from a Temperature of 1750 °C. Etched with Boiling Mixed Acids.

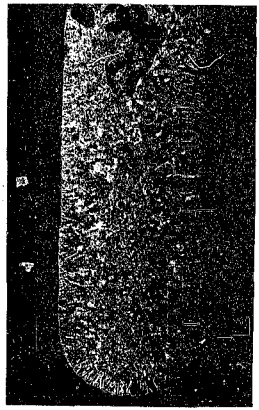

FIGURE 52 - Longitudinal Section of Suspension Cast Ingot (2,1 Percent Fe Powder) Poured from a Temperature of 1750 °C. Etched with Boiling Mixed Acids

TABLE VIII - Length of the Primary Pipe

Casting Code	Ingot Length (mm)	Length of Primary Pipe (mm)	% Length of Primary Pipe
CC0	214	99	46,26
CC20	228	98	42,98
CC40	218	93	42,66
CC60	212	87	41,04
CC80	198	87	43,94
		Average :	43,34%
		S.D. :	1,92
SC0	204	75	36,76
SC20	207	74	35,75
SC40	204	57	27,94
SC60	214	90	42,06
SC80	190	75	39,47
		Average :	36,40%
		S.D. :	5,33

4.2.2 The Macrostructure of Hot Rolled Ingots

Transverse sections of the hot worked ingots cast with and without iron additions are shown in Figures 53 a-d and 54 a-d respectively. The percentage recrystallisation for each ingot is tabulated in Table IX.

TABLE IX - Percentage Recrystallisation after Hot Rolling

Percentage Reduction in Area	Percentage Recrystallisation	
	Conventionally Cast	Suspension Cast
20	48	50
40	56	62
60	68	83
80	100	100

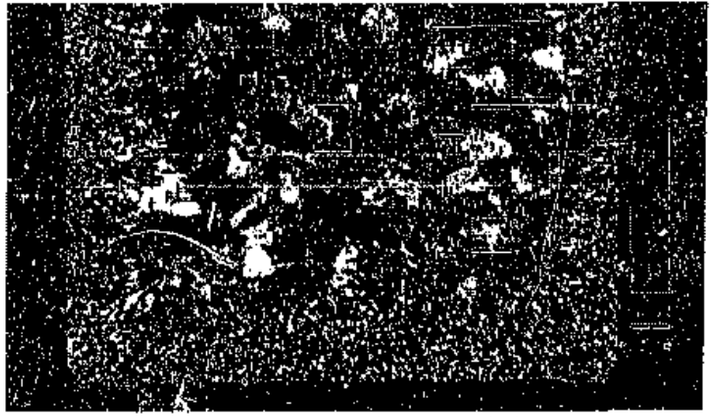

FIGURE 53a - Transverse Section of CC 20 Ingot

FIGURE 54a - Transverse Section of SC20 Ingot

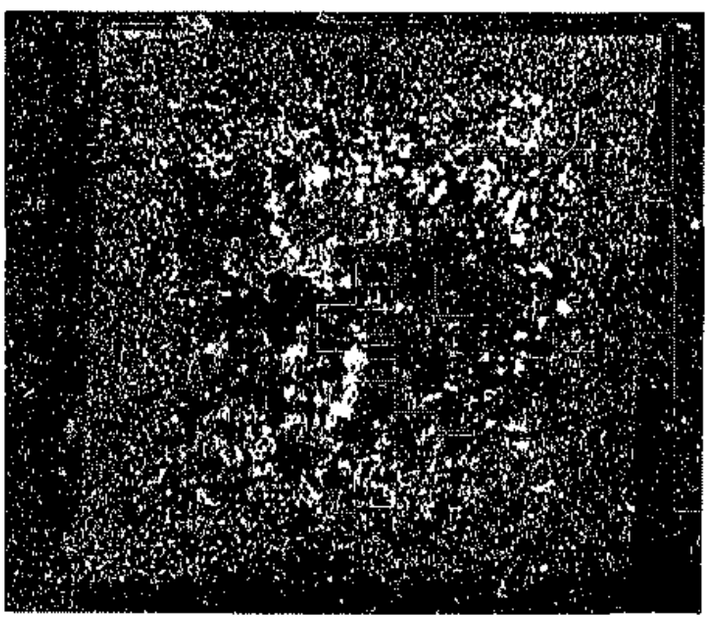

FIGURE 53b - Transverse Section of CC40 Ingot

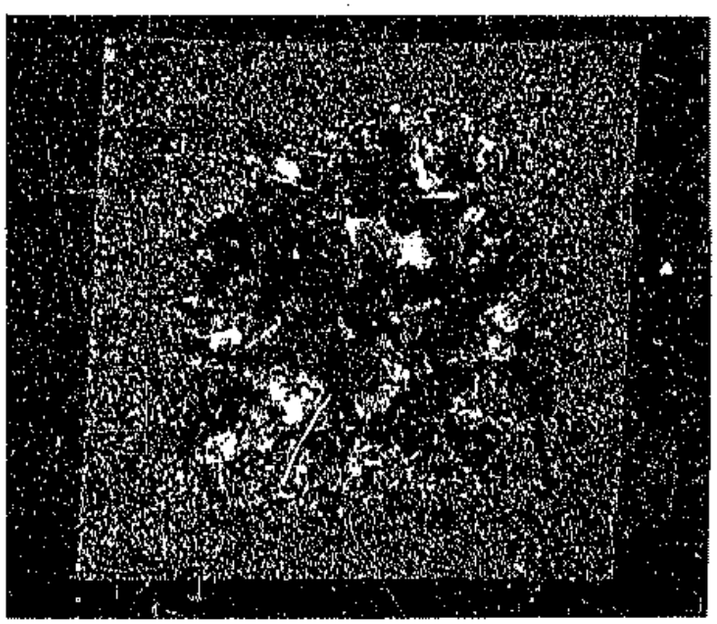

FIGURE 54b - Transverse Section of SC40 Ingot

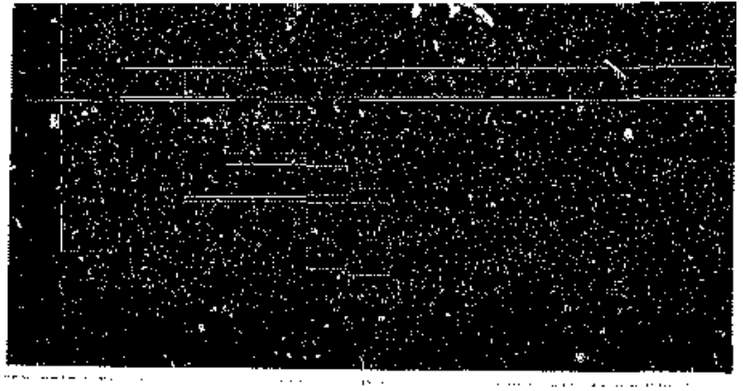

FIGURE 53c - Transverse Section of CC 60 Ingot

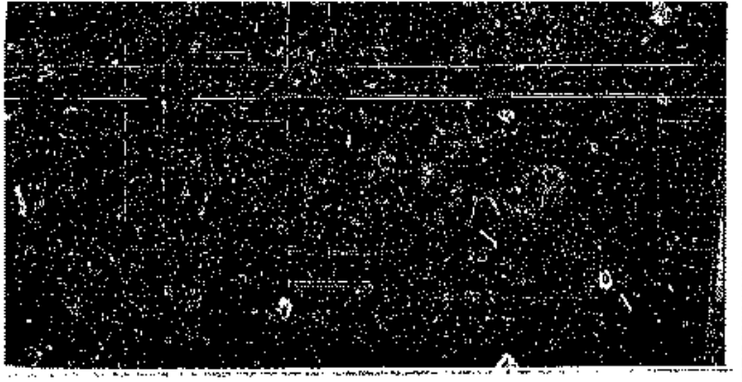

FIGURE 54c - Transverse Section of SC60 Ingot

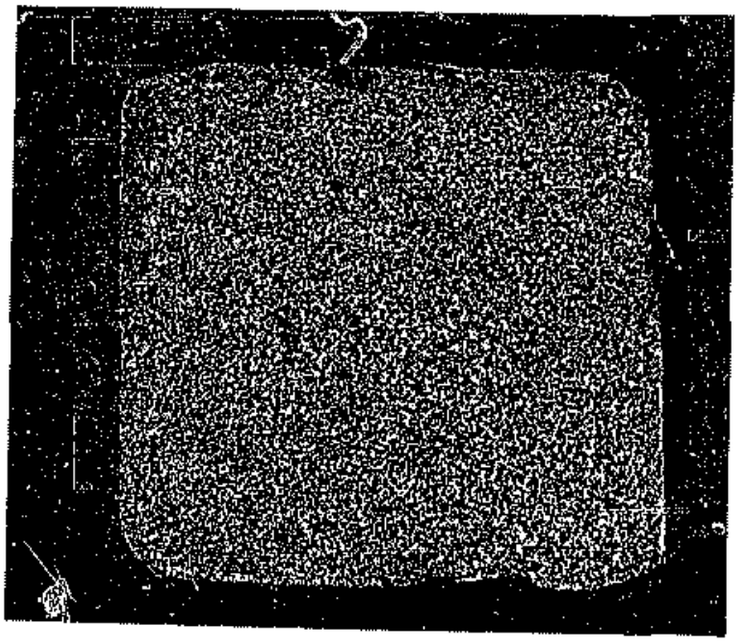

FIGURE 53d - Transverse Section of CC80 Ingot

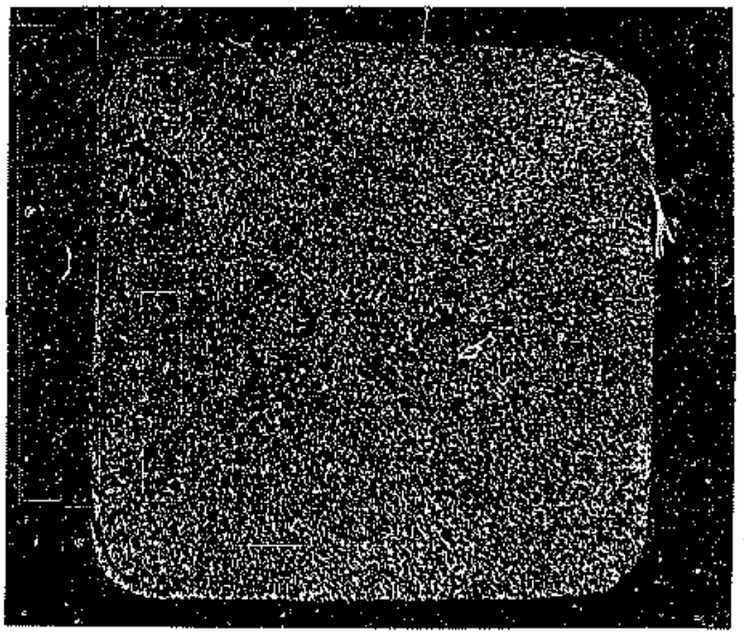

FIGURE 54d - Transverse Section of SC80 Ingot

The difference in the percentage recrystallisation of the conventionally cast and suspension cast ingots after 20 percent reduction in hot rolling was negligible. Both types of ingots showed a fully recrystallised structure after 80 percent reduction in hot rolling. The recrystallised grain size of the suspension cast ingot does, however, appear finer than that of the conventionally cast ingot.

The suspension cast ingots rolled by 40 and 60 percent showed a significantly greater degree of recrystallisation than the conventionally cast ingots. Furthermore, the grain size of the suspension cast ingots was again finer than that of the conventionally cast ingots.

The finer grain size of the suspension cast and hot rolled material, like that of the as cast material, should result in decreased segregation as well as improved mechanical and hot workability properties. The increased recrystallisation of the suspension cast ingots should result in decreased rolling load, shorter rolling schedules or lower rolling temperatures with concomitant economic benefits.

4.3 Microstructural Assessment

4.3.1 Optical Microscopy

In this section an optical microscopic examination of the overall appearance of specimens from suspension cast and conventionally cast ingots in the as polished condition will be made. The as cast microstructures for both types of ingots will then be compared and the microstructure of hot rolled material will be examined. Finally, an unexpected eutectoid-like structure which was observed in a CC40L specimen will be discussed.

Specimens from suspension and conventionally cast ingots showed a similar appearance in the polished condition with respect to the number, size and distribution of inclusions. The latter were small in size and evenly distributed as indicated in Figure 55 which shows inclusions in a specimen from ingot CC80L. Specimens from ingot CC40L showed some unique features which are discussed at a later stage. Some of the inclusions were identified as MnS but the majority appeared to be carbide particles.

Electrolytic etching in saturated oxalic acid revealed the nature of the grain boundaries and the form and distribution of precipitates. The etching also revealed that the ingots consisted entirely of austenite.

In the as cast condition the conventionally cast ingots had a typical non-random dendritic structure (Figure 56). The austenitic dendrites were aligned approximately normal to the surface of the casting. The effect of microchilling on the microstructure of this alloy can be seen clearly in Figure 57 where the austenite dendrites are smaller and randomly orientated. The number of interdendritic precipitate particles was appreciably lower in the microchilled material as can be seen from a comparison between Figures 56 and 57. These interdendritic precipitates probably resulted from segregation of alloying elements and carbon to interdendritic spaces during solidification and hence the lower number of precipitate particles in the microchilled ingot would suggest that microchilling decreased segregation.

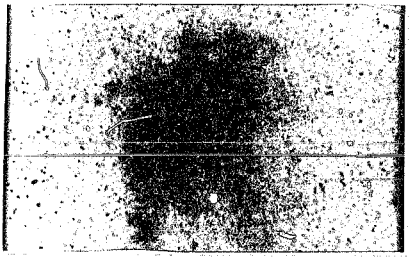

FIGURE 55 - Specimen CC80L in the As Polished Condition - x 250

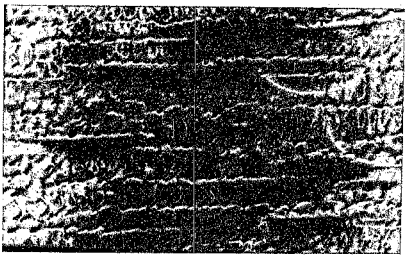

FIGURE 56 - The Microstructure of Specimen CC0L Showing a Non-Random Dendritic Structure - x125

The microstructure of the hot worked material showed a recrystallised equiaxed grain structure together with twinning. The intragranular precipitates appeared small and evenly dispersed. The microstructure of a specimen from the centre of the suspension cast ingot reduced by 20 percent is shown in Figures 58 and 59. These microstructures are typical of the hot worked material. Note that although the remnants of the cast structure were still discernible in the material reduced 20 percent, they were not observed in material which had had larger amounts of reduction (Figure 60).

Inclusions in both the suspension cast and conventionally cast materials were small and evenly distributed. They were also mainly intragranular (Figures 58 and 59). Grain boundary precipitates were however observed in the SC80L specimen (Figure 60). These precipitates were identified as $Cr(C,N)$ precipitates from their reflectivity and morphology. These precipitate particles are expected to be detrimental to the mechanical properties of the SC80L ingot.

A clear trend of decreasing grain size with increasing amount of deformation was observable. The grain size measurements are tabulated in Table X and plotted in Figure 61.

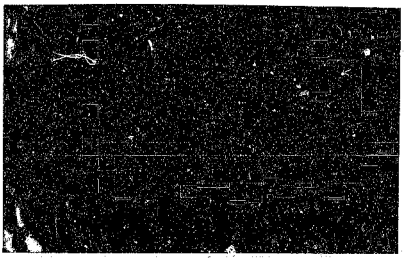

FIGURE 57 - The Microstructre of Specimen SC0L Showing a Random and Refined Dendritic Structure - x250

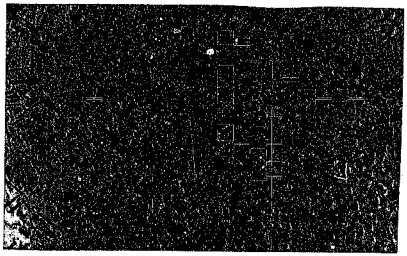

FIGURE 58 - The Microstructure of Specimen SC20L - x500

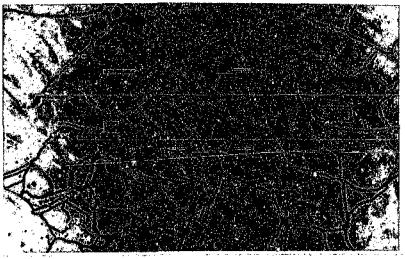

FIGURE 59 - The Microstructre of Specimen SC20L - x 1000

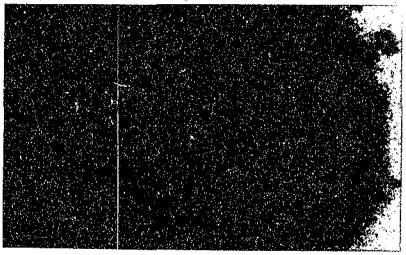

FIGURE 60 - The Microstructure of Specimen SC80L Showing Grain Boundary Precipitation - X1000

TABLE X - The Grain Size in Ingots Reduced by Different Amounts

Percentage Reduction in Area	Average Grain Size (μm)	
	Conventional Cast	Suspension Cast
0	411	371
20	196	190
40	100	90
60	57	50
80	57	35

The grain size of suspension cast ingots was consistently finer than that of the comparable ingots cast conventionally. This difference in grain size between conventionally cast and suspension cast ingots is most clearly illustrated in the as cast material and in material reduced by 80 percent.

A polished microsection of specimen CC40L is shown in Figure 62 at low magnification.

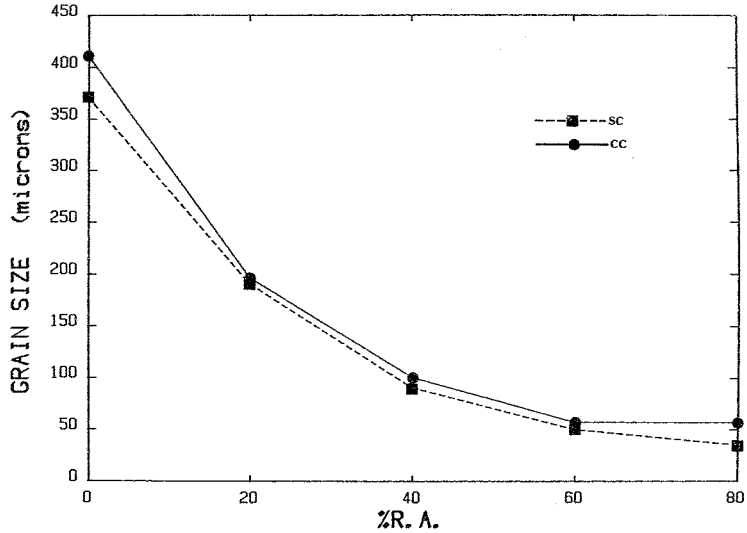

FIGURE 61 - Grain Sizes after Hot Deformation

The same specimen is shown at low and high magnifications after etching in Figures 63 and 64 respectively. An extensive network of precipitate particles was observed (Figure 62) consisting of intermetallic and non-metallic material. Upon etching, the areas showing precipitation revealed a eutectoid - like structure. This eutectoid-like structure has been described by Kane[67] as being a transformation production of δ-ferrite. None of the other ingots investigated showed this type of structure. The properties of the material might be expected to be affected adversely owing to the presence of these phases.

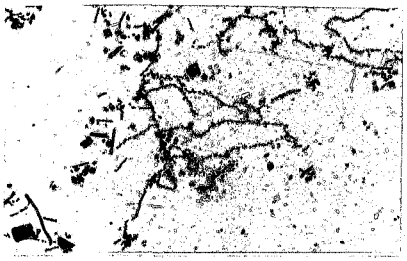

FIGURE 62 - Specimen CC40L in the As Polished Condition - x250

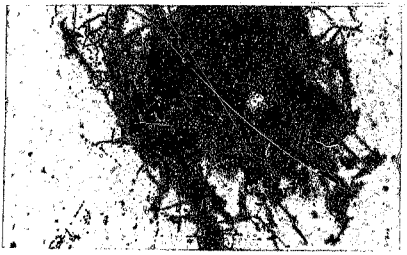

FIGURE 63 - Eutectoid-like Structure in Specimen CC40L - x250

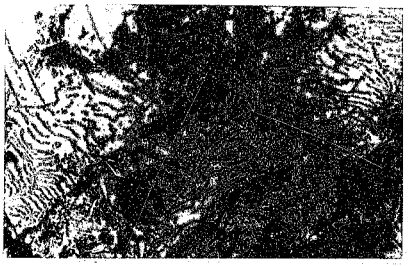

FIGURE 64 - The Microstructure of Specimen CC40L Showing a Eutectoid-like Structure and Blocky Non-Metallic Inclusions x 1000

4.3.2 Scanning Electron Microscopy

Scanning electron microscopy studies were undertaken in an attempt to characterise the precipitates found in the microstructure further.

Precipitates in both the suspension cast and conventionally cast materials were small and evenly distributed. They were also mainly intragranular (Figures 65 and 66). Grain boundary precipitates were however observed in the SC80L specimen (Figure 67). Qualitative analyses of these precipitates were carried out using an energy dispersive system (EDS) coupled to the scanning electron microscope. The results of these studies are presented in Figures 68 to 70. Most of the intragranular precipitates contained Cr, Fe, Ni and relatively large amounts of Si (Figure 68) indicating that the precipitates were probably mixed silicates.

The grain boundary as well as some of the intragranular precipitates had much higher Cr contents (Figures 69 and 70 respectively) than the matrix (Figure 71) and hence were thought to be either chromium carbonitrides or chromium carbides. However, in view of their reflectivity in the optical microscope these precipitates were identified as Cr (C,N) precipitates.

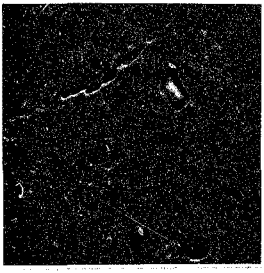

SEM x 2300

FIGURE 65 - Typical Intragranular Inclusion in Specimen SC80L

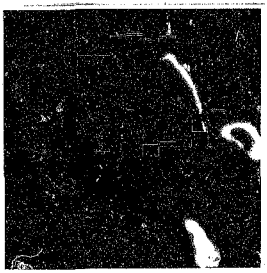

SEM x 5500

FIGURE 66 - Typical Intragranular Inclusion in Specimen SC80L

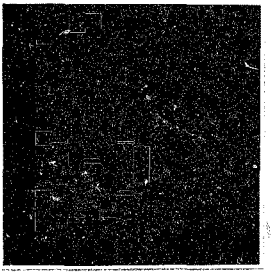

SEM x 5000

FIGURE 67 - Grain Boundary Inclusions in Specimen 3C80L

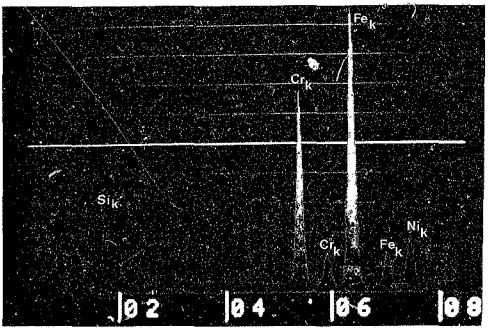

FIGURE 68 - Spectrum of an Intragranular Inclusion such as shown in Figure 65

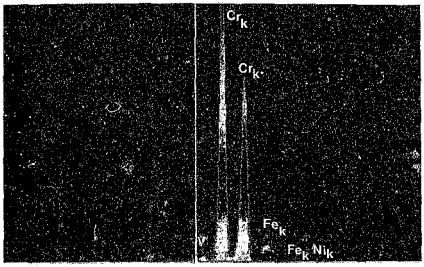

FIGURE 69 - Spectrum of a Grain Boundary Inclusion such as shown in Figure 67

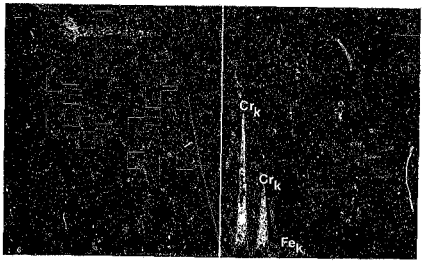

FIGURE 70 - Spectrum of an Intragranular Inclusion such as shown in Figure 66

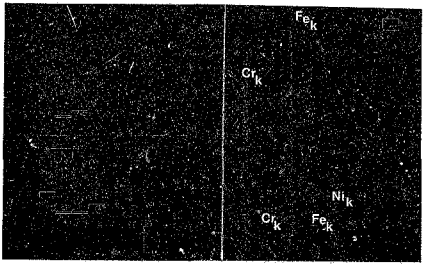

FIGURE 71 - Spectrum of the Matrix of Specimen SC80L

The eutectoid type structure found in specimen CC40L is shown in Figure 72. A typical example of the idiomorphic precipitates that were associated with the eutectoid-type structure can be seen. Qualitative analyses of these precipitates were carried out using the EDS and the results of these studies are presented in Figure 73 which shows the spectrum of the matrix and that of a precipitate particle superimposed.

Comparison of the two spectra indicated that the angular precipitate particle is substantially richer in chromium. This infers that the precipitate is a chromium oxide. The lower Ni concentration in the precipitate is also indicative of oxide as the free energy of formation of Cr_2O_3 is much more negative than that of NiO hence preferential oxidation of Cr occurs. The morphology and reflectivity of the particles (Figure 64) confirmed this conclusion.

A scanning electron micrograph of the network of precipitate particles with which the eutectoid-like structure was associated is shown in Figure 74. EDS analyses of precipitate particles showed the presence of Al, Si, K, Ca, Cr, Fe and Ni (Figure 75) indicating that the network of precipitate particles was caused by entrapment of slag during pouring. This would be entirely feasible in view of the fact that chromium rich slags form tenacious films on molten alloys.

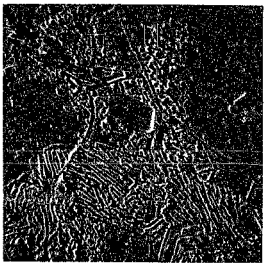

SEM x1100

FIGURE 72 - The Microstructure of Specimen CC40L in the Localised Regions that showed Phases other than Austenite

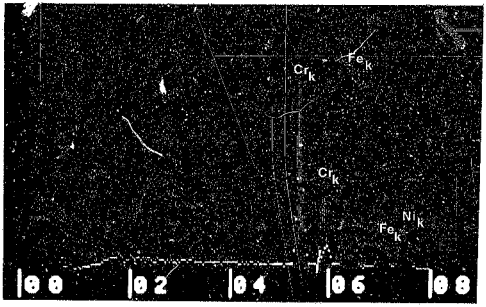

FIGURE 73 - Spectra of the Matrix (Dotted) and of an Idiomorphic Metallic Particle in Specimen CC40L showing Differences in Composition

SEM x 300

FIGURE 74 - Microstructure of the Network of Precipitate Particles with which the Eutectoid-like Structure found in Specimen CC40L was associated

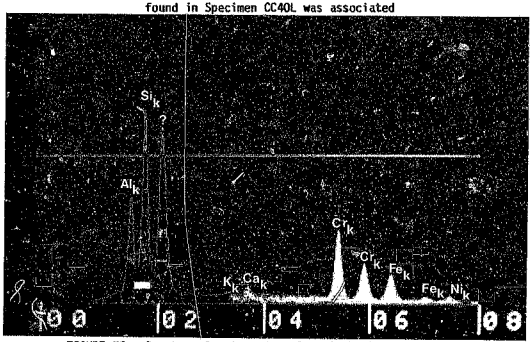

FIGURE 75 - Spectrum Obtained from Spot Analysis of a Slag Inclusion

4.4 Charpy Impact Tests

The results of the Charpy impact tests are summarised in Table XI and presented graphically in Figure 76.

TABLE XI - Charpy Impact Test Results

Percentage Reduction in Area	Impact Energy* (Joules)			
	Conventional Cast		Suspension Cast	
	Longitudinal	Transverse	Longitudinal	Transverse
0 (as cast)	203	156	217	178
20	196	163	195	172
40	203	-	202	-
60	231	-	267	-
80	298	-	248	-

* Mean of 4 determinations at room temperature

In the as cast condition the suspension cast material had a higher longitudinal and transverse impact toughness than the conventionally cast material. The impact energies of transverse specimens of conventionally cast material in the as cast condition and after a reduction of 20 percent were lower than those of longitudinal specimens as might have been expected.

The discrepancy between the transverse and longitudinal values of the suspension cast material however, was not anticipated. No difference in the impact energies of the SC20L and SC40L specimens compared to the CC20L and CC40L specimens is discernible. Suspension cast material reduced 60 percent had a higher impact toughness than the corresponding conventionally cast material but this trend was reversed in the case of material reduced 80 percent.

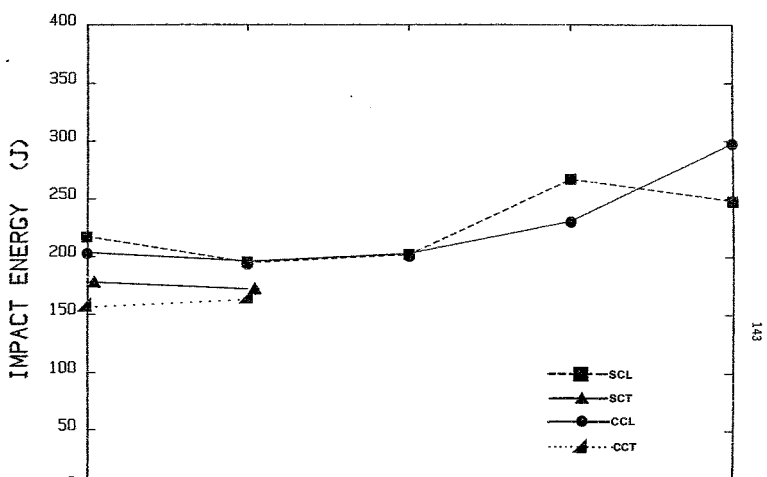

FIGURE 76 - Impact Energies of Conventionally Cast and Suspension Cast Material in the Longitudinal and Transverse Directions after Hot Deformation

The impact energies of both the conventionally cast and suspension cast materials increased with increasing amount of deformation. The reduced impact energy of the SC80L specimens was probably due to the high N_2 content of the ingot (see Table VII).

Although it is difficult to draw firm conclusions from a comparison of the results obtained with the two types of specimens it is clear that microchilling had no detrimental effects on impact properties. On the contrary, there are indications that this treatment improved impact strength (Figure 76).

4.5 Tensile Properties

Specimens taken from conventionally and suspension cast ingots after different amounts of deformation were tested under comparable conditions. Specimens from suspension cast material exhibited a higher yield stress and UTS. Typical curves of nominal stress against time and nominal stress against nominal strain for the SC80L and CC80L specimens are shown in Figures 77 and 78 respectively. Similar curves were obtained with material in the as cast condition and after 20, 40 and 60 percent reduction.

The results of the tensile tests are summarised in Table XII and presented graphically in Figures 79, 80, 81 and 82.

A significant difference in the ductility, as measured by percentage reduction in area and percentage elongation, between the suspension cast and conventionally cast specimens is apparent. The difference is more prominent than the differences in toughness as measured with the impact tests. The ductility of the suspension cast specimens in both the longitudinal and transverse directions are consistently higher than those of the conventionally cast specimens.

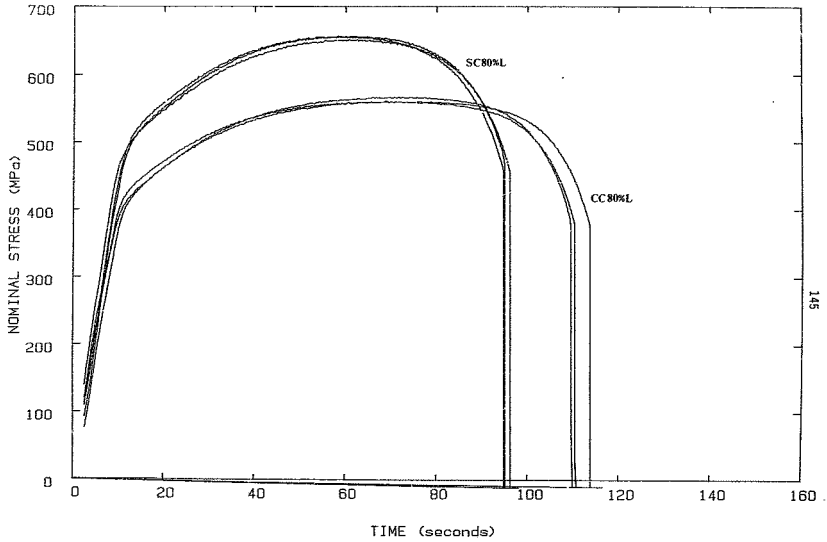

FIGURE 77 - Tensile Stress-Time Curves for Conventionally Cast and Suspension Cast Material in the Longitudinal Direction after 80 Percent Hot Deformation

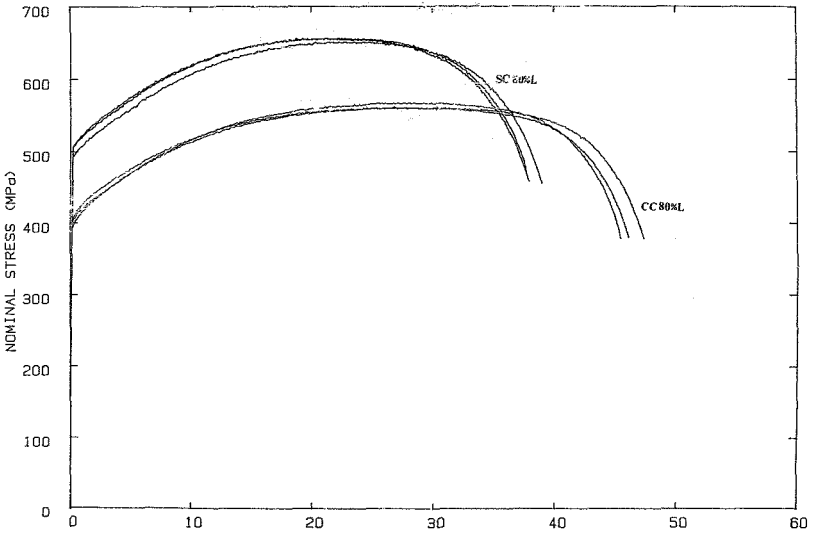

FIGURE 78 - Nominal Stress-Strain Curves for Longitudinal Specimens of Conventionally and Suspension Cast Materials after 80 Percent Hot Deformation

TABLE XII - Tensile Test Results

Specimen Code	Red. in Area (%)	Elongation (%)	Y.S. (MPa)	UTS (MPa)
CC0L	36	26	225	440
CC0T	58	43	215	426
CC20L	52	30	267	457
CC20T	45	23	284	389
CC40L	49	30	341	495
CC40T	57	28	271	450
CC60L	65	39	360	463
CC60T	65	27	356	436
CC80L	76	47	400	563
SC0L	62	51	226	468
SC0T	72	47	220	456
SC20L	64	40	420	564
SC20T	68	41	329	497
SC40L	72	43	396	573
SC40T	69	44	358	546
SC60L	74	46	410	576
SC60T	68	42	395	537
SC80L	76	36	502	655

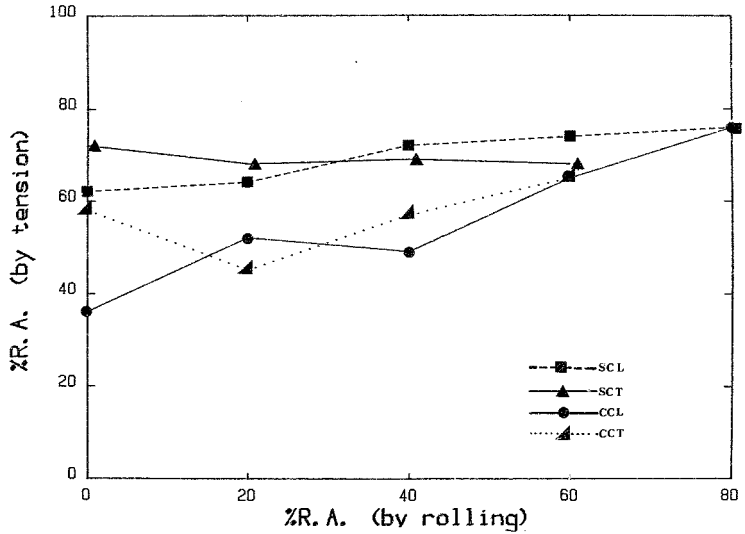

FIGURE 79 - Percentage Reduction in Area Obtained in the Tensile Tests for Conventionally Cast and Suspension Cast Materials Tested in the Longitudinal and Transverse Orientations after Hot Deformation

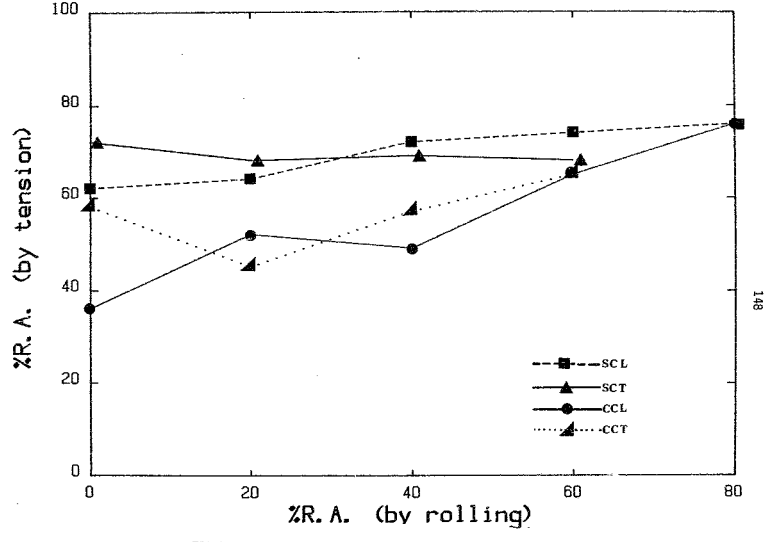

FIGURE 79 - Percentage Reduction in Area Obtained in the Tensile Tests for Conventionally Cast and Suspension Cast Materials Tested in the Longitudinal and Transverse Orientations After Hot Deformation

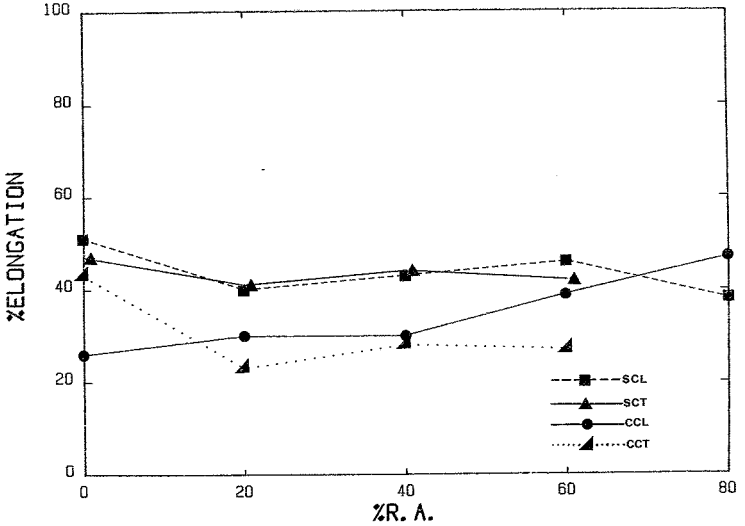

FIGURE 80 - Percentage Elongation Obtained in the Tensile Tests for Conventionally Cast and Suspension Cast Materials Tested in the Longitudinal and Transverse Orientations after Hot Deformation

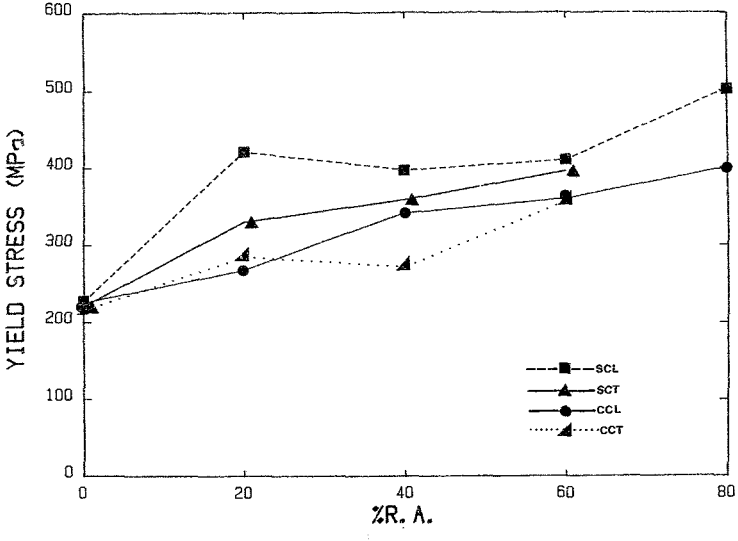

FIGURE 81 - Yield Stress Obtained in the Tensile Tests for Conventionally Cast and Suspension Cast Materials Tested in the Longitudinal and Transverse Orientations after Hot Deformation

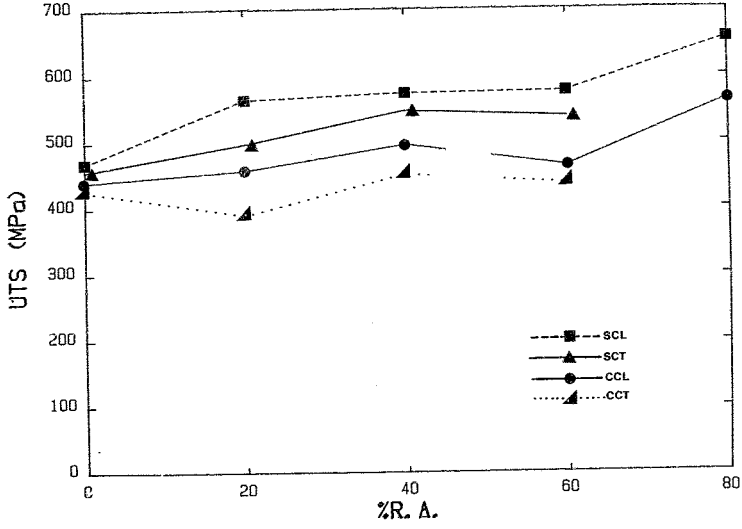

FIGURE 82 - UTS Obtained in the Tens[illegible]sts for Conventionally Cast and Suspension Cast [illegible]erials Tested in the Longitudinal and Transver[illegible]e Orientations after Hot Deformation

The general trend for both suspension and conventionally cast specimens is again one of increasing ductility with increasing amounts of deformation. The ductility of the SC80L specimens is much lower than the general trend of increasing ductility would tend to suggest (Figure 79). This could be due to the higher N_2 content of the SC80 material.

The ductilities of the longitudinal and transverse suspension cast specimens are, as one would expect for an equiaxed structure, very similar. The ductility of the CCOT specimen was unexpectedly higher than that of the CCOL specimen. If the ductility is considered in terms of percentage elongation, a difference between the conventionally cast longitudinal and transverse specimens is discernible, but not if the ductility is considered in terms of percent reduction in area.

The yield stress and UTS of the suspension cast specimens are higher than those of the conventionally cast specimens. Except in the case of the material cast conventionally and reduced by 20 percent, the longitudinal specimens had higher strengths than the transverse specimens. Furthermore, as the amount of deformation increased the strength of the material increased.

To conclude, suspension casting improved both the tensile strength and ductility of the material. These properties are also increased by increasing amounts of deformation and are dependent on the orientation of the specimen with respect to the rolling direction.

4.6 Hardness Tests

The hardness of the suspension cast ingots was higher than that of the conventionally cast ingots as can be seen from the results of the hardness tests which are summarised in Table XIII and presented in Figure 83.

TABLE XIII - Hardness Test Results

Percentage Reduction in Area	Average Hardness (HV_{30})			
	Conventional Cast		Suspension Cast	
	Longitudinal	Transverse	Longitudinal	Transverse
0 (as cast)	137,5	121,0	186,5	143,4
20	168,5	154,0	238,4	201,0
40	176,4	163,7	224,3	205,6
60	201,6	168,5	258,2	229,3
80	223,0	189,8	265,2	243,2

For both suspension cast and conventionally cast ingots, there was a difference in hardness between the longitudinal and transverse specimens. Also, there is an increase in hardness and therefore strength with increasing amounts of deformation.

4.7 Compression Tests

Typical examples of notches which were rated according to the extent and depth of cracking are shown in Figures 84 to 89. No significant buckling or barrelling of specimens was observed during testing and the compressed CC80L and SC80L series of specimens are shown in Figures 90 and 91 respectively. On the whole, the conventionally cast specimens showed greater frequency and severity of cracking. A visual appreciation of what is meant by the crack ratings 0 to 5 can be obtained from a study of Appendix A. The results of the compression tests are summarised in Table XIV and presented graphically in Figures 92, 93, 94, 95 and 96.

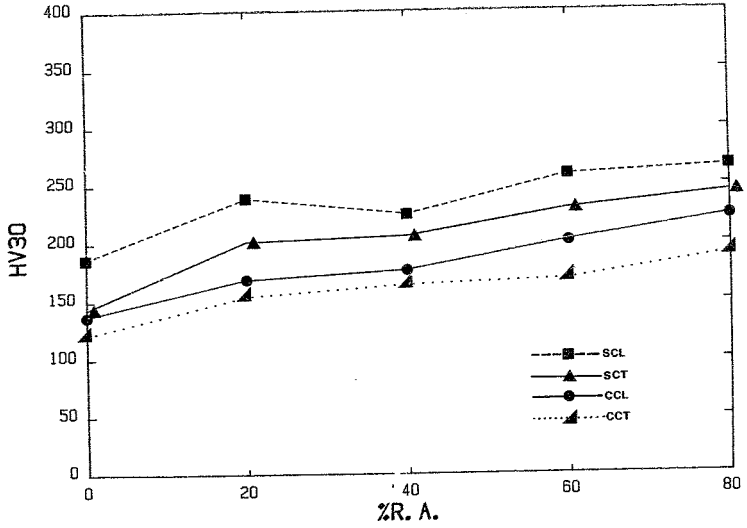

FIGURE 83 - Vickers Hardness (HV_{30}) for Conventionally Cast and Suspension Cast Materials Tested in the Longitudinal and Transverse Orientations after Hot Deformation

Except for the material reduced by 20 percent, the conventionally cast transverse specimens had the highest notch rating followed by the conventionally cast longitudinal specimens, the suspension cast transverse specimens and the suspension cast longitudinal specimens in that order. Hence, the formability of the materials follows the reverse order with the suspension cast material having consistently better formability. The only deviation in the material reduced by 20 percent was that the conventionally cast transverse specimens appeared to have better formability than the longitudinal specimens. However, in general the suspension cast material had higher formability.

With increasing percentage reduction in height there appeared to be a trend towards higher notch rating as would be expected but there were frequent exceptions. No trend between the notch rating and increased deformation by rolling was discernible.

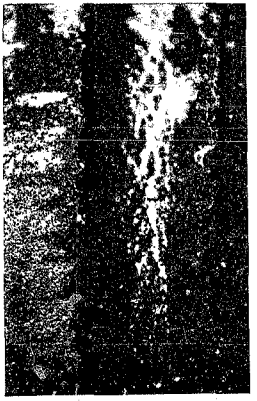

FIGURE 84 - Notch without Cracks Allocated a Rating of 0

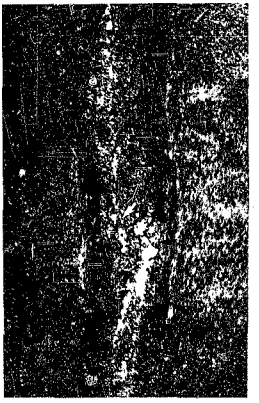

FIGURE 85 - Notch with an Isolated Crack Allocated a Rating of 1

FIGURE 84 - Notch without Cracks Allocated a Rating of 0

FIGURE 85 - Notch with an Isolated Crack Allocated a Rating of 1

FIGURE 86 - Notch with Extended Cracks Allocated a Notch Rating of 2

FIGURE 87 - Notch with Several Deep Interconnected Cracks Allocated a Notch Rating of 3

FIGURE 88 - Notch with increased Incidence of Cracking and Greater Crack Depth Allocated a Rating of 4

FIGURE 89 - Notch with Severe Rupture Allocated a Rating of 5

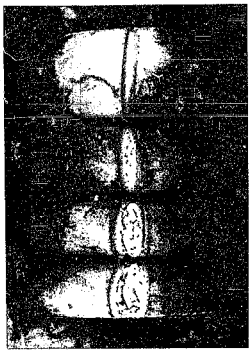

FIGURE 90 - The Compressed Specimens of CC80L

FIGURE 91 - The Compressed Specimens of SC80L

TABLE XIV - Compression Test Results

Specimen Code	Red. in Height (%)	Notch Rating	Specimen Code	Red. in Height (%)	Notch Rating
CC0L	50	1	SC0L	50	0
	60	2		60	0
	70	4		70	2
	80	5		80	1
CC0T	50	5	SC0T	50	1
	60	5		60	1
	70	3		70	1
	80	5		80	4
CC20L	50	0	SC20L	50	0
	60	1		60	0
	70	2		70	0
	80	5		80	2
CC20T	50	0	SC20T	50	0
	60	3		60	3
	70	4		70	3
	80	5		80	4
CC40L	50	0	SC40L	50	0
	60	3		60	1
	70	5		70	3
	80	5		80	4
CC40T	50	1	SC40T	50	1
	60	4		60	1
	70	5		70	5
	80	5		80	5
CC60L	50	2	SC60L	50	0
	60	2		60	1
	70	5		70	3
	80	5		80	3
CC60T	50	0	SC60T	50	1
	60	2		60	2
	70	5		70	4
	80	5		80	5
CC80L	50	1	SC80L	50	0
	60	3		60	3
	70	5		70	5
	80	5		80	5

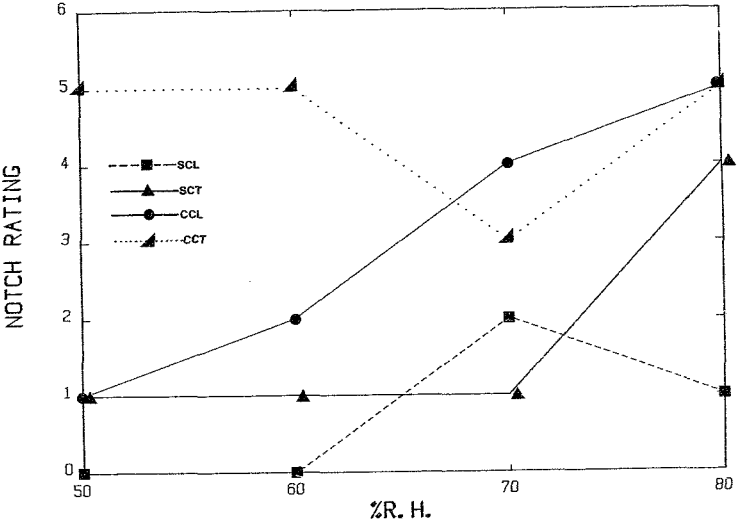

FIGURE 92 - Notch Ratings for Conventionally Cast and Suspension Cast Material in the As Cast Condition after Varying Amounts of Compression (% RH). The Specimens were Tested in the Longitudinal and Transverse Orientations

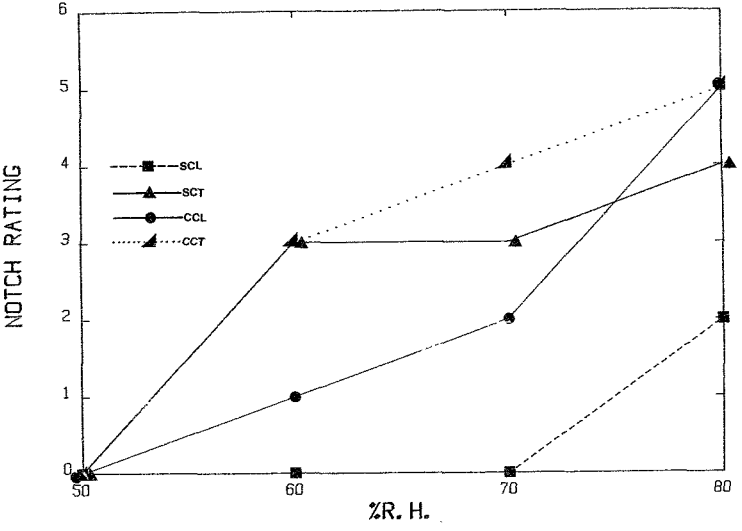

FIGURE 93 - Notch Ratings for Conventionally Cast and Suspension Cast Material Reduced by 20 Percent in Area. The Specimens were Compressed by Varying Amounts (% RH) in the Longitudinal and Transverse Orientations

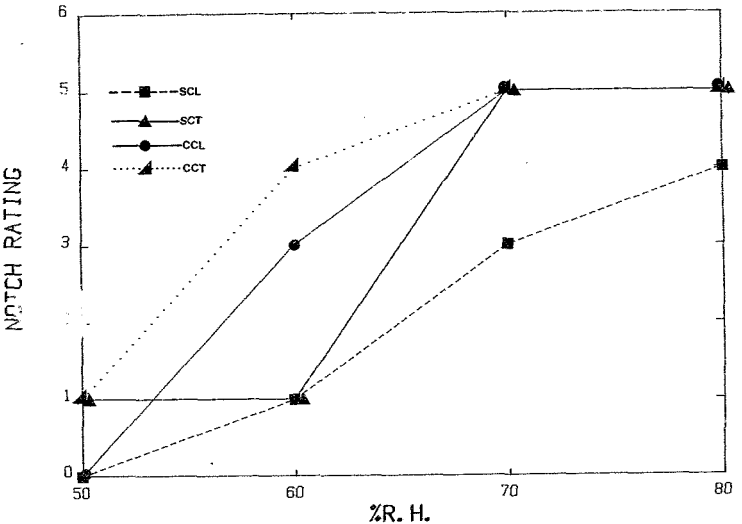

FIGURE 94 - Notch Ratings for Conventionally Cast and Suspension Cast Material Reduced by 40 Percent in Area. The Specimens were Compressed by Varying Amounts (% RH) in the Longitudinal and Transverse Orientations

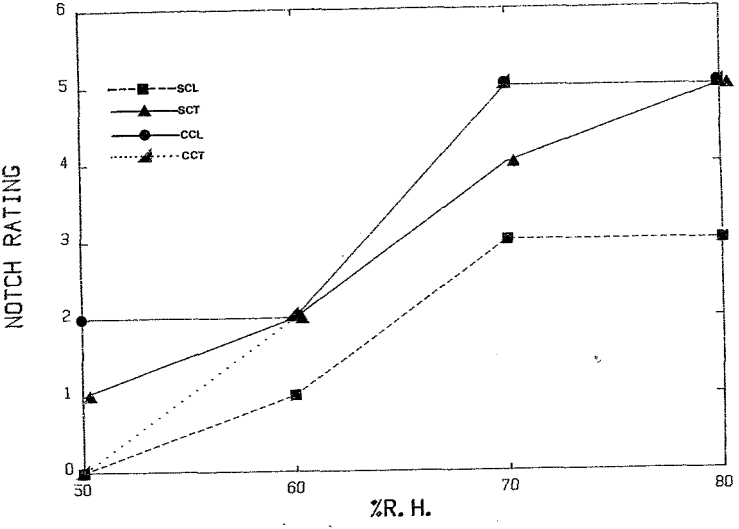

FIGURE 95 - Notch Ratings for Conventionally Cast and Suspension Cast Material Reduced by 60 Percent in Area. The Specimens were Compressed by Varying Amounts (% RH) in the Longitudinal and Transverse Orientations

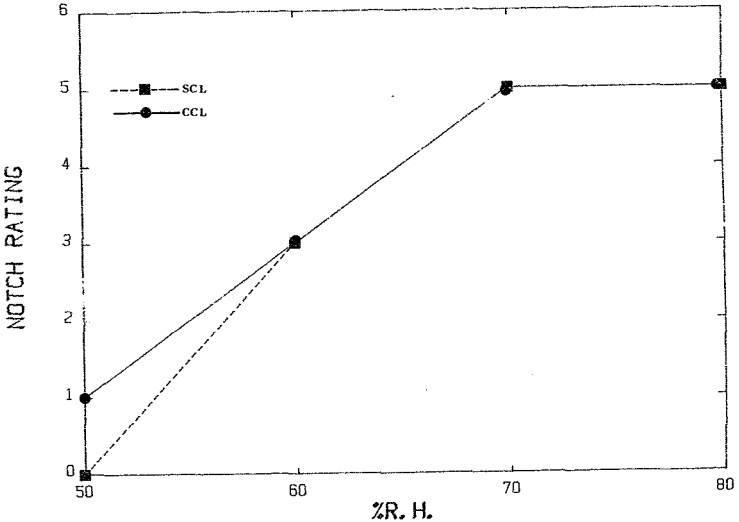

FIGURE 96 - Notch Ratings for Conventionally Cast and Suspension Cast Material Reduced by 80 Percent in Area. The Specimens were Compressed by Varying Amounts (% RH) in the Longitudinal Orientation

4.8 Fractography

Scanning electron microscopic examination of the tensile fracture surfaces revealed no differences in the fracture modes of the conventional and suspension cast specimens. All specimens failed in a typical cup and cone fracture mode (Figure 97). The fracture surfaces of both the suspension cast and conventionally cast specimens, when examined at high magnification, were found to consist entirely of dimples nucleated around non-deformable precipitates (Figures 98 and 99). This indicates that failure occurred by a mechanism of micro-void growth and coalescence characteristic of ductile materials. Analyses of the precipitates by the EDS system showed them to have a higher chromium concentration than the matrix (compare Figures 100 and 73).

The first CC40L specimen tested failed in an abnormal fashion as can be seen from Figure 101. The fracture surface consisted of regions which had failed by shear and abnormal regions where it appeared that some type of decohesion had occurred. A detailed view of a ductile region is shown in Figure 102 while Figure 103 shows a detailed view of ar area of apparent decohesion. It is evident from Figure 103 that this fracture is practically featureless suggesting little response to the breaking stresses. It should be borne in mind that specimens CC40L showed a network of intergranular precipitates (Section 4.3). This supports the view that failure took place partly by a type of decohesion.

SEM x20

SEM x20

FIGURE 97 - The Cup-and-Cone Tensile Fracture Surface Obtained with Specimen SC60L

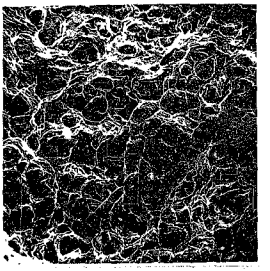

SEM x500

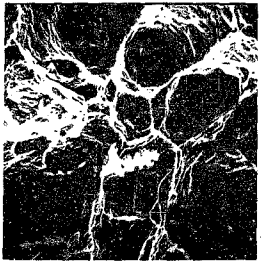

SEM x2000

FIGURE 98 - A Typical Fracture Surface of a Conventionally Cast Specimen at Two Magnifications (Specimen CCOL)

SEM x500

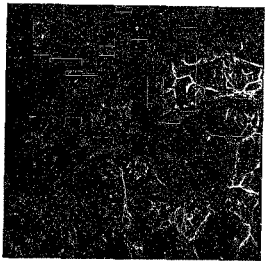

SEM x2000

FIGURE 99 - A Typical Fracture Surface of a Suspension Cast Specimen at Two Magnifications (Specimen SC80L)

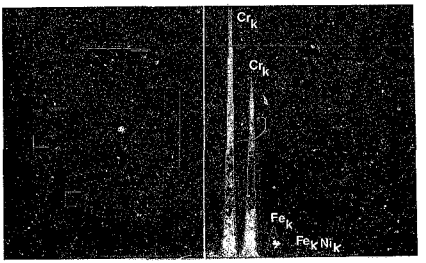

FIGURE 100 - Spectrum of Typical Precipitate found within a Dimple

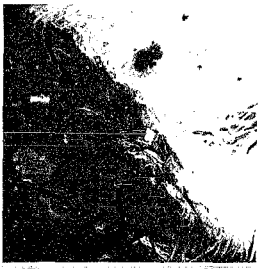

SEM x20

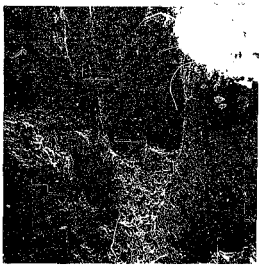

SEM x100

FIGURE 101 - Fracture Surface of Specimen CC4QL1 at Two Magnifications Showing Areas of Ductility and "Pits"

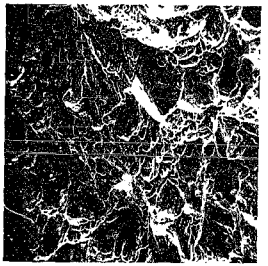

SEM x1000

FIGURE 102 - Ductile Dimpled Areas in Specimen CC40L1

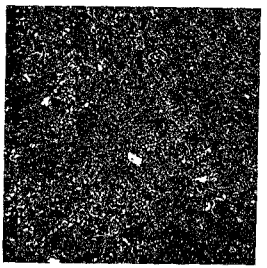

SEM x1000

FIGURE 103 - Surface of One of the "Pits" Present in Specimen CC40L1

5. DISCUSSION

5.1 Mechanism of the Suspension Casting Process

For nucleation to occur ahead of a solid/liquid interface, a specific quantity of energy must be provided. This energy may be derived from both supercooling, constitutional or thermal, and a region of high energy i.e. a nucleation site such as the surface of a solid particle suspended in the liquid. Thus, in order to produce an equiaxed zone there should be :

1. Constitutional supercooling

2. Nucleation sites to take advantage of the supercooling and allow nucleation to occur ahead of the solid/liquid interface

3. A combination of 1 and 2.

Constitutional supercooling allows stable nuclei to form in the remaining liquid upon further cooling of the casting. The size of the crystals formed will be dependent upon the degree of constitutional supercooling and the effect of solute segregation upon the actual freezing point of the liquid.

When powders are added to the steel, the effect is to provide an internal chilling mechanism in the molten metal, thus lowering its temperature. The amount of powder required is dependent upon the level of the superheat and the thermal properties of the powder.

It would appear then that the mechanism of refining is such that constitutional supercooling on a macroscale can provide suitable conditions for the stability of nuclei ahead of the initial solidification front. The nuclei formed within the melt (including falling crystallites and the tips of dendrites dislodged and transported by convection or turbulence) will then

be able to survive. Extraneous particles may provide the substrates for stable nuclei to form; in addition, these extraneous particles could be acting as microchills within the melt, allowing an envelope of constitutionally supercooled liquid to be formed around them and hence providing sites for growth of the solid. Under these conditions, showers of crystallites can inhibit the advance of columnar grains and result in a casting with a substantial equiaxed zone.

In order to see which of these two possible mechanisms is the more probable, a simple thermal energy balance (considering no heat loss to the surroundings) can be performed. This will allow the amount of powder required to decrease the temperature of the molten metal to the liquidus temperature of the steel, to be calculated to a first approximation.

In this study the metal was poured from a temperature of 1750 °C and the liquidus temperature of AISI type 310 stainless steel has been quoted as 1455 °C.[128]

Hence,

$$n\,(H^0_T - H^0_{298})_{Fe} + n\,\Delta H^0_f + n\,H_m^m + m\int_{T^0_B}^{T^0} Cp_{310}\,dT = 0 \qquad \ldots\ (15)$$

where n is the number of moles of microchilling powder added to m moles of steel at a pouring temperature of T^0_B. T^0 is the final temperature of the bath. $(H^0_T - H^0_{298})$ is the enthalpy increment in raising the powder from room temperature to T^0, ΔH^0_f is the enthalpy of fusion for the powder and H_m^m the enthalpy of mixing. The heat capacity, Cp, of AISI type 310 has

been reported as 6,66 cal/mol K.[128] The enthalpy of fusion of Fe is 3560 cal/g mol[129] and as we are considering an ideal situation, the enthalpy of mixing may be approximated to zero.

Substituting into equation 15,

$$\underset{g.mol^{-1}Fe}{\frac{x}{56}} (H^0_{1728} - H^0_{298})Fe + \Delta H^0_{f,Fe} + \overset{m}{H}_{m,Fe}$$

$$= \underset{g.mol^{-1}310}{\frac{100-x}{55,4}} \times Cp_{310} \times (2023 - 1728)$$

becomes

$$\frac{x}{56} [13\,378,4 + 3560 + 0] = \frac{100-x}{55,4} [6,66 \times 295]$$

and x, the amount of powder required to decrease the temperature from 1750 °C to 1455 °C is found to be 10,49% by mass of the steel casting.

If only 10,49% by mass Fe powder was required to decrease the temperature of the steel from the casting temperature of 1750 °C to the liquidus temperature and only 2,5% by mass Fe powder was used, it can be concluded that by the time the solidification temperature was reached, all of the Fe powder would have melted and become an integral part of the casting. Hence, the role of the powder is primarily to act as a microchill and increase the amount of supercooling. Very few, if any, Fe powder particles will be present during solidification to act as sites at which heterogeneous nucleation can commence.

5.2 Feasibility of the Suspension Casting Process

In order to obtain a uniform distribution of particles in the casting it is necessary to maintain a constant rate of metal flow and to match the pouring rate with the rate of powder flow. This was achieved in this study by the use of a pouring basin and a fixed diameter orifice to control the powder flow rate. The flowrate of the powder was to all intents constant at any given time during pouring but should larger amounts of powder be used, the effect of powder head in the funnel should be controlled. This could be accomplished by utilising a vibratory feeder or a worm screw for the feeding of the powder.

Vigorous turbulence at the entry of the mould cavity would also improve mixing and any further studies should utilise an ingot mould with a multi-stage cross sectional change in the runner to improve the turbulence and hence the efficiency of mixing. Alternatively, the powder could be injected into the melt under pressure. A more effective means of improving mixing would allow more powder to be added (only 2,5% powder was added and it has been shown that up to 10,5% could theoretically be added). This in turn should promote an even greater equiaxed zone.

In this study the conditions of a feasible application of the suspension casting process were determined empirically with a number of trial castings. The ingot macrostructure was successfully changed from a fully columnar structure to one with a large equiaxed zone. The equiaxed grain size was refined and a smaller primary pipe obtained. Hence, the control of the macrostructure via the suspension casting process was successfully demonstrated.

A thermal balance for the process has been performed. However, a theoretical heat transfer model, considering forced and natural convection, radiation and conduction in suspension castings with

regard to size, percentage additions and thermal properties of different powders should be determined.

No detrimental effects of suspension casting were observed during hot working and the microstructure of the hot worked suspension cast ingots showed a significantly finer grain size and a smaller number of interdendritic precipitates than the conventionally cast material. This suggests that segregation in the suspension cast material was minimal.

The improved macrostructure and refined grain size of the suspension cast ingots can be expected to improve both the mechanical properties and the hot workability of the material.

5.3 Effect of the Suspension Casting Process on the Mechanical Properties

The size and orientation of the grains clearly had a profound influence on the mechanical properties of AISI type 310 strainless steel.

The hardness and the strength of the suspension cast material were significantly higher than those of the conventionally cast material. The average hardness (HV_{30}) of the as cast material in the longitudinal direction increased from 137,5 for conventionally cast material to 186,5 for suspension cast material. The yield strength in the longitudinal direction increased from 400 MPa for conventionally cast material reduced by 80 percent in area to 602 MPa for suspension cast material reduced by 80 percent in area. For the same specimens the UTS increased from 563 MPa to 668 MPa.

This increase in the hardness and yield stresss of the material is due primarily to the decrease in grain size of the material obtained with suspension casting and hot deformation. The decrease in grain size results in an effective increase in the amount of grain boundaries which can act as barriers to dislocation motion. Also, it has been observed experimentally[62] that the dislocation density is an inverse function of grain size i.e. the smaller the grain size, the higher the dislocation density and hence the higher the yield stress and hardness of the material.

The increase in toughness of the material was not conclusive. The differences in charpy impact values were minimal (14J for as cast material and only IJ for material reduced by 20 and 40 percent). The results, however, indicate clearly that suspension casting had no detrimental effects on the impact values. A significant difference in the ductility of the two materials, as measured by percentage reduction in area and percentage elongation was however apparent. The percentage reduction in area in the longitudinal direction for the as cast material increased from 36 percent for conventionally cast specimens to 62 percent for suspension cast specimens. For the same specimens the percentage elongation increased from 26 percent to 51 percent. The reason for this anomalous behaviour of the two tests is to be found in their differing strain rates. The charpy test is done using impact loading whereas in the tensile test a much lower cross head speed of 0,1 $mm.s^{-1}$ was used. Hence, the tensile test is far more structure sensitive.

The anisotropic behaviour of conventionally cast material has been confirmed by the present work. However, the anticipated isotropic behaviour of suspension cast material was not observed and the material appeared to behave anisotropically. No explanation for this unexpected behaviour has been proposed.

This increase in the hardness and yield stresss of the material is due primarily to the decrease in grain size of the material obtained with suspension casting and hot deformation. The decrease in grain size results in an effective increase in the amount of grain boundaries which can act as barriers to dislocation motion. Also, it has been observed experimentally[62] that the dislocation density is an inverse function of grain size i.e. the smaller the grain size, the higher the dislocation density and hence the higher the yield stress and hardness of the material.

The increase in toughness of the material was not conclusive. The differences in charpy impact values were minimal (14J for as cast material and only 1J for material reduced by 20 and 40 percent). The results, however, indicate clearly that suspension casting had no detrimental effects on the impact values. A significant difference in the ductility of the two materials, as measured by percentage reduction in area and percentage elongation was however apparent. The percentage reduction in area in the longitudinal direction for the as cast material increased from 36 percent for conventionally cast specimens to 62 percent for suspension cast specimens. For the same specimens the percentage elongation increased from 26 percent to 51 percent. The reason for this anomalous behaviour of the two tests is to be found in their differing strain rates. The charpy test is done using impact loading whereas in the tensile test a much lower cross head speed of 0,1 $mm.s^{-1}$ was used. Hence, the tensile test is far more structure sensitive.

The anisotropic behaviour of conventionally cast material has been confirmed by the present work. However, the anticipated isotropic behaviour of suspension cast material was not observed and the material appeared to behave anisotropically. No explanation for this unexpected behaviour has been proposed.

5.4 Effect of Suspension Casting on Hot Workability

Hot compression tests were used to evaluate the effect of suspension casting on the hot workability of AISI type 310 stainless steel. In order to minimise the subjective nature of the test a crack rating system was utilised. This allowed a more objective assessment of the compression test results to be made.

The suspension cast specimens had consistently better formability. Both suspension cast and conventionally cast specimens appeared to behave anisotropically but the test procedure used was not sufficiently sensitive to allow any definite conclusions to be drawn in this respect.

It is not possible to draw a final conclusion on the effect of suspension casting on the hot workability by considering only the results of the hot compression tests. Further investigations such as the hot workability in tension and in torsion should also be performed. However, it can clearly be seen that suspension casting has a beneficial effect on the hot workability of the material as measured by compression tests.

6. CONCLUSIONS AND FUTURE WORK

i) The suspension casting process was used successfully to produce ingots of AISI type 310 stainless steel.

ii) Microchilling has a profound refining effect on the macrostructure of the material and on the microstructural level segregation appears to be decreased.

iii) Both the conventionally cast and microchilled material could be successfully hot worked to 80 percent reduction in area.

iv) The hardness and strength (σ_y and UTS) were improved by microchilling.

v) The toughness of the material as determined by the Charpy impact test was unaffected by microchilling but the ductility in tension increased significantly with microchilling.

vi) The fracture surfaces of both conventionally cast and microchilled materials indicated that failure occurred by a mechanism of micro-void coalescence and growth characteristic of ductile materials.

vii) The compressive hot workability of the material was improved by microchilling.

viii) Both the conventionally cast and microchilled material behaved in an anisotropic fashion.

ix) The results of this investigation show that suspension casting is a promising technique. However, more detailed investigations such as a theoretical heat transfer model should be determined.

APPENDIX A - Compression Specimens of the Suspension and Conventionally Cast Ingots Showing 50, 60, 70 and 80 Percent Deformation

FIGURE A1 : CCOL Compression Specimens

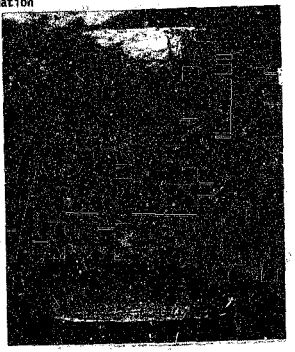

FIGURE A2 : SCOL Compression Specimens

FIGURE A3 - CCOT Compression Specimens

FIGURE A4 - SCOT Compression Specimens

FIGURE A5 : CC20L Compression Specimens

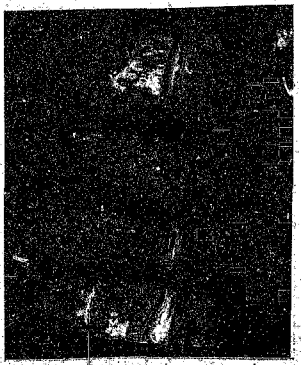

FIGURE A6 : SC20L Compression Specimens

FIGURE A7 - CC20T Compression Specimens

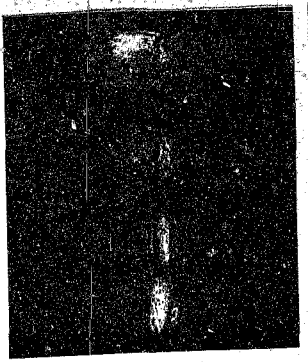

FIGURE A8 - SC20T Compression Specimens

FIGURE A9 : CC40L Compression Specimens

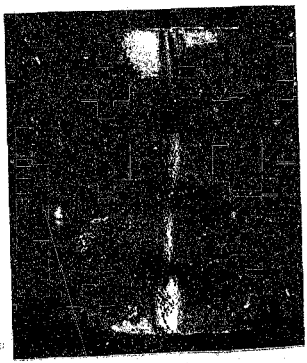

FIGURE A10 : SC40L Compression Specimens

FIGURE A11 - CC40T Compression Specimens

FIGURE A12 - SC40T Compression Specimens

FIGURE A13 : CC60L Compression Specimens

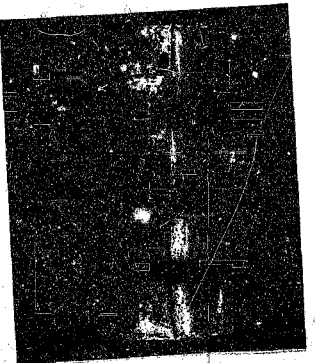

FIGURE A14 : SC60L Compression Specimens

FIGURE A15 - CC60T Compression Specimens

FIGURE A16 - SC60T Compression Specimens

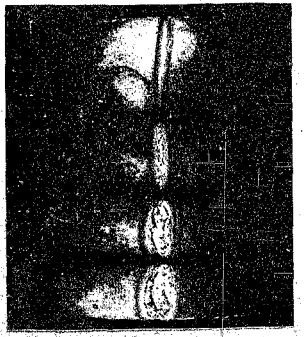

FIGURE A17: CC80L Compression Specimens

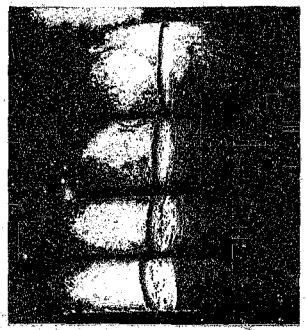

FIGURE A18 : SC80L Compression Specimens

REFERENCES

1. Chalmers, B. The Structure of Ingots, Journal of Australasian Institute of Metals, vol. 8, 1963, pp. 255-263.

2. Davies, G.J. Solidification and Casting, *Barking : Applied* Science Publishers Ltd., 1973.

3. Radhakrishna, K *and Seshan*, S. Internal Chills - Another Tool to Improve Casting Properties, Castings, Jan. 1980. *pp. 23-26.*

4. Smithells, C.J. ed., Metals Reference Book, *5th ed. Boston* : Butterworths, 1976.

5. Tiller, W.A., Jackson, K.A., *Rutter*, J.W. and Chalmers, B. The Redistribution of Solute Atoms During the *Solidification of Metals*, Acta Metallurgica, vol. 1, July 1953, pp. 428 - 437.

6. Chalmers, B. Principles of Solidification, New York : John Wiley, 1964.

7. Flemings, M.C. Solidification Processing, New York : McGraw-Hill, 1974.

8. Walker, J.L. Liquid Meta' and Solidification, Cleveland : American Society for Metals, 1958.

9. Bower, T.F. and Flemings, *M.C. Formation* of the Chill Zone in Ingot Solidification, Transactions of the Metallurgical Society of AIME, *vol.* 239, Feb. 1967, pp. 216-219.

10. Jackson, K.A., Hunt, J.D., Uhlmann, D.R. and Seward, T.P. On the Origin of the Equiaxed Zone in Castings, Transactions of the Metallurgical Society of AIME, *vol.* 236, Feb. 1966, pp. 149-158.

11. Walton, *D. and Chalmers*, B. The Origin of the Preferred Orientation in the Columnar Zone of Ingots, Transactions of the Metallurgical Society of AIME, vol. 215, June 1959, pp. 447-456.

12. Hellawell, A. and Herbert, P.M. The Development of Preferred Orientations during the Freezing of Metals and Alloys, Proceedings of the Royal Society, vol. A269, 1962, pp. 560-573.

13. Biloni, H. Relationship Between Segregation Substructures and Casting Structures, In : The Solidification of Metals, ISI P110, London : Iron and Steel Institute, 1968, pp. 74-82.

14. Morando, R., Biloni, H., Cole, G.S. and Bolling, G.F. The Development of Macrostructure in Ingots of Increasing Size, Metallurgical Transactions, vol. 1, May 1970, pp. 1407-1412.

15. Winegard, W.C. and Chalmers, B. Supercooling and Dendritic Freezing in Alloys, Transactions of the American Society for Metals, vol. 46, 1954, pp. 1214-1224.

16. Campbell, J. and Bannister, J.W. Grain Refinement of Electroslag Remelted Iron Alloys, Metals Technology, vol. 2, Sept. 1975, pp. 409-415.

17. Thomas, P.M. and Spittle, J.A. The Influence of Constitutional Convection during Solidification on Equiaxed Grain Formation in Large Ingots, Journal of the Institute of Metals, vol. 99, 1971, pp. 167-168.

18. Southin, R.T. Nucleation of the Equiaxed Zone in Cast Metals, Transactions of the Metallurgical Society of AIME, vol. 239, Feb. 1967, pp. 220-225.

19. Engler, S. and Ellerbrok, R. On the Formation of the Equi-axed Zone in Castings, In : Nieswaag, H. and Shut, J.W. Eds. Proceedings of Symposium on 'Quality Control of Engineering Alloys and the Role of Metals Science', Delft, 1977, pp. 121-129.

20. Ohno, A., Motegi, T. and Soda, H. Origin of the Equiaxed Crystals in Castings, Transactions of the Iron and Steel Institute of Japan, vol. 11, 1971, pp. 18-23.

21. Ohno, A. and Motegi, T. Formation Mechanism of Equiaxed Zones in Cast Metals, AFS International Cast Metals Journal, vol. 2, March 1977, pp. 28-36.

22. Murakami, K. and Okamoto, T. Formation of Equiaxed Zone in Castings, Metal Science, vol. 18, Feb. 1984, pp. 103-111.

23. Beeley, P.R. Foundry Technology, London : Butterworth Group, 1972.

24. El-Mahallawy, N.A. and Taha, M.A. Casting Process Developments for Improving Quality, Journal of Metals, vol. 37, No. 9, Sept. 1985, pp. 42-46.

25. Hellawell, A. Heterogeneous Nucleation and Grain Refinement in Aluminium Castings, In : Solidification and Casting of Metals, Proceedings of an International Conference on Solidification, London : The Metals Society, 1979, pp. 161-168.

26. Lane, D.H., Cunningham, J.W. and Tiller, W.A. The Application of Ulstrasonic Energy to Ingot Solidification, Transactions of the Metallurgical Society of AIME, vol. 218, Dec. 1960. pp. 985-994.

27. Abramov, O.V., Izotov, A.N., Astashkin, Yu. S., Kryuchkova, G.A., Manokhin, A.I., Markov, A.V. and Taran, V.P. Ultrasonic Treatment of Stream of Molten Metal, Steel in the USSR, vol. 15, April 1985, pp. 168-170.

28. Crossley, F.A., Fisher, R.D. and Metcalfe, A.G. Viscous Shear as an Agent for Grain Refinement in Cast Metal, Transactions of the Metallurgical Society of AIME, vol. 221, April 1961, pp. 419-420.

29. Wojciechowski, S. and Chalmers, B. The Influence of Mechanical Stirring on the Columnar to Equiaxed Transition in Aluminium-Copper Alloys, Transactions of the Metallurgical Society of AIME, vol. 242, April 1968, pp. 690-698.

30. Uhlmann, D.R., Seward, T.P. and Chalmers, B. The Effect of Magnetic Fields on the Structure of Metal Alloy Casting, Transactions of the Metallurgical Society of AIME, vol. 236, April 1966, pp. 527-531.

31. Tzavaras, A.A. and Brody, H.D. Electromagnetic Stirring and Continuous Casting - Achievements, Problems, and Goals, Journal of Metals, vol. 36, no. 3, March 1984, pp. 31-37.

32. Langenberg, F.C., Pestel, G. and Honeycutt, C.R. Grain Refinement of Steel Ingots by Solidification in a Moving Electromagnetic Field, Transactions of the Metallurgical Society of AIME, vol. 221, Oct. 1961, pp. 993-1001.

33. Johnston, W.C., Kotler, G.R., O'Hara, S., Ashcom, H.V. and Tiller, W.A. Grain Refinement via Electromagnetic Stirring During Solidification, Transactions of the Metallurgical Society of AIME, vol. 233, Oct. 1965, pp. 1856-1860.

34. Birat, J.P. and Chonê, J. Electromagnetic Stirring on Billet, Bloom, and Slab Continuous Casters : State of the Art in 1982, Ironmaking and Steelmaking, vol. 10, no. 6, 1983, pp. 269-281.

35. Orehoski, M.A. Improved Crystal Structure in Cast Steel Ingots, Journal of Metals, vol. 21, no. 5, May 1969, pp. 41-48.

36. Campbell, J. Effects of Vibration during Solidification, International Metals Review, vol. 26, no. 2, 1981, pp. 71-108.

37. Biloni, H. Solidification, In : Cahn, R.W. and Hassen, P. ed. Physical Metallurgy, 3rd ed. Amsterdam : North-Holland Physics Publishing, 1983, pp. 478-579.

38. Rapoport, D.B. Aerofoil Investment Castings for the Mach-3 Engine, Foundry Trade Journal, Feb. 1964, pp. 169-183.

39. Bryant, M.D. and Moore, A. Mould Coatings of Zinc/Ground Coke or Cobalt to Prevent Hot Checking in Malleable Iron Castings, The British Foundryman, vol. 64, June 1971, pp. 215-229.

40. Glasson, E.L. and Emley, E.F. Heterogeneous Nucleation in the Solidification of Aluminium and Magnesium Alloys, In : The Solidification of Metals, ISI P110, London : Iron and Steel Institute, 1968, pp. 1-9.

41. De Ross, A.B. and Mondolfo, L.E. Metallurgical Aspects of Casting Aluminium Alloys, In : Pampillo, C.A., Biloni, H. and Emburg, D.E. ed. Aluminium Transformation Technology and Applications, Proc. Conf., Ohio : American Society for Metals, 1980.

42. Perepezko, J.H. and LeBeau, S.E. Nucleation of Aluminium during Solidification, In : Pampillo, C.A. Biloni, H., Mondolfo, L. and Sacchi, F. ed. Aluminium Transformation Technology and Applications - 1981, Proc. Conf. Ohio : American Society for Metals, 1982.

43. Arnberg, L., Bäckerud, L. and Klang, H. Grain Refinement of Aluminium, Metals Technology, vol. 3, Jan. 1982, pp. 1-17.

44. Bäckerud, L. How Does a Food Grain Refiner Work ?, Light Metal Age, vol. 41, Oct. 1983, pp. 6-12.

45. Maxwell, I. and Hallawell, A. An Analysis of the Peritectic Reaction with Particular Reference to Al-Ti Alloys, Acta Metallurgica, vol. 23, Aug. 1975, pp. 901-909.

46. Sentarli, Y. Suspension Casting of a High Chromium White Iron, M.Sc. Dissertation, University of the Witwatersrand, Johannesburg, 1985.

47. Ryzhikov, A.A., Chudner, R.V., Gavrilin, I.V. and Starosel'skii, M.A. Improvements in the Suspension Casting Process, Russian Castings Production, Nov. 1975, pp. 457-458.

48. Zubov, L.A., Mandrik, E.A. and Tupchienko, V.I. Suspension Pouring of High-Speed Steel, Russian Castings Production, 1974, pp. 495-496.

49. Ryzhikov, A.A. and Mikryukov, R.A. Shaped Castings in Suspension Steel, Russian Castings Production, 1968, pp. 241-242.

50. Etelis, L.S., Blokhin, I.E., Plotnikov, V.A. and Babenko, V.G. Suspension Pouring of Iron, Russian Castings Production, Aug. 1975, p. 340.

51. Kostin, A.W., Schigol, V.B.M. and Bast, J. Influence of the Suspension Casting Process on the Properties of High-P Pig Iron, Giessereitechnik, Oct. 1977, pp. 317-318.

52. Panferov, V.N., Pisarev, I.E., Kim, G.P., Tokarev, V.M., Lusin, Yu. A. and Tyul'pin, A.V. Experience in the Automation of Suspension Pouring, Russian Castings Production, Nov. 1975. pp. 458-459.

53. Ivanov, V.T., Zubov, L.A., Grozov, D.P. and Kovshov, V.M. Influence of Micro-Chills on the Properties of Carbon Steel Castings, Russian Castings Production, 1974, pp. 29-30.

54. Bulavina, L.S., Milovanov, I.F. and Ageeva, N.A. Influence of Microchills on the Structure of Cast khN56VMTYu Heat-Resistance Alloy, Metal Science and Heat Treatment, vol. 26, nos. 5-6, May-June 1984, pp. 369-371.

55. Zatulovskii, S.S., Abramova, V.P. and Kuts, G.A. Effectiveness and Potentialities of the Use of Iron Powder for Improving the Quality of Steel, Poroshkovaya Metallurgiya, vol. 89, no. 5, May 1970, pp. 15-19, Translated by Consultants Bureau, a division of Plenum Publishing Co., 227 West 17th Street, New York, N.Y. 10011.

56. Borisov, E.S. and Larionov, A. Ya. Solidification Kinetics and Fluidity of Suspension-Poured Steel, Russian Castings Production, 1974, p. 71.

57. Sentarli, Y., Comins, N.R. and Koursaris, A. Suspension Casting of a High Chromium White Iron, The British Foundryman, Nov. 1985, pp. 459-464.

58. Pickering, F.B. Physical Metallurgy of Stainless Steel Developments, International Metals Reviews, vol. 21, Dec. 1976, pp. 227-268.

59. Peckner, D. and Berstein, I.M. Handbook of Stainless Steels, New York : McGraw Hill, 1977.

60. Sedriks, A.J. Corrosion of Stainless Steels, New York: John Wiley & Sons, 1979.

61. Ahlblom, B. and Sandström, R. Hot Workability of Stainless Steels : Influence of Deformation Parameters, Microstructural Components, and Restoration Processes, International Metals Reviews, vol. 27, no. 1, 1982, pp. 1-27.

62. Dieter, G.E. Mechanical Metallurgy, 2nd ed. Kogakushu : McGraw-Hill, 1981.

63. Ulvan, E. and Koursaris, A. Metal Formability in Bulk Deformation Processes, *Journal of Metals*, *vol.* 35, *no.* 12, Dec. 1983, pp. 20-26.

64. Ryan, N.D. and McQueen, H.J. Effects of Alloying Upon the Hot Workability of Carbon, Microalloyed, Tool, and Austenitic Stainless Steels, Journal of Mechanical Working Technology, vol. 12, no. 3, Feb. 1986, pp. 279-296.

65. Savvides, J. and Koursaris, A. The Hot Workability of Some Stainless Steels, Progress Report No. 1, Department of Metallurgy, University of the Witwatersrand, Johannesburg, Nov. 1982.

66. Rivlin, V.G. and Raynor, G.V. Critical Evaluation of *Constitution of Chromium-Iron-Nickel System*, International Metals Reviews, vol. 25, no. 1, 1980, pp. 21-38.

67. Kane, R.H. Structure and Hot Workability of AISI Type 310 Stainless Steel, In : Ballance, J.B. Ed. The Hot Deformation of Austenite, New York : American Institute of Mining, Metallurgical and Petroleum Engineers, 1977, pp. 457-498.

68. Stokowiec, Z., Holland, C.G., Dean, A.H. and Everill, A.C. Effect of Composition Balance and Trace Elements on the Hot Workability of Austenitic Stainless Steels, In : Stainless Steels, ISI P117, London : The Iron and Steel Institute, 1968, pp. 17-23.

69. Keown, S.R. Hot Ductility of Wrought Austenitic Stainless Steels - Part 1 : Effect of Alloying Additions, In : Sellars, C.M. and Davies, G.J. Eds. Hot Working and Forming Processes, London : The Metals Society, 1979, pp. 140-147.

70. Nicholson, A. and Moore, T.W. Selection of Optimum Conditions for Hot Rolling Stainless and Carbon Steels, In : Reheating for Hot Working, ISI P111, London : Iron and Steel Institute, 1968, pp. 46-55.

71. Harris, R. and Barnard, L. Experiences of Hot Shortness in the Forging of Certain Low-Alloy Steels, In : Deformation Under Hot Working Conditions, ISI P108, London : Iron and Steel Institute, 1968, pp. 167-177.

72. Post, C.B., Schoffstall, D.G. and Beaver, H.O. Influence of Rare-Earth Elements on Hot-Workability of Stainless Steels, Proceedings of Electric Furnace Steel Conference, 1951, pp. 115-133.

73. McQueen, H.J. and Jonas, J.J. Role of the Dynamic and Static Softening Mechanisms in Multistage Hot Working, American Society for Metals Journal of Applied Metal-working, vol. 3, no. 4, Jan. 1985, pp. 410-420.

74. Jonas, J.J., Sellars, C.M. and McG.Tegart, W.J. Strength and Structure under Hot-Working Conditions, Metallurgical Reviews, vol. 3., 1969, pp. 1-24.

75. Wray, P.J. Onset of Recrystallisation during the Tensile Deformation of Austenitic Iron at Intermediate Strain Rates, Metallurgical Transactions, vol. 6A, June 1975, pp. 1197-1203.

76. Norström, L.A. and Johansson, B. Hot Ductility - A Matter of Strain Rate, Scandinavian Journal of Metallurgy, vol. 11, 1982, pp. 139-142.

77. Rollason, E.C. Metallurgy for Engineers, 4th ed. London : Edward Arnold, 1980.

78. Reed-Hill, R.E. Physical Metallurgy Principles, 2nd Ed. Monterey : Brooks/Cole, 1973.

79. Dieter, G.E., Mullin, J.V. and Shapiro, E. Fracture of Inconel under Conditions of Hot Working, In : Deformation Under Hot Working Conditions, ISI P108, London : Iron and Steel Institute, 1968, pp. 7-13.

80. White, F.E. and Rossard, C. A Mechanism for the Fracture of Steel in High-Temperature Torsion and its Relation to Structural Changes, In : Deformation under Hot Working Conditions, ISI P108, London : Iron and Steel Institute, 1968, pp. 14-20.

81. Cotlingham, D.M. The Hot Workability of Low-Carbon Steels, In : Deformation Under Hot Working Conditions, ISI P108, London : Iron and Steel Institute, 1968, pp. 145-156.

82. Honeycombe, R.W.K. The Plastic Deformation of Metals, 2nd ed. London : Edward Arnold, 1984.

83. Sellars, C.M. and McG.Tegart, W.J. Hot Workability, International Metallurgical Reviews, vol. 17, 1972, pp. 1-24.

84. Honeycombe, R.W.K. Steels-Microstructure and Properties, London : Edward Arnold, 1981.

85. Gittens, A., Hinton, L.G. and McG. Tegart, W.J. Ductility of Steels in Hot Working, Manufacturing Engineering and Management, vol. 2, 1973, pp. 199-207.

86. Coward, M.D., Richardson, G.J. and Sellars, C.M. Influence of Inclusions on Hot Ductility of Fe-25Ni, Metals Technology, vol. 3, Dec. 1976, pp. 550-555.

87. Henning, H.J. and Boulger, F.W. Tests for Hot Workability, In : Smith, P.H. ed. Mechanical Working of Steel 1, 5th Technical Conference of AIME, vol. 21, New York : Gordon and Breach, 1964.

88. Ulvan, E. The Effect of Hot Rolling and Grain Size on the Cold Bulk Formability of Stainless Steels, PhD Thesis in preparation, University of the Witwatersrand, Johannesburg, 1986.

89. Ulvan, E. and Koursaris, A. The Effect of Grain Size on the Bulk Formability of Austenitic Stainless Steel Types 304 and 316, In press, 1986.

90. Hazzledine, P.M. and Newburg, D.E. Role of Grain Boundaries in Superplasticity, In : Chadwick, G.A. and Smith, D.A. ed. Grain Boundary Structure and Properties, London : Academic Press, 1976, pp. 235-264.

91. Duckworth, W.E. and Baird, J.D. Mild Steels, Journal of the Iron and Steel Institute, vol. 207, June 1969, pp. 854-871.

92. Datta, K.P. and Wood, W.E. On the Relationship of Toughness, Fracture Initiation Energy, and Specimen Deflection in Charpy Tests of 4340 Steel, ASTM Journal of Testing and Evaluation, vol. 9, no. 2, March 1981, pp. 111-117.

93. Bywater, K.A. and Gladman, T. Influence of Composition and Microstructure on Hot Workability of Austenitic Stainless Steels, Metals Technology, vol. 3, Aug. 1976, pp. 358-365.

94. Grünbaum, G. Värmningens inverkan pa duktibiteten vid varmbearbetring, U3 och U4's expertkonferens om varmduktilitet, Gernkontoret, 1976, Swedish, Reported In : Ahlblom, B. and Sandström, R. Hot Workability of Stainless Steels : Influence of Deformation Parameters, Microstructural Components and Restoration Processes, International Metals Review, vol. 27, no. 1, 1982, pp 1-27.

95. Norström, L.A. Influence of Grain Size on Flow Stress in an Austenitic Stainless Steel, Scandinavian Journal of Metallurgy, vol. 6, no. 4, 1977, pp. 145-150.

96. Mase, T. Hot-Workability Testing of Stainless Steel, Sumitomo Search, no. 3, May 1970, pp. 31-38.

97. Gueussier, A. and Castro, R. Relations entre les Fragibités à chaud et à froid dans les aciers austénitiques du type 18-8, Revue de Mètallurgie, vol. 55, no. 2, 1958, pp. 107-122.

98. Bellot, J. and Hugo, M. Contributions a l'étude de la forgeabilité des aciers inoxydables et réfractaires a l'état brut de coulée, Revue de Mètallurgie, vol. 63, Jan. 1966, pp. 7-16.

99. McG.Tegart, W.J. Influence of Reheating Temperature on Forming Properties, In : Reheating for Hot Working, ISI P111, London : Iron and Steel Institute, London, 1968, pp. 26-35.

100. Decroix, J.H. Neveu, A.M. and Castro, R.J. Some Observations on the Hot Workability of Stainless Steels in the As-Cast Condition, In : Deformation Under Hot Working Conditions, ISI P108, London : Iron and Steel Institute, 1968, pp. 135-144.

101. Samanta, S.K. Effect of Strain Rate on Compressive Strength of Tool Steel at Elevated Temperatures, In : Deformation Under Hot Working Conditions, ISI P108, London : Iron and Steel Institute, 1968, pp. 122-130.

102. Kemppinen, A.I. Simulation of Hot-Working Characteristics of Al-Mg Alloys by High Strain Rate Tensile Testing, In : Deformation Under Hot Working Conditions, ISI P108, London: Iron and Steel Institute, 1968, pp. 117-121.

103. Ludwick, P. Die Bedeutung des Gleit-und Reißwiderstandes für die Werkstoffprüfung, Zeitschrift des Vereines Deutscher Ingenieure, vol. 71, no. 43, 1927, pp. 1532-1538.

104. Nadai, A. Theory of Flow and Fracture of Solids, 2nd ed. New York : McGraw-Hill, 1950.

105. Nikkilä, K.A. Hot Torsion Test Simulating Rolling, Scandinavian Journal of Metallurgy, vol. 1, 1972, pp. 9-15.

106. Sandström, R. Mikro-strukturens roll vid varmbearbetning Del 2. Varmbearbetbarhet hos rostfria stal, Gernkontorets Ann., vol. 163, 1979, pp. 39-42, Swedish, Reported in : Ahlblom, B. and Sandström, R. Hot Workability of Stainless Steels : Influence of Deformation Parameters, Microstructural Components and Restoration Processes, International Metals Reviews, vol. 27, no. 1, 1982, pp. 1-27.

107. Aleszka, J.C. Low Energy Impact Behaviour of Composite Panels, ASTM Journal of Testing and Evaluation, vol. 6, no. 3, May 1978, pp. 2-2-211.

108. Allen, B.C. and Bartlett, E.S. Elevated Temperature Tensile Ductility Minimum in Silicide Coated Cb-10W and Cb-10W - 2.5 Zr, Transactions of American Society for Metals, vol. 60, 1967, pp. 295-304.

109. Guy, A. Essentials of Materials Science, New York : McGraw-Hill, 1968.

110. Fontana, M.G. and Greene, N.D. Corrosion Engieering, 2nd Ed. New York : McGraw-Hill, 1978.

111. Moore, P. Methods for Studying Hot Workability : A Critical Assessment, In : Deformation Under Hot Working Conditions, ISI P108, London : Iron and Steel Institute, 1968, pp. 103-106.

112. Dieter, G.E. Tension Testing, In : Dieter, G.E. ed. Workability Testing Techniques, Cleveland : American Society for Metals, 1984, pp. 21-36.

113. Nicholson, A., Smith, D. and Shaw, P. Hot Workability Testing at United Steel Companies, In : Deformation Under Hot Working Conditions, ISI P108, London : Iron and Steel Institute, 1968, pp. 161-166.

114. Min, B.K. A Plane Stress Formulation for Elastic-Plastic Deformation of Unidirectional Composites, Journal of the Mechanics and Physics of Solids, vol. 29, no. 4, 1981, pp. 327-352.

115. Ertürk, T. Anisotropy of Bulk Forming Limits in Hot-Rolled Steel Bars, Metallurgical Transactions, vol. 12A, May 1981, pp. 743-748.

116. Costin, L.S. and Duffy, J. The Effect of Loading Rate and Temperature on the Initiation of Fracture in a Mild, Rate-Sensitive Steel, Journal of Engineering Materials and Technology, vol. 101, no. 3, July 1979, pp. 258-264.

117. Proud, L.W. and Wynne, E.J. Hot Workability of High-Carbon Chrome Bearing Steel, In : Deformation under Hot Working Conditions, ISI P108, London : Iron and Steel Institute, 1968, pp. 157-160.

118. Kuhn, H.A., Lee, P.W. and Otto, W.L. A Criterion for Ductile Fracture in Metalworking Processes, In : [Proc. Conf. on] The Microstructure and Design of Alloys, vol. 1, Cambridge : The Institute of Metals, Monograph and Report Series, no. 36, 1973, pp. 355-359.

119. Atkinson, M.W. A Study of the Fabrication and Machining Characteristics of Some Abrasion - Corrosion Resistant Alloys, M.Sc Dissertation, University of the Witwatersrand, Johannesburg, 1984.

120. Sangdahl, G.S., Aul, E.L. and Sachs, G. An Investigation of the Stress and Strain States Occurring in Bending Rectangular Bars, Proceedings of the Society for Experimental Stress Analysis, vol. 6, no. 1, 1948, pp. 1-18.

121. Fitzsimons, G., Kuhn, H.A. and Venkateshwar, R. Deformation and fracture Testing for Hot Working Processes, Journal of Metals, vol. 33, no. 5, May 1981, pp. 11-17.

122. Male, A.T. and Dieter, G.E. Hot Compression Testing, In : Dieter, G.E. ed. Workability Testing Techniques, Cleveland: American Society For Metals, 1984, pp. 51-72.

123. Semiatin, S.L. Workability in Forging, In : Dieter, G.E. ed. Workability Testing Techniques, Cleveland : American Society For Metals, 1984, pp. 197-248.

124. Sabroff, A.M., Boulger, F.W. and Henning, H.J. Forging Materials and Practices, Ohio : Reinhold Book Corporation, 1968.

125. Daykin, R.P. Unpublished research, Ladish Co., Cudahy, WI, June 22 1951, Reported in : Semiatin, S.L. Workability in Forging, In : Dieter, G.E. ed. Workability Testing Techniques, Cleveland : American Society For Metals, 1984, p. 214.

126. De Ridder, A.J. and Koch, R. Forging and processing of High-Temperature Alloys, In : Abrams, H., Maniar, G.N., Nail, D.A. and Solomon, H.D. eds. Micon 78 : Optimisation of Processing, Properties, and Service Performance Through Microstructural Control, ASTM STP 672, Philadelphia : American Society for Testing and Materials, 1979, pp. 547-563.

127. Haberling, E., Bennecke, R. and Köster, K. Properties of High Speed Steels with Increased Sulphur Content, In : Thyssen Edelstahl Technische Berichte, Krefeld : Thyssen Edelstahlwerke AG, Forschungsinstitut, Dec. 1983, pp. 31-37.

128. Technical Data Sheet of Southern Cross, Middleburg, S.A. 01.10.82.

129. Fine, H.A. and Geiger, G.H., Handbook on Material and Energy Balance Calculations in Metallurgical Processes, Warrendale : The Metallurgical Society of AIME, 1979.